AAS, XRPD, SEM/EDS, AND FTIR STUDIES OF THE EFFECT OF CALCITE AND MAGNESITE ON THE UPTAKE OF Pb^{2+} AND Zn^{2+} IONS BY NATURAL KAOLINITE AND CLINOPTILOLITE

A Thesis Submitted to
the Graduate School of Engineering and Sciences of
İzmir Institute of Technology
in Partial Fulfillment of the Requirements for the Degree of

MASTER OF SCIENCE

in Chemistry

by

BANU ZÜNBÜL

January 2005
İZMİR

We approve the thesis of **Banu ZÜNBÜL**

Date of Signature

.....

14.01.2005

Asst. Prof. Talal SHAHWAN

Supervisor

Department of Chemistry

.....

14.01.2005

Assoc. Prof. Ahmet E. EROĞLU

Co-supervisor

Department of Chemistry

.....

14.01.2005

Prof. Dr. Çetin GÜLER

Ege University,

Facult of Science, Department of Chemistry

.....

14.01.2005

Assoc. Prof. Hürriyet POLAT

Department of Chemistry

.....

14.01.2005

Assoc. Prof. Serdar ÖZÇELİK

Department of Chemistry

.....

14.01.2005

Assoc. Prof. Ahmet E. EROĞLU

Head of Department of Chemistry

.....

Assoc. Prof. Semahat ÖZDEMİR

Head of the Graduate School

ACKNOWLEDGEMENT

I wish to express my grateful thanks to my supervisor Assist. Prof. Dr. Talal R.A. Shahwan for his guidance, motivations and endless supports during this project.

I would like to thank my co-supervisor, Assoc. Prof. Dr. Ahmet E. Eroğlu, for his supports and helps.

I would like to thank Sinan Yılmaz, Betül Öztürk at Chemistry Department for their help in AAS and FTIR measurements and Duygu Oğuz, Gökhan Erdoğan, Evrim Yakut at Material Research Center at İzmir Institute of Technology for their help in performing the SEM/EDS and XRPD analysis.

Special thanks go to all friends, research assistants, technicians and all staffs in İzmir Institute of Technology for their helps and friendships.

Finally, I would like to express my endless thanks to my beloved family for their endless support and motivation throughout the course of my studies.

ABSTRACT

In this study, the effect of magnesite and calcite on the uptake of lead and zinc ions by mixtures of these carbonates with kaolinite and clinoptilolite was investigated at various loadings and mixture compositions. The concentration of both ions in the liquid phase was in measured using AAS, while XRPD, SEM/EDS, and FTIR techniques were used in characterizing the solid samples. The study included the determination of kinetics and sorption isotherms of lead and zinc on pure kaolinite and clinoptilolite. Moreover, the sorption behavior of lead and zinc at different concentrations and pH conditions was investigated on mixtures of calcite and magnesite with kaolinite and clinoptilolite at carbonate mass percentage compositions of 5, 10, 25, 60 in addition to pure calcite and magnesite. The morphologies of the formed precipitates, the plausible structural change in the lattice of calcite, magnesite, kaolinite, and clinoptilolite originating from sorption of lead and zinc ions was examined. According to obtained results, the sorption affinity of kaolinite and clinoptilolite towards lead is larger than their affinity towards zinc. Within the operating experimental conditions, the sorption capacity increased with increasing the amounts of calcite, and magnesite. The overall order of retention of lead and zinc was observed as magnesite ≥ calcite> clinoptilolite> kaolinite under neutral and alkaline pH conditions and high loadings. When the initial concentration of zinc and lead ions is raised to saturation conditions, rapid overgrowth of cerussite and hydrozincite was observed. Increasing the initial pH to 10,0 caused enhancement in the dissolution of calcite and magnesite, leading to the enhancing the precipitation of hydrozincite, and an increased formation of hydrocerussite instead of cerussite. The uptake of Zn^{2+} and Pb^{2+} ions by calcite and magnesite have lead to modifying the geometry of the carbonate groups, the thing reflected as variation in their vibrational bands.

ÖZ

Bu çalışmada, Pb^{2+} ve Zn^{2+} iyonlarının kaolinit ve klinoptilolit minerallerince tutulmasındaki kalsit ve magnezit etkisi çeşitli deneysel ortamlarda araştırılmıştır. XRPD, SEM/EDS, ve FTIR teknikleri katı örnekleri karakterize etmek için kullanılırken, her iki iyonun sıvı faz içindeki konsantrasyonu AAS kullanılarak ölçüldü. Bu çalışma saf kaolinit ve klinoptilolit üzerindeki kurşun ve çinkonun kinetik ve sorpsiyon izotermlerini de içermektedir. Ayrıca, farklı konsantrasyon ve pH koşullarında kurşun ve çinkonun sorpsiyon davranışları saf kalsit ve magnezit ile olan etkileşimine ek olarak, yüzde (kütle) 5,10, 25, ve 60 karbonat içeren klinoptilolit ve kaolinit karışımları ile olan etkileşimi de araştırıldı. Oluşan çökelti morfolojisi, kurşun ve çinko iyonlarının sorpsiyonundan dolayı kalsit, magnezit, kaolinit ve klinoptilolitteki olası yapısal değişimi incelenmiştir. Elde edilen sonuçlara göre, kaolinit ve klinoptilolitin kurşuna karşı sorpsiyon afinitesi, çinkoya karşı olan afinitesinden daha büyüktür. Çalışılan deney koşullarında, kurşun ve çinko iyonlarının tutulma sırası magnezit≥ kalsit> klinoptilolit> kaolinit şeklinde saptanmıştır. Çinko ve kurşun iyonlarının başlangıç konsantrasyonları doygunluk koşullarına yükseltildiği zaman, serusit ($PbCO_3$) ve hidroserusit ($Pb_3(CO_3)_2(OH)_2$) çökeltilerin hızlı bir büyüme gösterdiği gözlenmiştir. Magnezit ve kalsitin çözünürlüğünün artmasına neden olan başlangıç pH ının 10' a yükselmesi, hidrozinkitin çökmesinin artmasına ve serusit yerine hidroserusit formunun oluşmasına yol açmıştır. Zn^{2+} ve Pb^{2+} iyonlarının kalsit ve magnezit tarafından tutulması, karbonat gruplarının geometrisinin biraz değişmesine yol açmakta, buda titreşim bantlarını etkilemektedir.

TABLE OF CONTENTS

LIST OF FIGURES

Figure **Page**

LIST OF TABLES

CHAPTER 1

INTRODUCTION

1.1. General Consideration

The term ‘heavy metal’ is used to describe any metallic chemical element which has a relatively high density and is toxic or poisonous even at low concentrations. Heavy metals are natural components of the Earth's crust which cannot be degraded or destroyed. Therefore, they tend to accumulate in soils and sediments. Examples of heavy metals include lead, zinc, copper, nickel, mercury, chromium, and cadmium. [Pierzynski et al. 1995, p.167, Hooda et al. 1998, p.121]

Heavy metals can be toxic to living things at certain levels. Although they occur naturally, they might also come from many different sources. These include some mining industries, burning of fossil fuels, like coal, burning garbage or tobacco, and even forest fires, the thing leading to release of a variety of heavy metals into the environment. [Allen et al. 1995, p.255, Sekar et al. 2004, p.1]

Heavy metals can enter our bodies via food, drinking water and air to a small extent. Although some heavy metals are very important to maintain the metabolism of the human body as trace elements, they can lead to poisoning at higher concentrations. Heavy metal poisoning could result, for example, from drinking-water contamination (e.g. lead pipes), high ambient air concentrations near emission sources, or intake via the food chain. There are a lot of health effects of heavy metals. These include various types of cancer, kidney damage, and even death in some instances of exposure to very high concentrations. [Appel et al. 2002, p.582]

1.2. Heavy Metals in the Environment

1.2.1. Significance of Lead and Zinc

1.2.1.1. Lead:

Lead is a well- known metal toxicant which has an atomic number of 82, an atomic mass of 207.19, and is located in Group IVA of the Periodic Table. It is a bluish - white, soft metal with a density of 11.34 gr\cm^3, a melting point of 327.5 ^{o}C, and boiling point about 1740 ^{o}C.

Lead is a naturally occurring element which consists of 52 % ^{208}Pb, 24% ^{206}Pb, 23% ^{207}Pb, and 1 % ^{204}Pb. Radioactive ^{210}Pb, from radon decay, plays also a role, for example, in waters and sediments. It can be found in all environmental media (air, soil, rocks, sediments, water) and in all components of the biosphere. The most important lead minerals are galena (lead sulfide), cerussite (lead carbonate), and anglesite (lead sulfate). [Ohnesorge et al. 1991, p. 971-974].

Although lead is used in batteries, petrol additives, extruded products, alloys, pigments, cable sheathing, lead pollution, irrespective of source, is of major concern because of its long residence time in the soil and its possible association with cognitive development in children. Lead can be transported into water bodies by natural circulation and consequently threaten human life because of its well known toxicity, accumulation in food chains and persistence in nature. Accumulation of lead is mainly in the bones, brain, kidney and muscles and may cause, many serious disorders like anemia, kidney disease, nervous disorders and sickness even death. [Yu et al. 2001, p.83, Prasad et al. 2000, p.3034]

1.2.1.2. Zinc:

Zinc plays an important role as an essential trace elements in all living systems from bacteria to humans. Zinc is a bluish white, rather soft metal, which solidifies in

hexagonal crystals and belongs to the group IIB elements of the Periodic Table. It is a member of transition elements. Its atomic number is 30, its atomic mass 65.39, and its density 7,14 g/cm^3. The melting point is 419.58 ^{o}C and the boiling point 907 ^{o}C. [Ohnesorge et al. 1991, p.1309]

Zinc is used in soldering compounds, galvanized wire, batteries, steel works with galvanizing lines, fiber production, newsprint paper production and certain paints. Zinc is not very toxic. Significiant excesses are toxic and produce signs similar to lead poisoning. It usually enters the body when a person consumes food, drink, or dietary supplements containing the element. For humans and animals, a deficiency of Zn can cause anorexia and growth depression. Normally, zinc leaves the body in urine and feces. There are alot of health effects of zinc if people are exposed with elevated levels. It may interfere with the body's immune system and affect the body's ability to utilize other essential minerals and cause digestive problems such as stomach cramps, nausea, and vomiting. When large amounts of zinc are inhaled, a short-term disease called metal fume fever may occur. Scientists doubt that zinc plays a role in cancer. [Pardo-Botello et al. 2004, p.292, Nachtegaal et al. 2004, p.14].

Turkey contains natural deposits of some heavy metals. Lead and Zinc deposits occur mainly in Balıkesir (Balya Mine), Çanakkale (Yenice Mines), Yozgat, Niğde, Adana (Horzum), Kayseri, Sivas (Koyulhisar ve Aktepe Mines) WEB_1 (1996).

1.3. Soil Fractions: Clays, Zeolites, Carbonates

1.3.1. Clays:

Clay is a naturally occuring, inorganic component of most soils. Clays are the products of the weathering of rocks and are widely distributed. Clay minerals are essentially hydrous aluminum silicates of very small particle size (<2 μm). In some, Mg and Fe substitute in part for aluminum and alkali or alkaline earths may be present as essential constituents as a result of isomorphous substitution. [Rouquerol et al. 1999, p.355, Van Olphen 1977, p.59] . As indicated by Figure 1.1, [Yariv et al. 2002, p.7,9], the structure of a pure clay mineral is made up of two basic blocks. The first is the sheet

formed of silicon tetrahedral units and the second is another sheet composed of aluminum octahedral units. The stacking of these sheets into layers, the bonding between layers, and the substitution of other ions for Al and Si determines the type of the clay minerals. Among the properties of clay minerals are their plasticity, when mixed with a small amount of water, their low permeability, thermal stability, and wide availability. Although a clay may be made up of a single clay mineral, there are usually several mixed with other minerals such as fieldpars, quartz, carbonates, and micas. [Shahwan 2000, p.8]

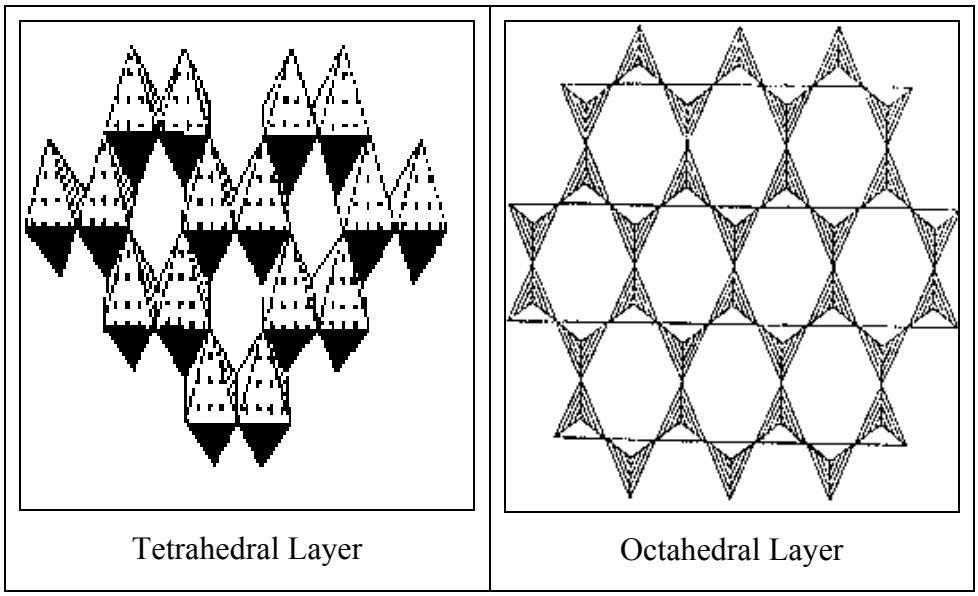

Figure 1.1. Structure of tetrahedral sheet and octahedral sheet of clay

Clay deposits can be found in estuaries, coastal plains, continental shelves, and offshore islands of various parts of the world. These geographic zones are usually the economic, industrial, commercial, and residential hubs of regions [Lim et al. 2002, p.806]. Turkey has plenty of clay deposits. Deposits of clays, suitable for ceramics manufacture, are produced in Bilecik regions, İstanbul, Şile and Beykoz. Most of Kaolin deposits in Turkey are concentrated in the Marmara Sea Region, particularly in Balıkesir zone. WEB_1 (1996)

1.3.3.1. Kaolinite:

Kaolinite is the most known example of 1:1 type clay. The ideal formula of kaolinite is $Al_2Si_2O_5(OH)_4$. As Figure 1.2, [Shahwan 2000, p.10], indicates, kaolinite consists of an octahedrally coordinated sheet of aluminium ions and tetrahedrally coordinated sheet of silicon ions. When these sheets stack, OH ions of one sheet, O ions of its neighbour sheet provide connection between tetrahedral silicate (SiO_4) and octahedral gibbsite layers ($Al(OH)_2$). As a result the structure of kaolinite becomes tightly bound by H bonding. Therefore, most sorption activity occurs along the edges and surfaces of the structure. It is nonexpandable and possess a cation exchange capacity (CEC) of 3-15 meq /100 g. [Coles et al. 2002, p.40, Rouquerol et al. 1999, p.358, Hu et al. 2003, p.1279].

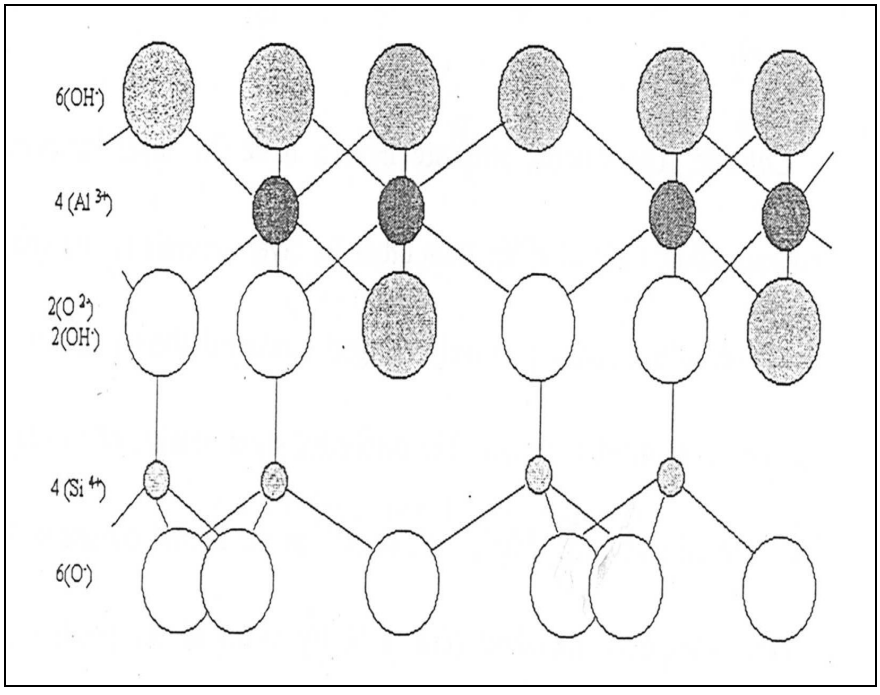

Figure 1.2. Structure of kaolinite

Kaolinite which is essential to the production of ceramics and porcelain is also used as a filler for paint, rubber and plastics because of relatively inert and long

lasting, but the greatest demand for kaolinite is in the paper industry to produce a glossy paper such as is used in most magazines.

Three kaolin production areas, which are dominate the world markets, are the sedimentary kaolins in Georgia and South Carolina in the United States; the primary kaolins in the Cornwall area of Southwestern England; and the sedimentary kaolins in the lower Amazon basin in Brazil. Other kaolin deposits, which are regionally important, are located in China, Australia, Argentina, Czech Republic, France, Germany, Indonesia, Iran, Mexico, South Korea, Spain, Turkey, and Ukraine. [Kissel et al. 1989, p.488]. The natural kaolinite used in this study was obtained from the Sındırgı, located on the western part of Anatolia.

1.3.2. Zeolites:

Zeolites has three dimensional crystal structure. They are naturally occuring crystalline, hydrated aluminasilicates of alkali and alkaline earth cations which are characterized by cage-like structures, high surface areas (hundreds of m^2/g) and high cation exchange capacities (at least hundreds of meq/kg), [Sheta et al. 2003, p.127] .

Natural zeolites can occur in greater sized aggregates and are free of shrink swell behavior observed in some clays. Most zeolites are rich in Na^+, K^+, and Ca^{2+}, which are usually exchangeable with other metal ions. Although zeolites have been known for centuries, their value as adsorbent material was only realized some 4 decades ago. Adsorption properties of zeolite are affected by structure, location and size of its cations and presence of molecules formerly adsorbed [Feng et al. 2000, p.360]. Figure 1.3, WEB_2 (1996), shows a typical zeolite crystal formation with the open-cage structure and the position of oxygen and silicon atoms. When silicon is replaced by aluminium, an overall negative charge results, a well- known property of zeolites.

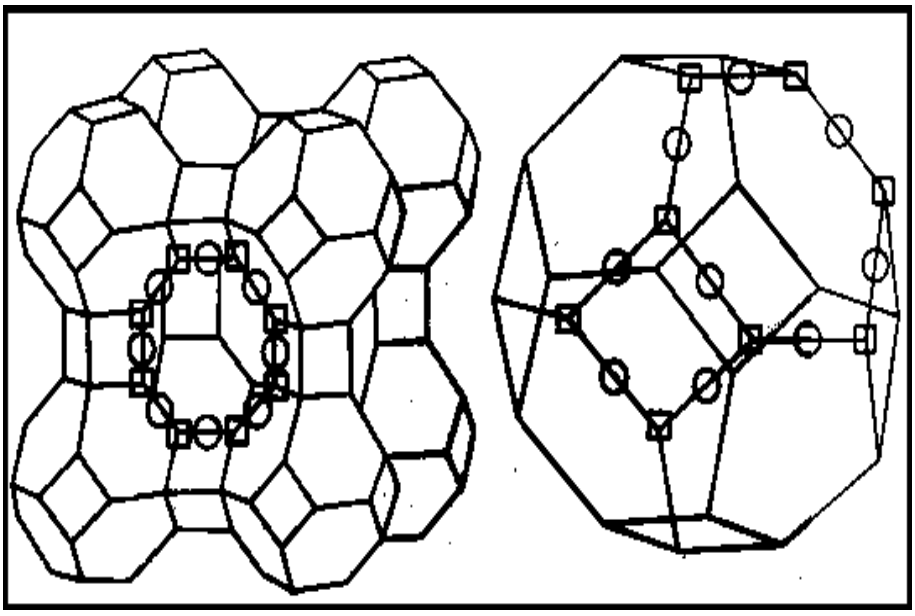

Figure 1.3. Illusration of typical zeolite crystal formation (circle = oxygen, square = silicon, aluminium)

Each zeolite mineral has a separate capacity and an ion exchange selectivity. Several factors, which can affect both the ion exchange selectivity and capacity of the specific zeolite mineral, must be considered in this process. These include ionic strength, pH, temperature and the presence of other competing cations in the solution.

Alteration of glassrich volcanic rocks with fresh or saline water in playa lakes or by seawater form most common natural zeolites. Also, zeolites are deposited in lava flows. Because of their specific structure and physical and chemical properties, natural zeolites have found applications in the field of pollution control, including control of hardness, ammonium nitrogen, heavy metals, air pollutants, and radioactive contaminants [Badillo-Almaraz et al. 2003, p.424, Trgo et al. 2003, p.167].

Internationally, zeolite deposits are found in Canada, Japan, New Zealand, Bulgaria, USA, British Columbia, Austria and Turkey. Clinoptilolite and Analcime, two types of zeolites, are found in Turkey with great amounts. Locations and types of natural zeolites in Turkey are given in Table 1.1. [Özkan 1996, p.2, Narin 2001, p.15]

Table 1.1. Natural zeolite deposits in Turkey and types

Region	*Type*
İzmir, Urla	*Clinoptilolite*
Balıkesir, Bigadiç	*Clinoptilolite*
Kapadokya Region (Tuzköy, Karain village)	*Clinoptilolite*
	Chabazite
	Mordenite
	Erionite
Gördes	*Clinoptilolite*
Emet, Yukarı Yoncaağaç	*Clinoptilolite*
Bahçecik, Gülpazarı, Göynük	*Analcime*
Polatlı, Mülk, Oğlakçı, Ayaş	*Analcime*
Nalıhan, Çayırhan, Sabanözü	*Analcime*
Kalecik, Çandar, Hasayar	*Analcime*

1.3.2.1. Clinoptilolite:

Clinoptilolite is the most abundant zeolite in nature because of wide geographic distribution and the large size of deposits. The ideal formula of Clinoptilolite is $(Na,K,Ca)_6Al_6Si_{30}O_{72}*24H_2O$. [Tanaka et al. 2003, p.713]. As Figure 1.4 [Top 2001, p.23] shows, the structure of clinoptilolite consists of two dimensional systems of three types of channel. A channel contains of 10 member ring, B channel

contains of 8 member ring, and perpendicularly intersected by C channel is 8 memberring.

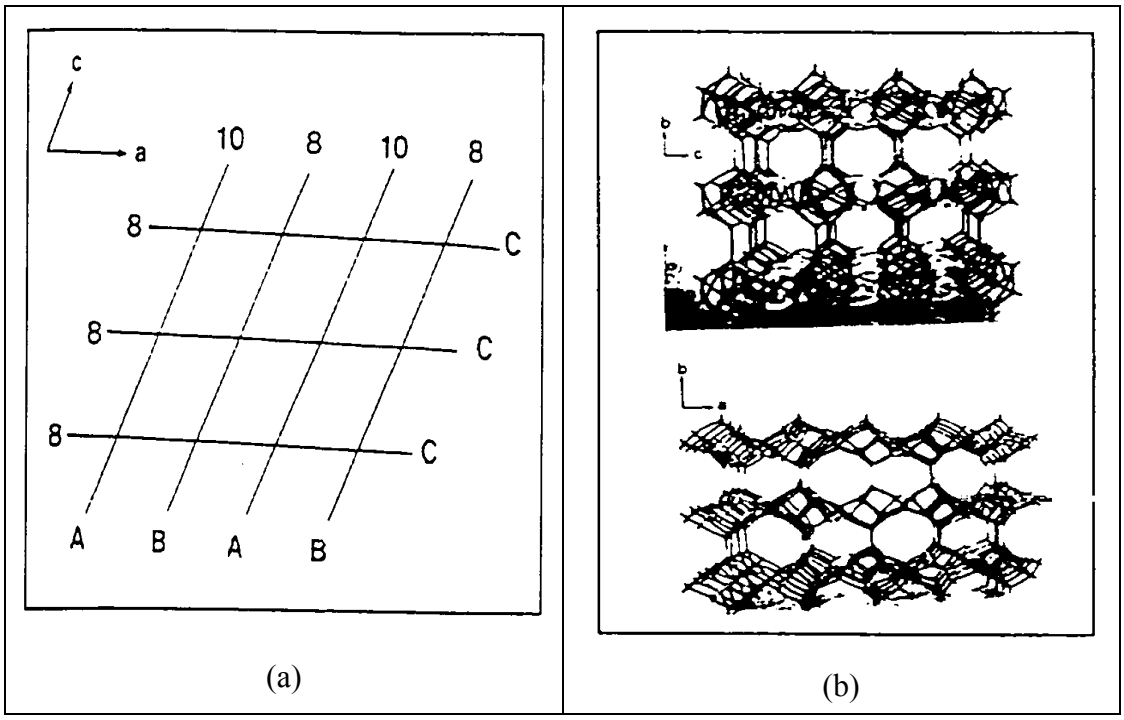

Figure 1.4. a) Orientation of clinoptilolite channel axis b) Model framework for the structure of clinoptilolite.

As illustrated by Figure 1.5 [Top 2001, p.24], the structure of clinoptilolite include cation sites. In this structure, the main cation positions; M(1), M(2), M(3) located in channel A, B, C. In clinoptilolite, these channels are predominantly occupied by Na, K, Ca and H_2O. Na resides in the larger A channel, Ca resides in the smaller B channel, K resides in the C channel. Na bonds to 2 framework O atoms and 5 of water molecules, Ca bonds to 3 framework O atoms and 5 of water molecules, K bonds to 6 framework O atoms and 3 of water molecules.The CEC of clinoptilolite was reported that to be 222-238 meq/100 g. [Langella et al 2000, p.339]

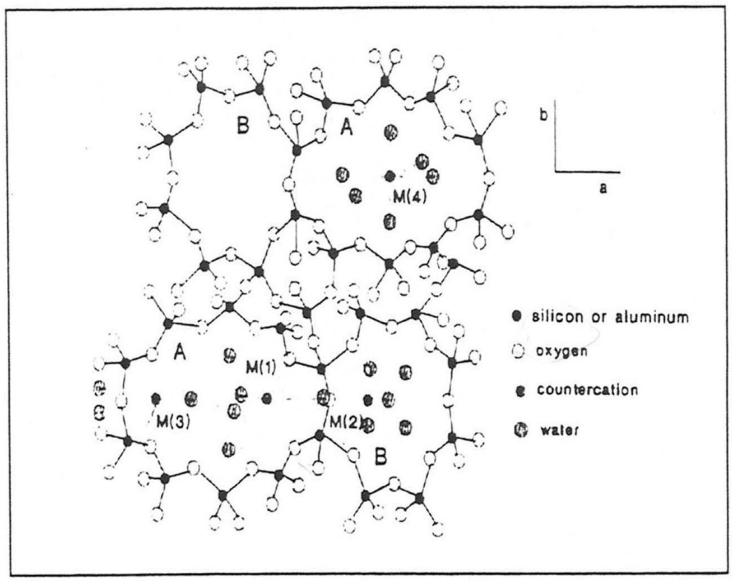

Figure 1.5. The c-axis projection of the structure of clinoptilolite.

Clinoptilolite is used in various applications such as adsorption processes, ion exhanger, in gas seperation. This mineral has been used since several years as an additive to feed for sheep, pigs, cattle and chickens. [Tanaka et al. 2003, p.713]

1.3.3. Carbonates:

Carbonates are common constituents of the Earth's near-surface crust. They comprise about 4 % by weight of Earth's Crust. They tend to originate in sedimentary rocks where calcite and dolomite are the most abundant carbonate minerals, beside them siderite, $FeCO_3$ and rhodocrysite, $MnCO_3$, may be present. The large availability of carbonate minerals makes them among the most important minerals that can affect the biogeochemical cycles of heavy metals in the environment.Carbonate minerals are essential due to the fact that they regulate the aquatic environments via precipitation, dissolution and sorption reactions which are controlled by chemical process and which take place at the interface between mineral lattice and bulk solution. [Shahwan et al. 2002, p.563]. Due to the fact that carbonates are soluble in aqueous solutions the determination of surface charge by potentiometric titration is diffucult.

When associated with clays and zeolites, carbonate minerals can affect the uptake properties of them due to the difference in their sorption characteristics and capacities.

1.3.3.1. Calcium Carbonate ($CaCO_3$):

It is one of the most common minerals on the surface of the Earth and also have an additional biological importance. $CaCO_3$ can exist in three polymorphs; calcite, aragonite, and vaterite. Calcite is the most thermodynamically stable one at room temperature and atmospheric pressure. Also, calcite can exist as limestone or marble. Limestone transforms marble under the effect of heat and pressure of metamorphic events. Calcite occurs in all colors, sometimes even multicolored. [Smyth et al 1997, p.1595]. It has hexagonal structure with the trigonal carbonate ions being coplanar as seen in Figure 1.6 WEB_4 (1996).

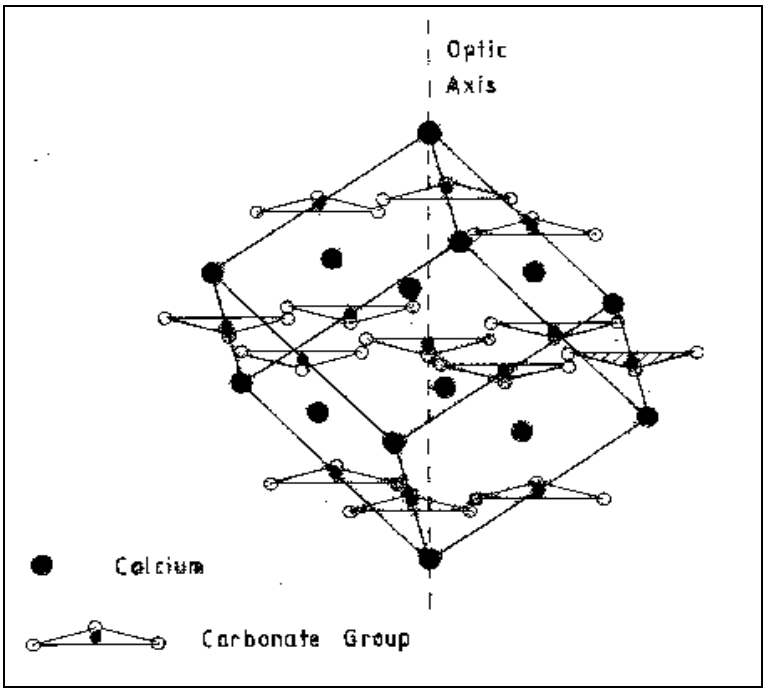

Figure 1.6. The structure of calcite

1.3.3.2. Magnesium Carbonate ($MgCO_3$):

Magnesium carbonate, $MgCO_3$, known also as magnesite, is another example of the most widely available carbonate minerals. It is either white, greyish, tinted yellow or brown in colour, and its hardness is slightly greater than that of human nail.

Magnesite play an important role in regulating the aquatic environments as a result of precipitation, dissolution and sorption reactions. Magnesite does not ordinarily form good crystals, but can make up a substantial portion of some rock types. It forms commonly from the alteration of magnesium-rich rocks during low grade metamorphism while they are in contact with carbonate-rich solutions. Based on a linear free energy correlation model, magnesite was predicted to have the largest trace metal partition coefficients among the carbonate minerals possessing a calcite structure [Wang et al. 2001, p. 1529]. Many of the properties of magnesite are either identical or similar to those of calcite. It has hexagonal structure with the trigonal carbonate ions being coplanar as calcite. Figure 1.7 WEB_5 (2002) shows a model of a crystal structure of magnesite.

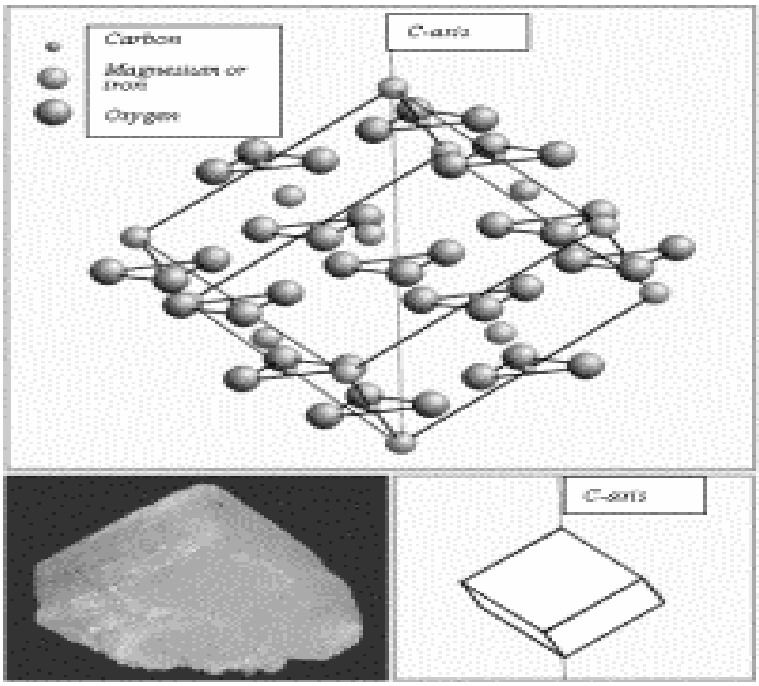

Figure 1.7. Crystal-chemical structure of magnesite.

1.4. The Interaction Processes of Metal Ions and Soil

Soil is both a heavy metals's adsorbent and a source of them. The residence time of most heavy metals is very long. The interaction of metal ions with natural soil particles is complex therefore, it involves multiple mechanisms [Pierzynski et al. 1994, p.167; Allen et al. 1995, p.255]. Sorption is an important process that can regulate the transport of chemical species through the hydrosphere. The term "sorption" is generally used to refer to three important processes: adsorption, surface precipitation, and fixation. Adsorption is a two-dimensional accumulation of matter at the solid/water interface and is understood primarily in terms of intermolecular interactions between solute and solid phases. The surface complexation model is able to describe the adsorption behavior at low cation concentrations very exactly but it is not able to describe the adsorption curves obtained at higher concentrations. In the first case, the curves can be described approximately by a Langmuir isotherm where a saturation of the adsorption capacity is reached. In the second case a continuous increase without saturation at the surface is observed, which is fitted better by a Freundlich isotherm. To explain this behavior the so-called surface precipitation model has been developed, which takes into account precipitation reactions in addition to adsorption reactions at the surface. The third principal mechanism of sorption is fixation or absorption, which involves the diffusion of an aqueous metal species into the solid phase. Like surface precipitation or coprecipitation, absorption is three-dimensional in nature. Heavy metals that are specifically adsorbed onto clay minerals and metal oxides may diffuse into the lattice structures of these minerals. The metals become fixed into the pore spaces of the mineral structure (solid-state diffusion). In order to remove the heavy metals, the total dissolution of the particles in which they are incorporated may be required. [Bradl 2004, p.6]

Sorption of heavy metal ions on soils and soil constituents is influenced by a variety of parameters. These are pH, metal ion, soil type (composition, aging). Soil pH is the most important parameter influencing metal-solution and soil surface chemistry. The dependence of heavy metal adsorption on, e.g., clays on solution pH has been noticed early. The number of negatively charged surface sites increases with pH. In general, heavy metal adsorption is small at low pH values. At high pH values, the metal

ions are completely removed. The pH is a primary variable, which determines cation and anion adsorption onto oxide minerals. [Bradl 2004, p.10]

The soil type and composition plays an important role for heavy metal retention. In general, coarse-grained soils exhibit lower tendency for heavy metal adsorption than fine grained soils. The fine-grained soil fraction contents soil particles with large surface reactivities and large surface areas such as clay minerals, iron and manganese oxyhydroxides, humic acids, and others, and displays enhanced adsorption properties. Clays are known for their ability to effectively remove heavy metals by specific adsorption and cation exchange as well as metal oxyhydroxides. Depending upon the variability in physical and chemical characteristics of metals , their affinity to soil components governs their speciation [Pendias et al. 1992, Bradl 2004, p.11]. Alternatively, the sorption mechanism on the calcite fractions can plausibly occur via various processes; ion exchange, burial of the ions within the lattice of carbonate upon recrystallization, formation of surface complexes with >CaOH and $>CO_3H$ groups, precipitation as metal-carbonate, metal hydroxide, or both, and solid state diffusion. [Xu et al. 1996, p.2801].

Generally consistent rules of metal selectivity cannot be given as it depends on a number of factors such as the chemical nature of the reactive surface groups, the level of adsorption (i.e., adsorbate/adsorbent ratio), the pH at which adsorption is measured, the ionic strength of the solution in which adsorption is measured, which determines the intensity of competition by other cations for the bonding sites, and the presence of soluble ligands that could complex the free metal. All these variables may change the metal adsorption isotherms. Competition from monovalent metal in background electrolytes has relatively little effect on adsorption on heavy metals. Preference or affinity is measured by a selectivity or distribution coefficient. The reduction of this selectivity with increased adsorption is observed for metal adsorption on both clays as soil components and pure minerals. [Bradl 2004, p.10)

The distribution ratio, R_d, is widely used in the description of the partition of a sorbed cation/anion among the solid and liquid phases. R_d in an emprical constant, that is subjective to the operating experimental conditions, and thus is not a fully equilibrium constant.

Several types of reactions can be attributed to forces associated with charge sites. The term for trading ions with the surrounding water is "ion exchange". Ion

exchange is an important process in soils. For the ion exchange reaction to take place, three concurrent processes usually should take place. (1) diffusion of ions through the solution film that surrounds the soil particles, usually called film diffusion; (2) diffusion of ions through the hydrated surface of the soil particle, named as particle diffusion; and (3) chemical exchange reaction of ions from the particle surface, referred to as chemical reaction. [Liu et al. 1995, p.838).

The ordinary clays in many agricultural soils have a limited capacity for ion exchange because of their two dimensional framework structure. Zeolites were the first known materials capable of ion exchange since they have three dimensional structure. The affinity for sorption differs depending on (i) the charge of the ion, (ii) the ionic radious and the degree of hydration. The larger the charge on the ion, the greater is the force that the functional groups of the opposite charge of the ion exchanger attract. The greater the volume of the ion, the weaker is its electric field in the solution and therefore, the smaller is its degree of hydratation. The hydrodynamic radii of ions decrease with increasing atomic weight and hence their exchange energy when the ion is transported from the solution to the ion exchanger. [Shahwan 2000, p.18].

1.5. The Present Study

1.5.1. Aim of Present Study

The primary aim of this study is to elucidate the effect of calcite and magnesite on the uptake of lead and zinc by mixtures of these carbonates with kaolinite and clinoptilolite. The study have also included determination of kinetics and sorption isotherms of lead and zinc on pure kaolinite and clinoptilolite. In addition, the study is discussing the mechanisms of uptake of lead and zinc at different concentration levels for different mixtures and pH conditions, the morphologies of the formed precipitates, the plausible structural changes in the lattice of calcite, magnesite, kaolinite, clinoptilolite resulting from sorption of lead and zinc ions.

The sorption behavior of and/ Zn^{2+} or Pb^{2+} on kaolinite was investigated in a number of studies. The uptake of Zn is reported to proceed via fast kinetics and to obey Fruendlich and Dubinin –Radushkevich types of isotherm [Erten et al. 1994, p.375]. In another study, it was concluded that the interactions of the heavy metals (Pb, Zn) with

kaolinite could affect the structure of this mineral and influence properties such as swelling capacity, compaction capability and the double layer behaviour. [Miranda-Trevino et al. 2003, p.133, Coles et al. 2002, p.39-40, Nachtegaal et al. 2004, p.14]. Also, it was found that Pb^{2+} adsorption is higher than Zn^{2+} on clay minerals for the higher concentrations. [Auboiroux et al.1996, p.117, Ikhsan et al. 1999, p.408, Saha et al. 2001, p.694, Bradl 2004, p.14, Badawy et al. 2002, p.167, Gupta et al. 2001, p.1131, Jain et al. 1997, p.157, Singh et al. 2001, p.1961]

The uptake of both cations on clinoptilolite was reported in several studies. According to these studies, clinoptilolite favors Pb^{2+} over Zn^{2+} [Peric et al. 2004, p.1893, Badillo-Almaraz et al. 2003, p.424, Li et al. 2002, p.1106, Inglezakis et al. 2003, p.49, Çulfaz et al. 2003, p.94, Langella et al. 2000, p.337].

Retention of Pb^{2+} and /or Zn^{2+} on pure calcite was the subject of a number of investigations. [Godelitsas et al. 2003, p.424, Sipos et al. 2004, p.363, Lin et al. 1995, p.303-309, Mercy et al. 1998, p.739-745, Mesquita et al. 1996, p.137-146, Elzinga et al. 2002, p.3943]. On the contrary, the number of sorption studies of both ions on magnesite is very limited. Calcite is reported to retard Pb in higher quantity, compared to Zn [El-Korashy 2003, p.1709, Echeverria et al. 1998, p.275, Godelitsas et al. 2003, p.3353]. The retardation mechanism of Pb^{2+} and Zn^{2+} is believed to range from ion-exchange to precipitate formation (cerussite, hydrocerussite for Pb, hydrozincite for Zn). It was found that upon of Pb^{2+}, calcite disappeared almost totally, yielding the formation of cerussite, $PbCO_3$. Increasing the pH and initial concentration have caused the formation of hydrocerussite. [Godelitsas et al. 2003, p.3351, Sipos et al. 2004, p.369, Lin et al. 1995, p.303]. Mercy et al. 1998, p.739 concluded that hydrocerussite is the most stable in waters. According to Prasad et al. 2000, p.3034 natural minerals (carbonic rock) are effective in removing 65-99% of lead ions. On the other hand, Zn^{2+} retention on calcite occurs by precipitation as hydrozincite, $Zn_5(OH)_6(CO_3)_2$ under appropriate loading and pH conditions. [Garcia-Sanchez et al. 2002, p.539]

The primary motivation of this study is the scarcity in literature resources of studies dealing with the effect of association of clays and zeolites by calcite and magnesite on the uptake capacities and mechanisms of these clays and zeolites. A limited number of studies is available on the uptake of Pb^{2+} and/or Zn^{2+} by different calcareous soils, but, to our knowledge, none is available on magnesite association with soils. A radiotracer study of the sorption characteristics of Zinc (II) by calcareous soil

suggests that the contribution of calcite to the Zn^{2+} sorption by the two calcareous soils was approximately 70 % of the total amount sorbed, thus the calcite in calcareous soil is undoubtedly the most significant sink for zinc at high pH range.[Wenming et al. 2001, p.371]

The techniques applied in this study include Atomic Absorption Spectroscopy (AAS), X Ray Powder Diffraction (XRPD), Infrared Spectroscopy (FTIR) and Scanning Electron Microscope / Energy Dispersive Xray Spectroscopy (SEM/EDS). Taking into consideration that most of the studies performed on sorption are carried out using bulk techniques, applying a surface technique like SEM/EDS will be helpful in figuring out sorption, as a surface phenomena, on a microscopic scale. Moreover, the application of XRPD is helpfull in elucidating the structural stability of solids upon uptake of Zn^{2+} and Pb^{2+} ions. In this study we report also how FTIR spectroscopy can be used to follow the change in the vibrational modes of carbonate upon Zn^{2+} and Pb^{2+} fixation.

1.5.2. Applied Methods:

1.5.2.1. Atomic Absorption Spectroscopy (AAS):

Atomic-absorption spectroscopy (AAS) is based on the absorption of light emitted from a hollow cathode lamp by gas –phase atoms of an atomized liquid sample to find the concentration of these atoms. Ions or atoms in a sample must undergo desolvation and vaporization in a high-temperature source such as a flame or graphite furnace. The typical atomization temperature achieved by both the flame and furnace in atomic absorption methods (2500-3100 ^{o}C). The majority of the atoms will remain in the ground state. It is this factor which gives atomic absorption its characteristically good sensitivity as an analytical technique for elemental determinations. Flame AAS can only analyze solutions, while graphite furnace AAS can accept solutions, slurries, or solid samples. [Haswell 1991, p.22]

The main parts of an AAS instrument are given in Figure 1.8 WEB_ 6 (1996). Flame AAS uses a slot type burner to increase the path length, and therefore to increase the total absorbance. Sample solutions are usually aspirated with the gas flow into a

nebulizing/mixing chamber to form small droplets before entering the flame. The analyte concentration is determined from the amount of absorption. Applying the Beer-Lambert law directly in AAS is difficult due to variations in the atomization efficiency from the sample matrix, and nonuniformity of concentration and path length of analyte atoms (in graphite furnace AA). Concentration measurements are usually determined from a working curve after calibrating the instrument with standards of known concentration.

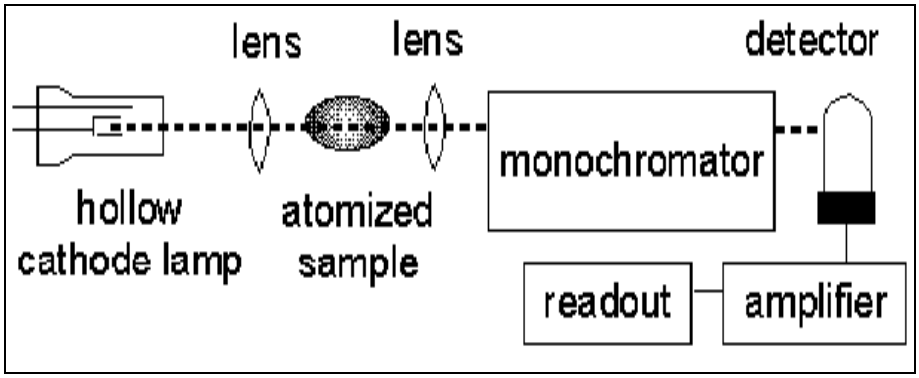

Figure 1.8. Illustration of the AAS

The optical system essentially consists of the light source. Light source emits the characteristic narrow line spectrum of the elements of interest and a monochromotor which enables, through spectral dispersion, the selection of the specific emission lines [Haswell 1991, p.22]. Generally, the light source is a hollow-cathode lamp of the element that is being measured. Lasers are also used in research instruments. Since lasers are intense enough to excite atoms to higher energy levels, they allow AA and atomic fluorescence measurements in a single instrument. The disadvantage of these narrow-band light sources is that only one element is measurable at a time.

AA spectrometers use monochromators and detectors for UV and visible light. Monochromator isolates the absorption line from background light due to interferences. This is the main purpose of the monochromator. Simple dedicated AA instruments often replace the monochromator with a band pass interference filter. Photomultiplier tubes are the most common detectors for AA spectroscopy.

Inspite the fact that AAS enables determination of a wide range of elements, it still has some limitations. These include the restriction to single elemental determination, the limited working calibration range, and the sensitivity to matrix effects that complicates the accurate measurements of some elements.

In this study, AAS is used to determine the concentration of Zn^{2+} and Pb^{2+} in solution, which is then used to calculate the concentration of both ions on the solids in addition to percentage sorption.

1.5.2.2. X-ray Diffraction (XRD):

X ray diffraction is a versatile analytical technique that is used in examining crystalline solids. Those solids include ceramics, metals, electronic materials, organics, and polymers. Samples to be analyzed may be introduced as powders, single crystals, multilayer thin films, sheets, fibers, or irregular shapes, depending on the desired measurement. X ray diffractometers fall broadly into two classes: single crystal and powder. Single-crystal diffractometers are most often used to determine the molecular structure of new materials. Powder diffractometers are routinely used for phase identification and quantitative phase analysis but can be configured for many applications, including variable – temperature studies, texture and stress analysis, grazing incidence diffraction, and reflectometry.The operative equation in X ray diffraction is the Bragg equation [see Figure 1.9]

$$n\lambda=2d\sin\theta \qquad 1.1$$

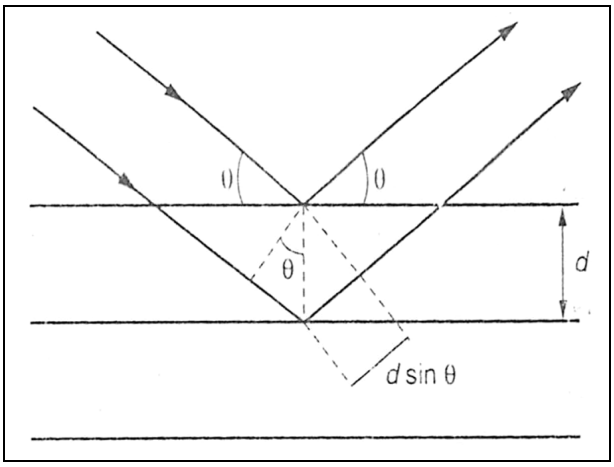

Figure 1.9. Illustration of Bragg's Law

In this formula, n is the order of a reflection, λ the wavelength of the X-ray radiation, d is the distance between parallel lattice planes, and θ is the angle between the incident beam and a lattice plane, known as the Bragg angle. When the pathlength in the crystal (2dsinθ) is a multiple of the wavelength, constructive interference occurs and diffracted intensity is obtained. In general, the d –spacing is a function of the lattice parameters (a, b, c) and angles (α, β, γ) defining the unit cell, and the miller indices (b, k, l) denoting a particular reflection. As such, it is the geometry of the crystal lattice that determines the positions of the peaks in an X ray diffraction pattern. In general, the more symmetrical the material, the fewer peaks in its diffraction pattern and the more intense these peaks are. Moreover, the type and arrangement of atoms within the crystal lattice determine diffracted intensities associated with those peaks.

The radiation used in a typical diffraction measurement, contains several wavelengths. It is denoted by $K_{\alpha 1}$, $K_{\alpha 2}$, and K_{β}, which are characteristic of the material producing the X rays. When the wavelength is small, the radiation is energetic and penetrating. Longer wavelength radiation spreads out the peaks in a diffraction pattern, which may overcome line overlap problems or enhance small peak shifts due to stress. The choice of radiation also depends on the sample characteristics.

XRPD is applied in this study to determine the mineralogical composition, and test the structural stability of the minerals upon sorption. The formation of carbonate phases of Pb^{2+} and Zn^{2+} will also be elucidated. (Setle 1997, p.341-342).

1.5.2.3. Infrared Spectroscopy (FTIR):

Infrared Spectroscopy is an important technique in chemistry. It is an easy way to identify the presence of certain functional groups in a molecule. Also, one can use the unique collection of absorption bands to confirm the identity of a pure compound or to detect the presence of specific impurities. This technique measures the absorption of various infrared light wavelengths by the material of interest. With the advent of Fourier Transform Infrared Spectroscopy (FTIR) the range of applications and the materials amenable to study has increased sensitivity, speed, wavenumber accuracy and stability.

The FTIR instrument consists of an IR light source, a sample container, a prism to separate light by wavelength, a detector, and a recorder (which produces the infrared spectrum).

One of the important features of FTIR is the ability to signal average a large number of scans in a relatively short amount of time. Thus spectra on very small quantities of material, or on highly absorbing materials, in which the signal to noise ratio of individual scans is very poor, can be achieved. The second major advantage of FTIR over conventional dispersive instruments is the high throughput of infrared radiation, since narrow slits are no longer necessary to achieve resolution. [Connor et al. 2003, p.203-205]

In this study, FTIR will in particular be used in revealing the effect of uptake of Zn^{2+} and Pb^{2+} on the stretching and bending modes of calcite and magnesite at different loading conditions.

1.5.2.4. Scanning Electron Microscope (SEM)

SEM is a powerful technique applied in micro-imaging of a variety of surfaces. This technique can be used in exploring the surface structure to determine particle size and texture on that surface. The surface of a solid sample is scanned in a raster pattern with a beam of energetic electrons. Several types of signals are produced from a surface in this process, including backscattered, secondary, and Auger electrons; X ray fluorescence photons; and other photons of various energies. All of these signals have

been used for surface studies, but the two most common are (1) backscattered and secondary electrons, which serve as the basis of SEM, and (2) X ray emission, which is used in electron microprobe analysis [Skoog et al. 1971, p.549].

Figure 1.10 [Connor et al. 2003, p.91] shows the essential elements of SEM. The electron gun, fitted with a W, LaB_6 or Field Emission (FE) gun operates typically over the range 0.1-30 kV accelerating voltage. A condenser lens produces a demagnified image of the source, which in turn is imaged by the probe forming lens onto the specimen. The electron path and sample chamber are evacuated. Scanning coils deflect the probe over the rectangular raster, the size of which, relative to the display screen, determines the magnification. Detectors collect the emitted electron signals, which after suitable amplification can be used to modulate the intensity of the beam of the display video screen, which is rastered in synchronism with the probe.

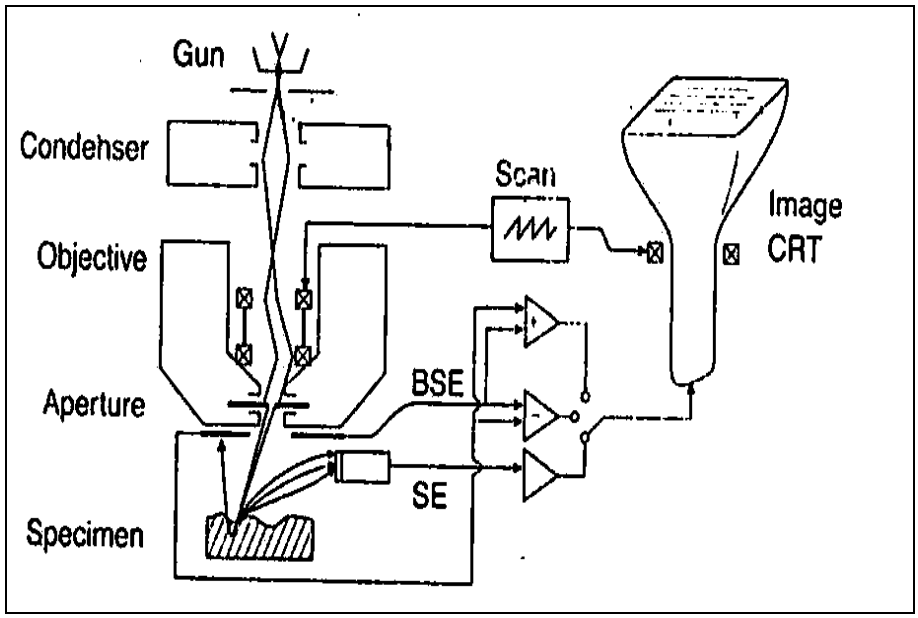

Figure 1.10. Basic features of the SEM (showing electron gun, condenser and objective lenses, scanning system detectors and image display CRT).

In this work, SEM is applied in the morphological characterization of the minerals prior to and following the sorption of Zn^{2+} and Pb^{2+} ions.

1.5.2.5. Energy Dispersive X- Ray Spectroscopy (EDS):

EDS is a technique that can be applied in determination of elemental composition of surfaces. The technique makes use of X- rays emitted by elements within the surface that are initially excited by bombarding electrons. X rays are generated by the incident probe within a volume similar to, but rather larger than, that for the backscattered electrons. Peaks at energies characteristic of the elements within that volume can be identified and the concentrations of the elements can be calculated. Thus the composition of the sample, and of the individual grains in a polycrystalline sample can be determined for comparison with surface analytical data.

The dimension of the interaction volume depends on the mean atomic number and the density of the material, and on the beam energy and the emitted X ray energy. The sampling depth in EDS is approximately 1 μm. Diameters range from 0.03 μm to several μm. Thus conventional EDS spectrometry will not reveal compositional changes due to surface segregation. It is possible, however, by analysing a point at several different beam energies, to determine the thicknesses and composition of this surface layers. X ray maps of surfaces, with spatial resolutions of 0.1-1.0 μm are often valuable in revealing compositional variation across a sample, especially if scanning Auger microscopy is not available. [Connor et al. 2003, p.98]

EDS was used in this study to perform spot analysis of the elemental composition at different points on the solid surface, and to examine the distribution of structural and sorbed ions on the surfaces of the minerals via mapping analysis.

CHAPTER 2

EXPERIMENTAL

2.1. Preparation of Samples

The natural sample of kaolinite and clinoptilolite applied in this work originated, respectively, from natural resources in Sındırgı and Manisa regions located in the western part of Anatolia. The samples were dry-sieved and the particle size of kaolinite used in this study was 75-300 μm, while that of clinoptilolite was >38 μm. The particle size of calcite ($CaCO_3$; PRC Panreac 141212) used through out this was 48-600μm, and the particle size of magnesite ($MgCO_3$; Fluka Chemika 63032) used through out this was 53-300μm. The experiments were performed using 50-ml polyethylene tubes. To each tube, 0.50 g. of the solid mixture were added, followed by the addition of 50.0 ml of aqueuos $Zn(NO_3)_2.6H_2O$ and $Pb(NO_3)_2$ solutions prepared at different concentrations, and run under experimental conditions as described in the following sections.

2.1.1. Kinetic Experiments

Batch method was used through all the experiments. 50 ml samples of 1, 100, 1000 mg/L of $Pb(NO_3)_2$ and $Zn(NO_3)_2$.$6(H_2O)$ solutions were mixed with 0.5 g. samples of kaolinite and clinoptilolite and contacted for 10 minutes, 30 minutes, 2 hours, 8 hours, 24 hours and 48 hours in a lateral shaker. Initial and final pH of the solution medium was measured. At the end of the mixing period the solid phase was separated from the solution by filtrated and dried. All the experiments were performed under 25 ^{o}C temperature and atmospheric pressure.

2.1.2. Experiments on Mixtures

50 ml samples of 1, 100, 500, 3000, 10000 mg/L of $Pb(NO_3)_2$ and $Zn(NO_3)_2.6(H_2O)$ solutions were added to mixtures of kaolinite or clinoptilolite with calcite or magnesite at the compositions of 5%, 10%, 25%, 60%. The same experiments were also performed for pure kaolinite, clinoptilolite, calcite, and magnesite. The experiments were conducted in two sets for the concentration of 10000 mg/L, one of them with no pH control and the second with the initial pH raised to a value of 10.0 units using a 0.1 M solution of NaOH. The solid phase was separated from solution by filtration and dried at the end of the mixing period. The experiments were carried out under 25 ^oC temperature and atmospheric pressure.

The initial pH (at the start of mixing) and final pH (at the end of mixing) values of all the mixtures are given in Appendix D. In fresh water media, up to neutral pH conditions, the chemical forms of zinc and lead predominantly present will be Pb^{2+} and Zn^{2+} ions. As the pH increases beyond ~7, the hydroxy- ions, $ZnOH^+$ and $PbOH^+$, start to compete with the above ions (Stumm et al., 1996, p. 296). The speciation curves of Zn^{2+} and Pb^{2+} in aqueous media are provided in Figure D3-1, Figure D3-3. The fraction of hydroxy species of both ions is expected to decrease as the initial concentration is increased. In order to elucidate the effect of pH on the morphology of the evolving Zn- and Pb-carbonate species, separate sets of the experiments with initial concentrations of 10000 mg/L were performed at initial pH of 10. The pH was modified using a 0.1 M NaOH solution.

2.2. Analysis of Aqueous Solutions

2.2.1. AAS:

Flame AAS analysis was performed using a Thermo Elemental SOLAAR M6 Series Atomic Absorption Spectrometer with air-acetylene flame. Pb and Zn hollow cathode lamps (λ(Pb)=217 nm, λ(Zn)=213.9 nm) were applied as sources. Standarts of 0.1, 0.5, 1, 5, 10, 20 mg/L of Pb and Zn were prepared from 1000 mg/L stock solutions.

The aqueous solutions of Zn and Pb ions were analyzed after making the necessary dilution whenever required.

2.3. Analysis of Solid Phases

2.3.1. FTIR:

FTIR technique was applied to collect the spectra of the solid samples using a Nicolet Magma 550 type instrument. The samples were introduced as pellets prepared from powders mixed with KBr and the spectra were recorded in the range 400-4000 cm^{-1}. KBr powder pellets were used as a background. A total of 32 scans were recorded with a resolution of 4 cm^{-1} for each spectrum. Omnic 1.3 software was used to process the results.

2.3.2. XRPD:

The XRPD analysis was performed using a Philips X' Pert Pro diffractometer located at the Center of Material Research at İzmir Institute of Technology. The samples were first ground , mounted on holders then introduced for analysis. The source consisted of Cu Kα radiation (λ=1.54 Å). Each sample was scanned with a step size of 0.020 in the 2 theta range of 2-60. The features in the patterns of different powders were idendified by a search- match procedure that was excuted using the software X' Pert Graphic & Identify.

2.3.3. SEM/EDS:

The SEM/EDS characterization was carried out using a Philips XL- 30S FEG type instrument located at the Center of Material Research at İzmir Institute of Technology. Prior to analysis, the solid samples were sprinkled onto adhesive aluminum

/carbon tapes supported on metallic disks. Images of the sample surfaces were then recorded at different magnifications. Elemental analysis was performed at different points randomly selected on the solid surface and the average of the results was reported. EDS mapping was conducted at magnification of x500 and a voltage of 18 kV under vacuum conditions of 3.5×10^{-5} mbar.

CHAPTER 3

RESULTS AND DISCUSSION

3.1. Characterization of the Minerals

3.1.1. Natural Kaolinite: XRPD, SEM/EDS, and FTIR Characterization

The mineralogical purity of natural kaolinite was tested using XRPD. The results showed that the natural kaolinite samples were composed of kaolinite in addition to quartz as an impurity (Fig. 3.1). In the figure, kaolinite is characterized by the marked 001 and 002 features and the presence of quartz in the sample is evident from the well known 101 and 100 peaks.

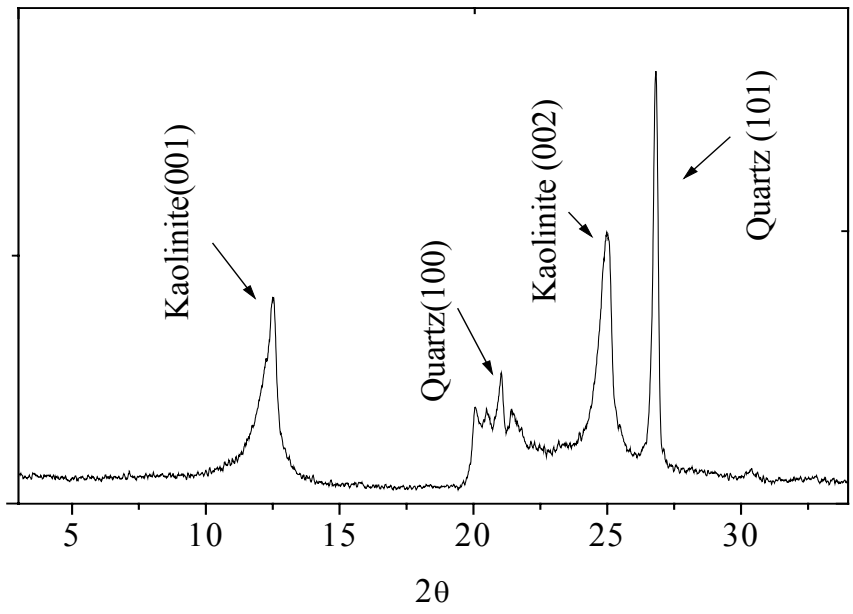

Figure 3.1. XRPD-mineralogical analysis of kaolinite.

SEM was used to reveal the morphology and particle size of kaolinite crystals. SEM microimages indicated that kaolinite has a well-defined crystal structure revealed by its hexagonal plates with edge sizes ranging from 300-500 nm. A typical SEM graph is given in Figure 3.2.

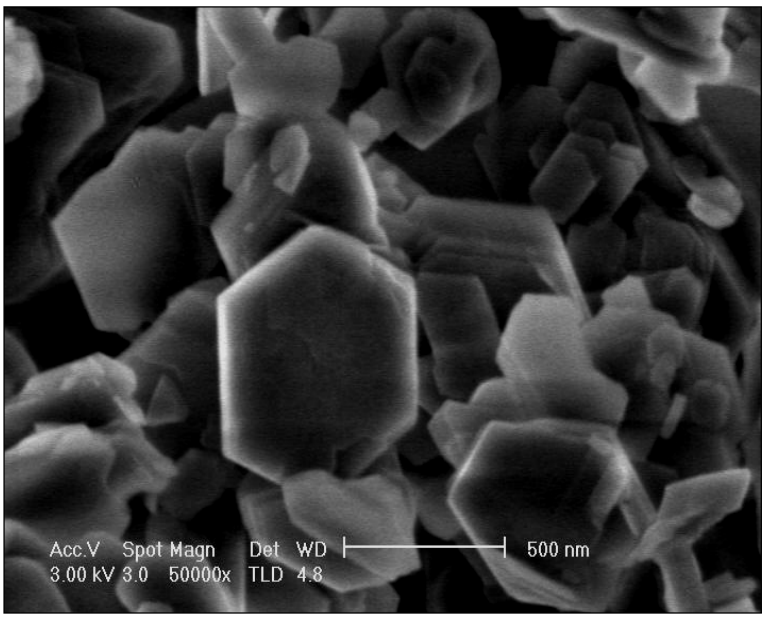

Figure 3.2. A typical SEM image of kaolinite applied in our studies.

The elemental composition of kaolinite surface was determined using EDS. In this analysis, 3 different random points on the surface were selected, and the results were reported as an arithmetic average. A summary of the EDS results of kaolinite are given in Table 3.1. The results revealed that the elemental content of kaolinite was O, Si, Al in addition to minor quantities of Na, K, Mg, and Ca probably stemming from a non-kaolinitic impurity that is below the detection limit of XRPD. The amount of Si is seen to exceed that of Al by about 20 %. Taking into account that in pure kaolinite, on molar basis, the quantity of Al and Si is equal, it can be concluded that the extra amount of Si is primarly originating from the quartz impurity in the natural clay, which seems to consequently account for about one fifth of the molar quantity of the clay. The fact that quartz fraction gave a more intense signal in the XRPD diagram of natural kaolinite (Fig. 3.1.), is due to the higher “impact factor” of the usually better crystalline quartz phase. Another factor that frequently leads to the decrease in kaolinite signal compared

to quartz, is the smaller particle size of the former, thus increasing the internal scattering of kaolinite particles and as a result decreasing the reflected signal.

Table 3.1. Elemental content of kaolinite as obtained by EDS

EDS Analysis	% Atomic
O	66.84±0.80
Na	0.47±0.04
Mg	0.34±0.05
K	0.14±0.12
Al	14.09±1.95
Si	17.61±0.66
Ca	0.50±0.71

The FTIR spectrum of kaolinite is given in Figure 3.3. Kaolins can be readily distinguished from other clays by differences in position and relative intensities of their OH stretching bands. The OH stretchings occurring around the 3700-3620 cm^{-1} doublet are characteristic for kaolin clays. The feature near 3700 cm^{-1} lies well separated from those of most other mineral bands. The OH deformation bands near 938-916 cm^{-1} are also typical for the kaolin group minerals and arise from vibrations of the inner and inner surface OH groups within the clay matrix. Other features appearing in the spectrum belong to a variety of Al-O and Si-O stretching and bending vibrations. [Wilson 1994, p.52-55]. A detailed assignment of all the bands arising in the kaolinite spectrum is given in Table 3.2.

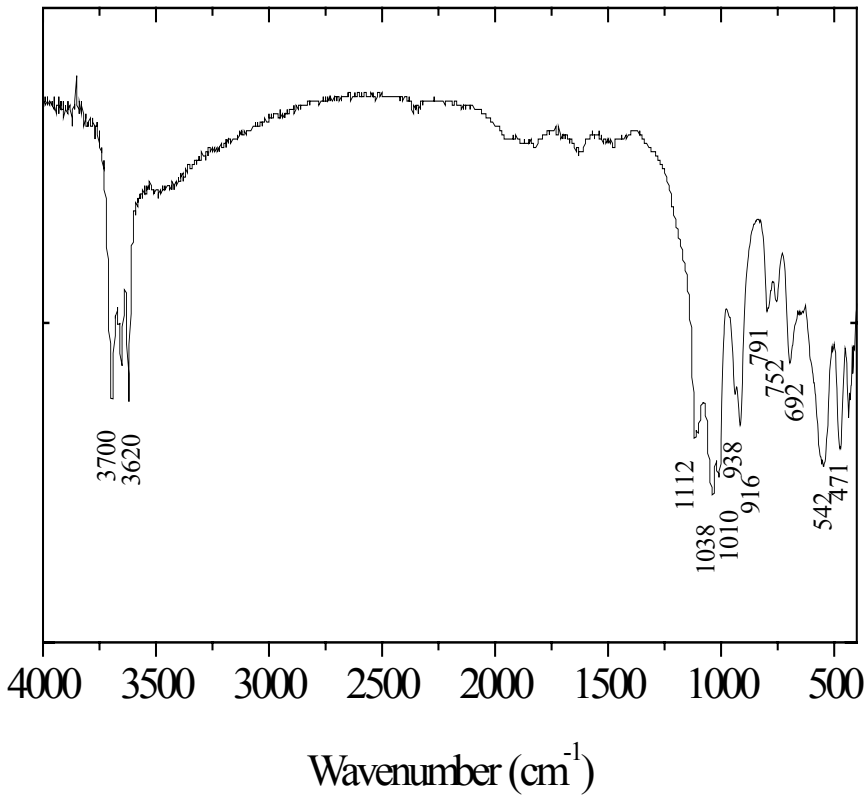

Figure 3.3. FTIR spectra of natural kaolinite used in our studies

Table 3.2. Assignments of the bands appearing in the FTIR spectrum of natural kaolinite.

Band Position (cm^{-1})	**Vibration Assignment**
3700	Inner surface –OH stretching vibration
3620	Inner –OH stretching vibration
1112, 1038, 1010	Si-O bending vibration
938, 918	Al-OH bending vibration
792, 754	Si-O-Al compound vibrations
692	Si-O stretching vibration
540	Si-O-Al compound vibrations
471, 433	Si-O vibrations

3.1.2. Natural Clinoptilolite: XRPD, SEM/EDS, and FTIR Characterization

The natural clinoptilolite was characterized using XRPD. The results indicated that clinoptilolite appeared to be almost pure. Its peaks are sharp as seen in Figure 3.4, the thing indicative of a good crystallinity of the mineral.

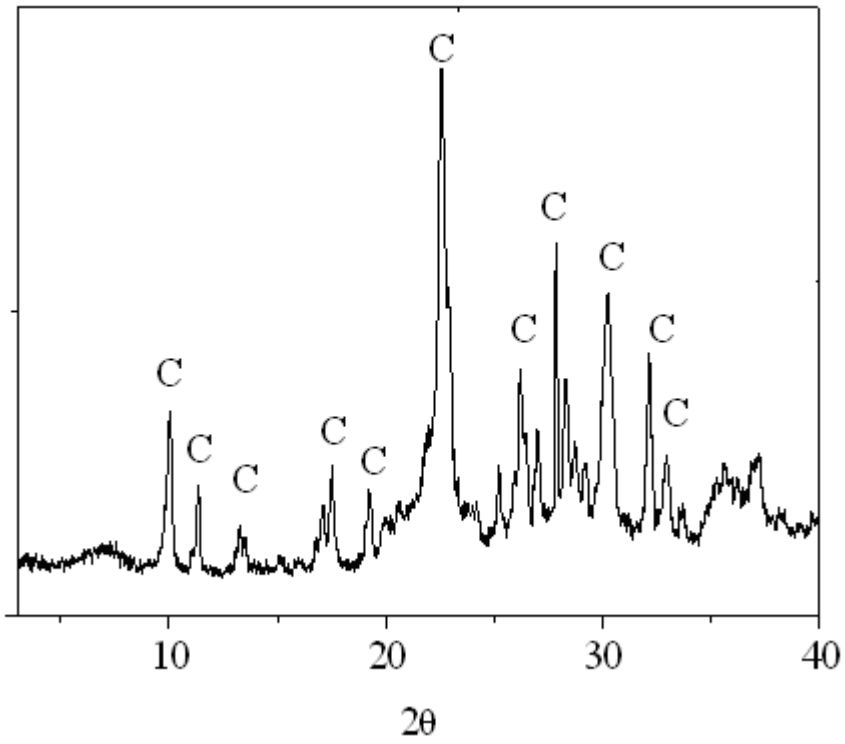

Figure 3.4. XRPD-pattern of clinoptilolite used in our research, C:Clinoptilolite

The shape and size of clinoptilolite crystals was elucidated using SEM imaging. The SEM microimages indicated that clinoptilolite seems to be composed of crystals with well-defined shape, and a particle size that amount to several micrometers. A typical SEM image is given in Fig. 3.5.

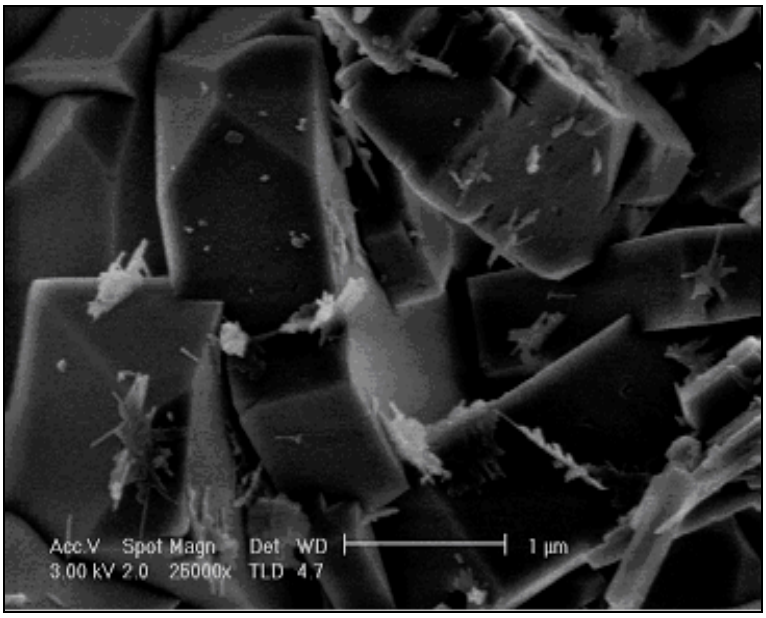

Figure 3.5. A typical SEM image of clinoptilolite

The average elemental composition of clinoptilolite was found using EDS performed with 3 different random points. The arithmetic average of these points is given in Table 3.3. As the Table shows, the major elements of clinoptilolite were O, Si, Al in addition to small amounts of Na, K, Mg, and Ca. If the ratio of Si/Al in the analyzed mineral is compared to that in a pure clinoptilolite which has the formula [(Na, K, Ca)$_6$Al$_6$Si$_{30}$O$_{72}$. 24H$_2$O], it can be seen that a value of 4.5 is obtained. This is slightly below the ideal value of 5.0 (calculated using the above formula). This might be stimming from impurities that could not be detected using XRPD, the detection limit of which is around 5-10 %. Another reason for such a difference might be caused by the difference in bulk and surface composition, as EDS is capable of detecting the upper 1-2 µm of the surface. The element Si is partially replaced by Al in zeolites, the thing believed to be responsible for the development of a negative charge on the zeolitic structure, and lead to a local modification in the Si/Al ratio.

Table 3.3. Elemental composition of clinoptilolite as obtained by EDS

EDS analysis	%Atomic
O	61.94±0.7
Na	0.56±0.12
Mg	0.86±0.13
K	1.61±0.12
Al	5.30±0.02
Si	23.73±0.89
Ca	1.05±0.11
N	5.02±0.306

The FTIR spectrum of clinoptilolite is given in Figure 3.6. The fact that zeolites are significantly hydrated is illustrated by the discrete water absorption bands in the 3500 and 1640 cm^{-1} region. These bands, which were centered at 3450 and 1633, refer to water molecules associated with Na and Ca in the channels and cages in the of the zeolite structure. [Wilson 1994, p.45]. As can be seen from the figure, other bands appear near 1204, 1057, 799 and 471 cm^{-1}. The 1111 cm^{-1} band arises from asymmetric stretching vibration modes of internal T-O bonds in TO_4 tetrahedra (T=Si and Al). The 799 and 471 cm^{-1} bands are assigned to the stretching vibration modes of O-T-O groups and the bending vibration modes of T-O bonds, respectively. [Tanaka et al 2002, p.719]

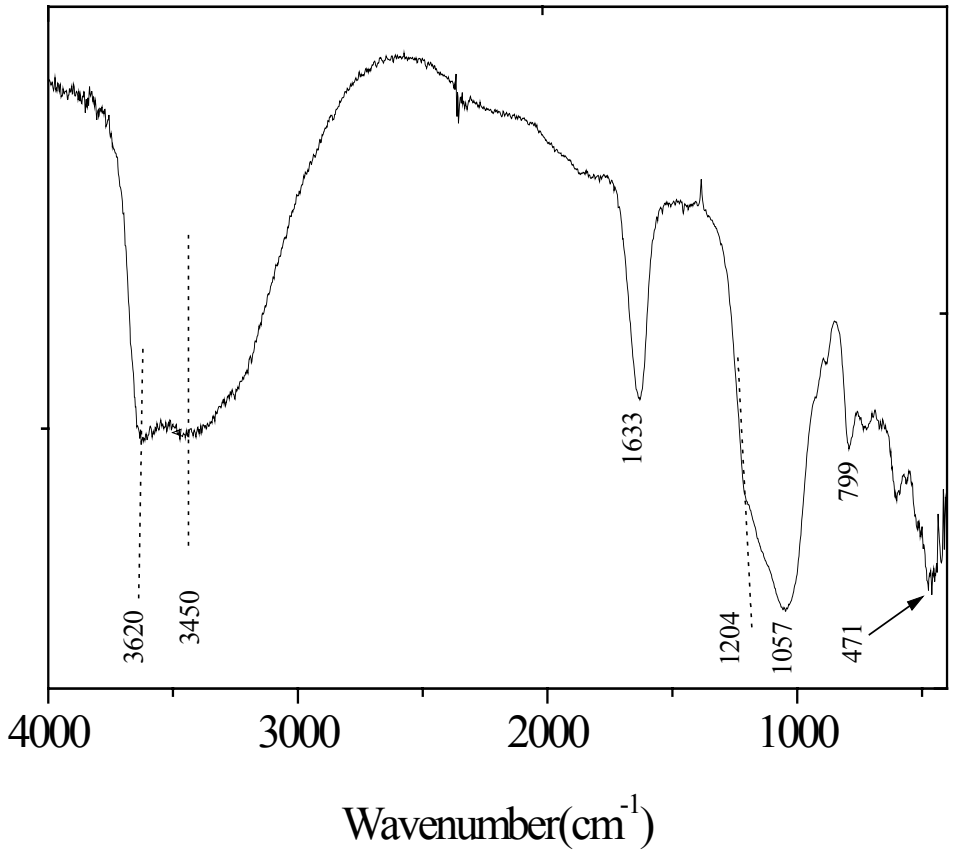

Figure 3.6. FTIR spectrum of clinoptilolite used in this work.

3.1.3. $CaCO_3$: XRPD, SEM/EDS, and FTIR Characterization

$CaCO_3$ is a mineral known to be present in three polymorphs; calcite, aragonite, and vaterite. Among these, calcite is the thermodynamically stable polymorph and vaterite is the least stable. The XRPD analysis showed that the $CaCO_3$ fractions applied in our research were completely composed of calcite polymorph. The calcite features occur mainly at d_{104}=3.069 Å, d_{110}=2.488 Å, d_{202}=2.092 Å , d_{108}=1.949 Å, d_{116}=1.892 Å as shown in Figure 3.7.

The calcite samples were also characterized using SEM. The pictures obtained at various locations on the surface showed that the mineral is composed of aggregates of various sizes as given in Figure 3.8, with no specific regular morphological structure.

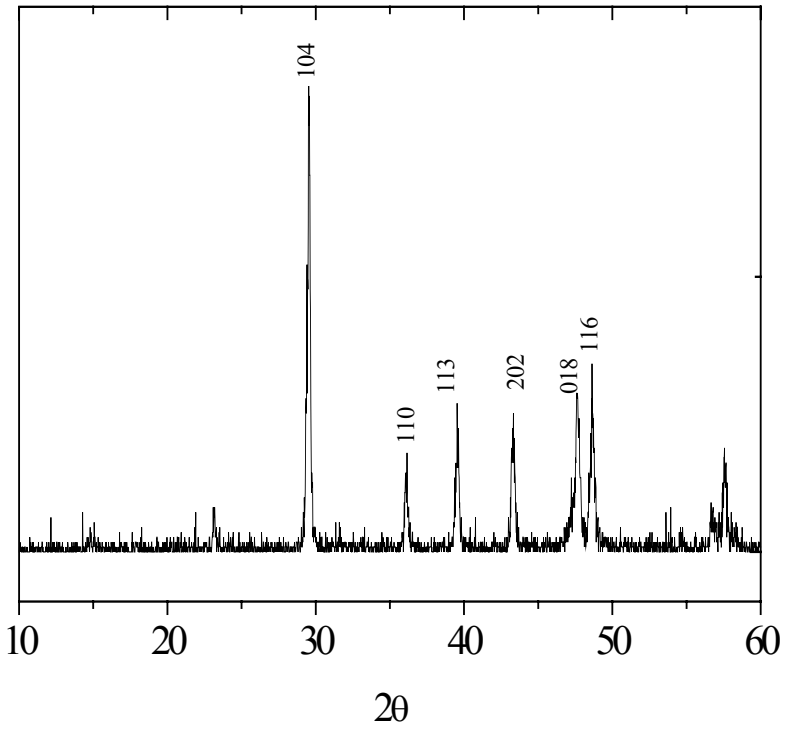

Figure 3.7. XRPD diagram of calcite applied in this study

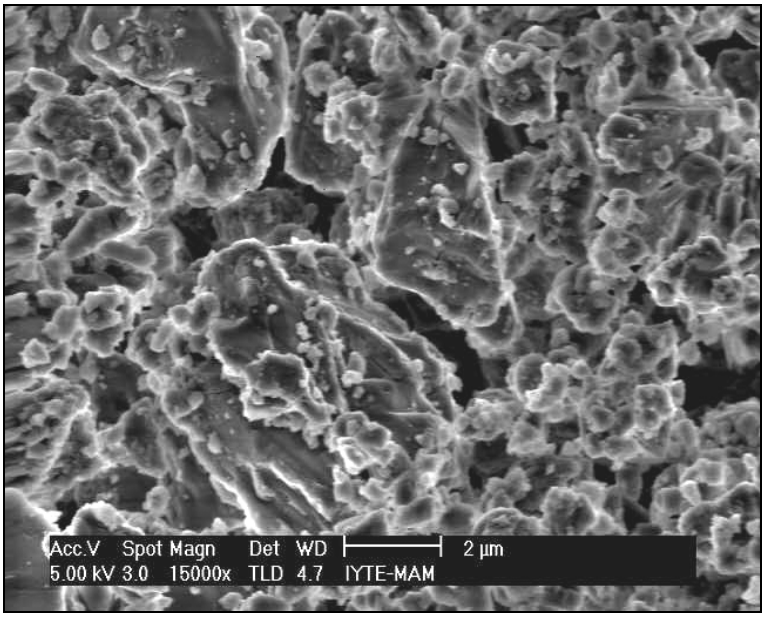

Figure 3.8. A typical SEM image of calcite used in this study.

The EDS results showed that the mineral consists of C, O, and Ca with atomic percentages of 36.9± 6.9, 47.3±3.2, 15.8 ±3.7. No other elements were detected, the thing that illustrates the high purity of the mineral.

The FTIR spectrum of calcite is shown in Figure 3.9. The bands appearing near 1428, 878, and 714 cm^{-1} are diagnostic for calcite (Wilson 1995, p. 52-55). The vibrational spectra of carbonate minerals contains modes arising from the symmetric stretching mode (ν1), out-of-plane bending (ν2), the asymmetric stretching (ν3), the in-plane-bending (ν4), in addition to the two combination modes (ν1+ν3) and (ν1+ν4) (Böttcher et al. 1997, p.1379-1385). Based on this, the bands at 712, 878, 1437, 1789, and 2509 cm^{-1} in the FTIR spectrum of pure calcite were assigned to the vibrational modes ν4, ν2, ν3, ν1+ν3, and ν1+ν4, respectively. The band corresponding to the vibrational mode ν1 was not observed. In calcite, the carbonate ion has a D_{3h} point group (Reig et al. 2002, p.811), for which the symmetric stretching mode (ν1) is IR inactive. According to the theory of vibrational spectroscopy, in gaseous phase, the carbonate ion possesses a trigonal planar shape with a point group of D_{3h}. This molecule possesses, as was previously stated, four first order internal modes; ν1, ν2, ν3, and ν4 with the last two modes being doubly degenerate adding up to a total of six normal modes as predicted by the 3N-6 rule that applies for nonlinear polyatomic molecules. Due to symmetry considerations, the selection rules predict that the ν1 mode is IR inactive. Because of the intermolecular interactions, the symmetry of carbonate ion might be lowered in a crystalline state and the selection rules might consequently be affected, the thing leading to activating initially inactive bands and splitting the degenerate vibrations. When considering molecular vibrations in crystalline states, rather than the isolated gaseous states, the concept of site symmetry is used to predict the plausible changes in the vibrational modes. The site symmetry concept refers to the local symmetry around the center of gravity of a molecule in a unit cell. This approach explains why, for example, calcite and aragonite have different vibrational spectra in spite of the fact that they have the same chemical composition as both of the minerals are polymorphs of $CaCO_3$. It can be theoretically shown that the D_{3h} symmetry of carbonate ion is lowered to D_3 in the case of calcite and C_s in the case of aragonite the thing that leaves the carbonate vibrational modes unchanged in the case of calcite but activates the ν1 mode and causes the ν3 and ν4 modes to split in the case of aragonite (Nakamoto 1986, p.86-87). Experimental observations are in agreement with these

predictions, the thing also in line with our FTIR characterization of calcite samples applied in this work.

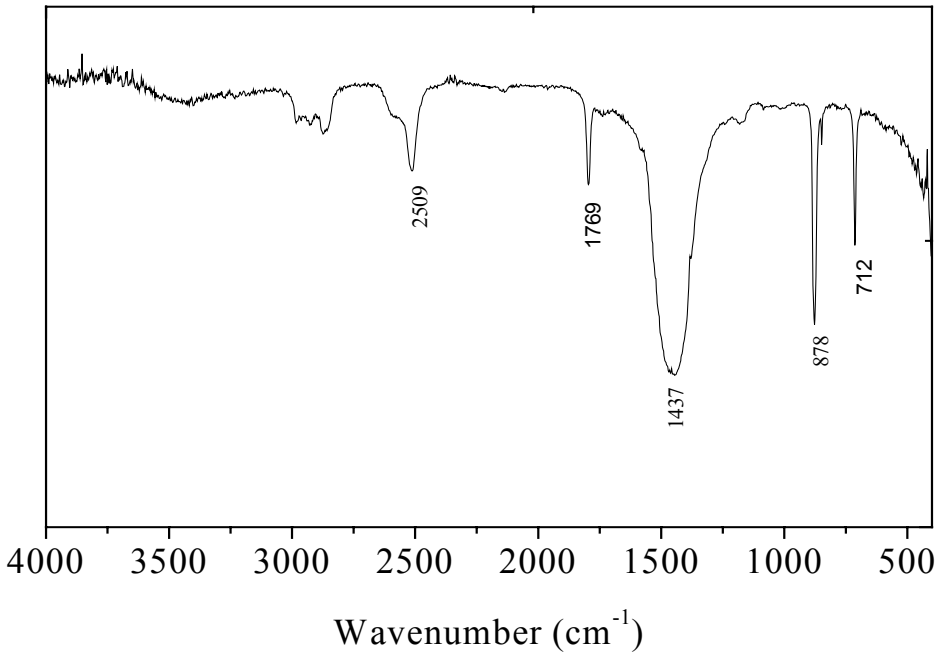

Figure 3.9. FTIR spectrum of calcite used in our research

3.1.4. $MgCO_3$: XRPD, SEM/EDS, and FTIR Characterization

$MgCO_3$ was tested using XRPD. Characterization of this mineral validated its purity as given in Figure 3.10. The major peaks of magnesite occurs at d_{104}= 2.742 Å, d_{006}=2.503 Å,d_{113}=2.102 Å,d_{202}=1.939 Å as shown in Figure 3.10.

Moreover, the SEM microimages indicated that $MgCO_3$ was composed mostly of aggregates with sizes generally below 1 μm. A typical image is given in Figure 3.11.

The elementel content of magnesite was determined using EDS. The analysis showed that the mineral is composed of Mg, C, and O with percentage composition of 17.6±0.74, 21.2±1.48, 61.2±0.94, respectively. Again, the results correspond to arithmetic averages of 3 data points obtained from randomly selected locations on the surface of magnesite.

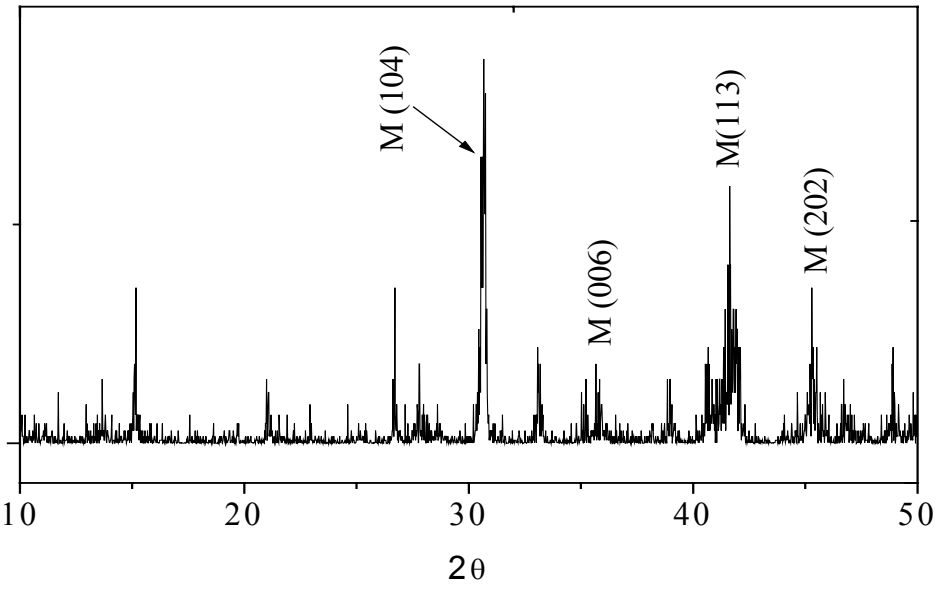

Figure 3.10. XRPD of magnesite used in our research, M:magnesite

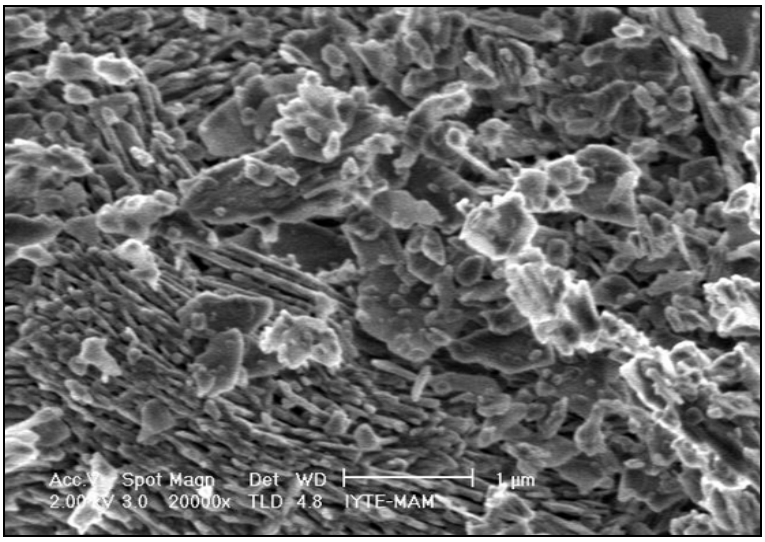

Figure 3.11. A typical SEM image of magnesite used in this study.

As previously discussed, the FTIR spectra of carbonate minerals contains modes arising from out-of-plane bending (ν2), the asymmetric stretching (ν3), the in-plane-bending (ν4), and the combination modes (ν1+ν3) and (ν1+ν4). The symmetric stretching mode (ν1) is usually very weak and hardly detected and its presence is referred to a disorder in the symmetry of carbonate group. The FTIR bands of magnesite

are demonstrated in Figure 3.12. The doublet at 1490, 1419 cm^{-1} correspond to asymmetric stretching vibrations of carbonate. The reason for the split of this peak into a doublet is unclear. The band at 1117 cm^{-1} correspond to symmetric stretching of carbonate, and those at 886, 795 cm^{-1} are assigned to inplane and out-of-plane bending vibrations of carbonate ion.

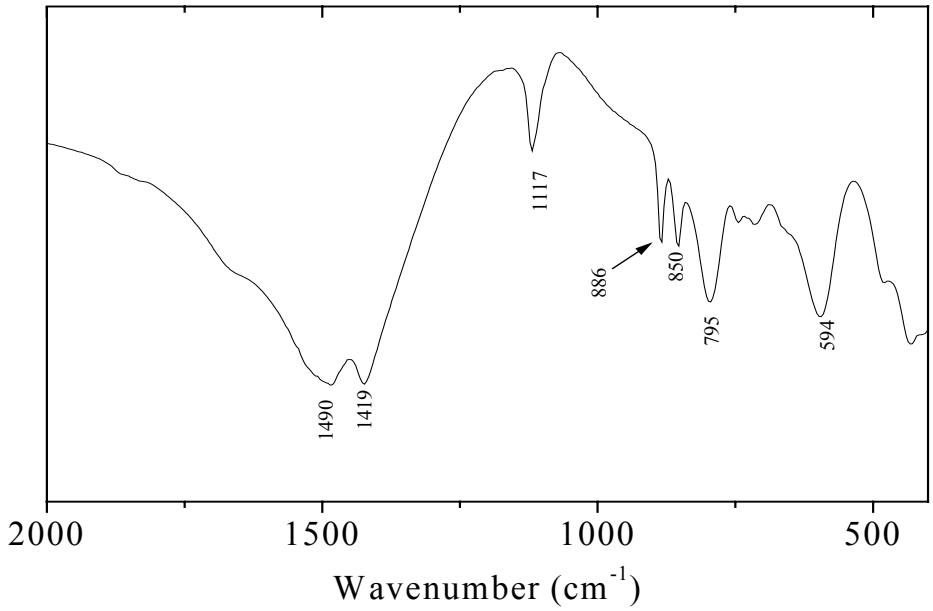

Figure 3.12. FTIR spectrum of magnesite used in this study.

3.2. Sorption Studies on Natural Kaolinite and Natural Clinoptilolite

3.2.1. Sorption of Zn^{2+} and Pb^{2+} on Natural Kaolinite

3.2.1.1. Effect of Time

The effect of time on sorption was examined by mixing aliquots of 1, 100, 1000 mg/L of $Pb(NO_3)_2$ and $Zn(NO_3)_2$ $.6H_2O$ solutions with kaolinite samples for 10 minutes, 30 minutes, 2 hours, 8 hours, 24 hours and 48 hours. The results are given in Figure 3.13 and Figure 3.14. It is clear that equilibrium was achieved at the initial

concentrations of 1 and 100 mg/L faster than at the higher concentration of 1000 mg/L due to the increasing competition between the sorbate ions as concentration is increased. In general, equilibrium is observed to be attained within the first 24 hours of mixing for both ions.

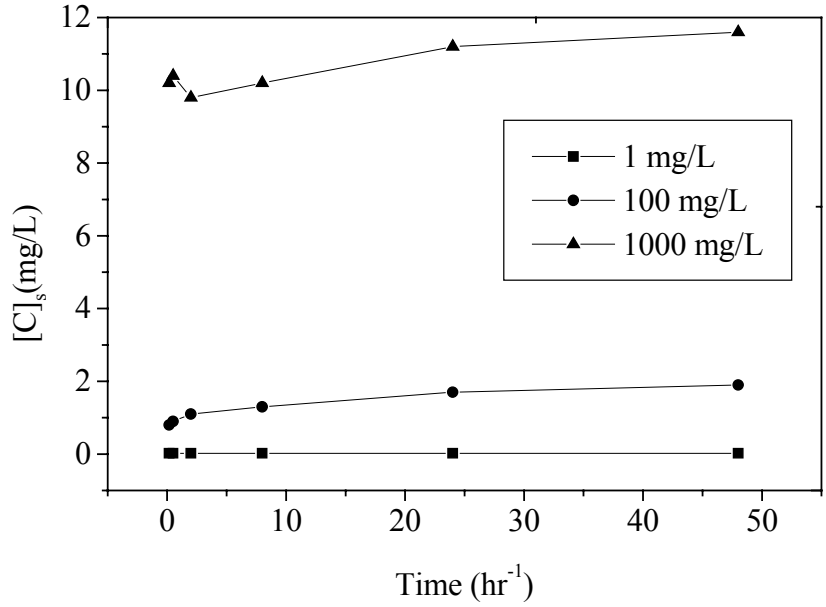

Figure 3.13. The effect of time of mixing on the sorption of Zn ions on kaolinite.

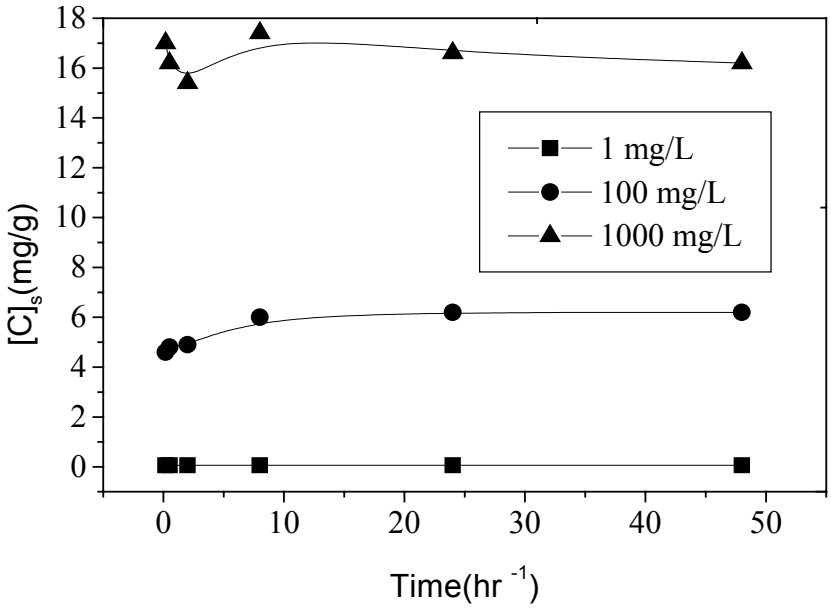

Figure 3.14. The effect of time of mixing on the sorption of Pb ions on kaolinite.

3.2.1.2. Effect of Concentration

The effect of concentration on the uptake of aqueous Zn^{2+} and Pb^{2+} ions by kaolinite was investigated at the initial concentration of 1, 100, 500, 3000, and 10000 mg/L of $Pb(NO_3)_2$ and $Zn(NO_3)_2$ .6(H_2O) solutions, while keeping the mixing time fixed at 48 hours. The experimental data were then fitted to Langmuir and Freundlich isotherm models, and the latter was found to describe the data more adequetly as shown in the next section. Moreover, the data was used to calculate percentage sorption using the equation:

$$PS = ([C]_o - [C]_l)/ [C]_o \times 100 \qquad 3.1$$

where;

PS : percentage sorption

$[C]_o$ and $[C]_l$: initial and equilibrium concentration of Zn^{2+} or Pb^{2+} in solution (mg/L).

The calculated values for both ions are given in Table 3.4. For the initial concentrations of 1 and 100 mg/L, the results indicate almost a 100% removal of both ions by kaolinite. The percentage sorption decreased with further increase in the initial concentrations. Up to the initial concentration of 500 mg/L, Pb^{2+} sorption seems to be favoured more, however, beyond this concentration Zn^{2+} uptake starts to exceed that of Pb^{2+}.

Table 3.4. The values of percentage sorption of Zn^{2+} and Pb^{2+} on individual kaolinite

	% Sorption on Kaolinite	
Initial Conc (mg/L)	Zn^{2+}	Pb^{2+}
1	>99.9	>99.9
100	86.4	98.4
500	36.4	45.4
3000	31.8	28.3
10000	9.5	5.2

3.2.1.3. Freundlich Isotherms of Loaded Kaolinite

The linear form of Freundlich isotherm is defined as follows.

$$\log[C]_s = \log k + n\log[C]_l \qquad 3.2$$

Where;

$[C]_s$: equilibrium concentration of the sorbate on the solid (mg/g),

$[C]_l$: equilibrium concentration of the sorbate in solution (mg/L),

n, k: Freundlich constants

This isotherm model was widely used in describing sorption of various ions on kaolinite (Erten et al 1994, p.375, Jain et al. 1996, p.161). It is best adequate for describing sorption taking place on heterogeneous surfaces which are composed of different types of sites, each possessing varying capacity and sorption affinity. This model does not predict any overall sorption capacity of the solid, thus allowing for multilayer sorption. Freundlich plots are given in Figure 3.15 and Figure 3.16, and the values of n and k are provided in Table 3.5. The non-linearity of the sorption indicated by the relatively low n values implies that, within the studied concentration range, the energy barrier against sorption becomes increasingly effective as loading is increased, the thing resulting in a significant decrease in the fixation ability of kaolinite. The k values are indicative of the larger sorption affinity of kaolinite towards lead compared to its affinity towards zinc.

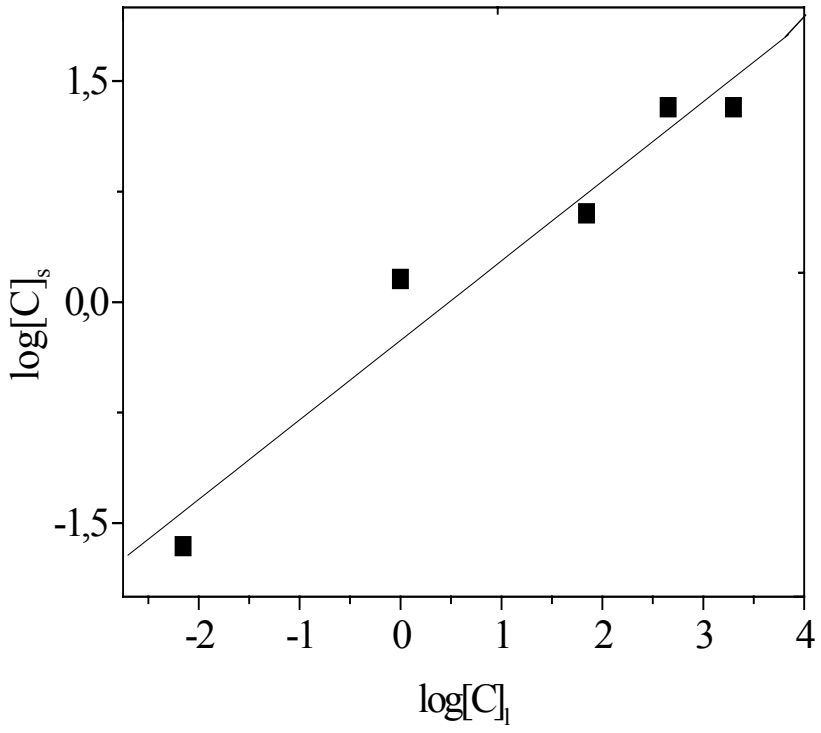

Figure 3.15. Freundlich plots corresponding to sorption of Zn ions on kaolinite.

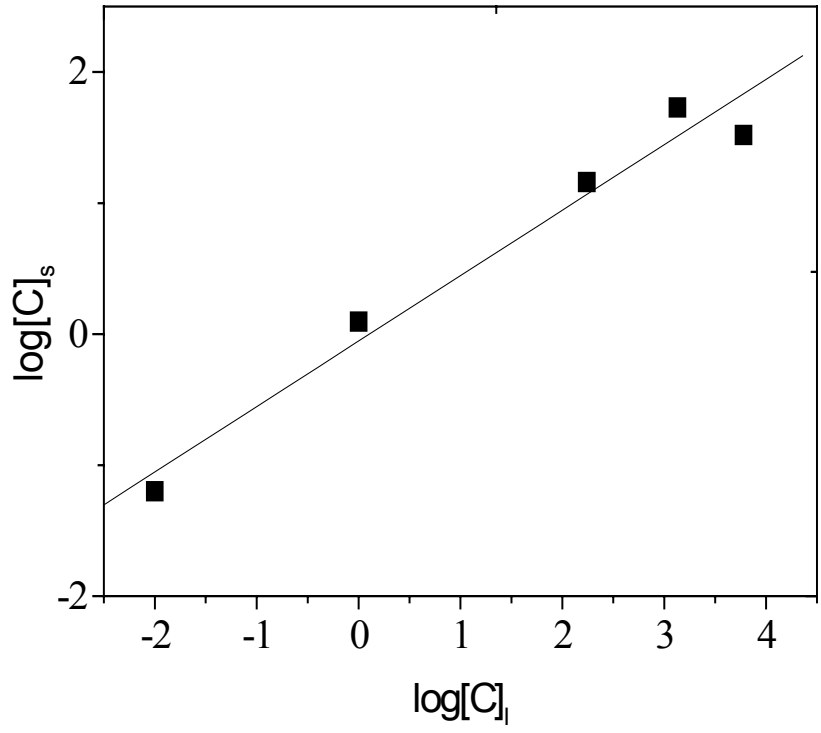

Figure 3.16. Freundlich plots corresponding to sorption of Pb on kaolinite.

Table 3.5. Freundlich parameters, n and k, obtained from the fits of the sorption data of Zn^{2+} and Pb^{2+} ion on kaolinite. R corresponds to the linear correlation coefficient of the plots.

	n	k	R
Zn-kaolinite	0.54	0.55	0.9741
Pb-kaolinite	0.5	0.88	0.9829

3.2.1.4. XRPD and SEM/EDS Analysis of Sorbed Kaolinite

The XRPD characterization of Zn-, and Pb-reacted kaolinite samples showed that no significant changes in the peak positions or peak intensities of the basic 001, 002 reflections of kaolinite have taken place. The fact that the initial reflections were retained upon loading, indicates the structural stability of the clay upon sorption, within the conditions of our studies.

In line with the XRPD predictions, SEM micro-images demonstrated no distinguishable change in the kaolinite surface for the mineral samples, prior to or following loading. The stability of kaolinite matrix is expected, as this clay is well known to be non-expanding, i.e its interlayer structure is tightly bound by hydrogen bonds, the thing that makes the interlayer sites inaccessible to 'foreign' ions. In literature, it was reported that sorption on kaolinite takes place mainly on the sorption sites located at the edges and external surface of the clay (Miranda-Trevino et al 2003, p.134). Moreover, kaolinite is known to be among the most stable clay minerals against attack by external factors. (Coles et al 2002, p.39-40).

The distribution of Zn^{2+} and Pb^{2+} ions on kaolinite surface was analyzed using EDS mapping. The maps of these ions together with those of Al and Si are given in Figure 3.17. This figure revealed that while Pb is distributed equally on the kaolinite surface, Zn appears to show some sort of selectivity to Si richer regions on the kaolinite. This might be indicative that Zn^{2+} is fixed by sorption sites different than those of Pb^{2+}. However, to validate this, a more precise and closer examination of the structural environment of both cations on kaolinite is required, the thing that necessitates the

application of advanced techniques like ‘ Extended X-ray Absorption Fine Structure’, EXAFS.

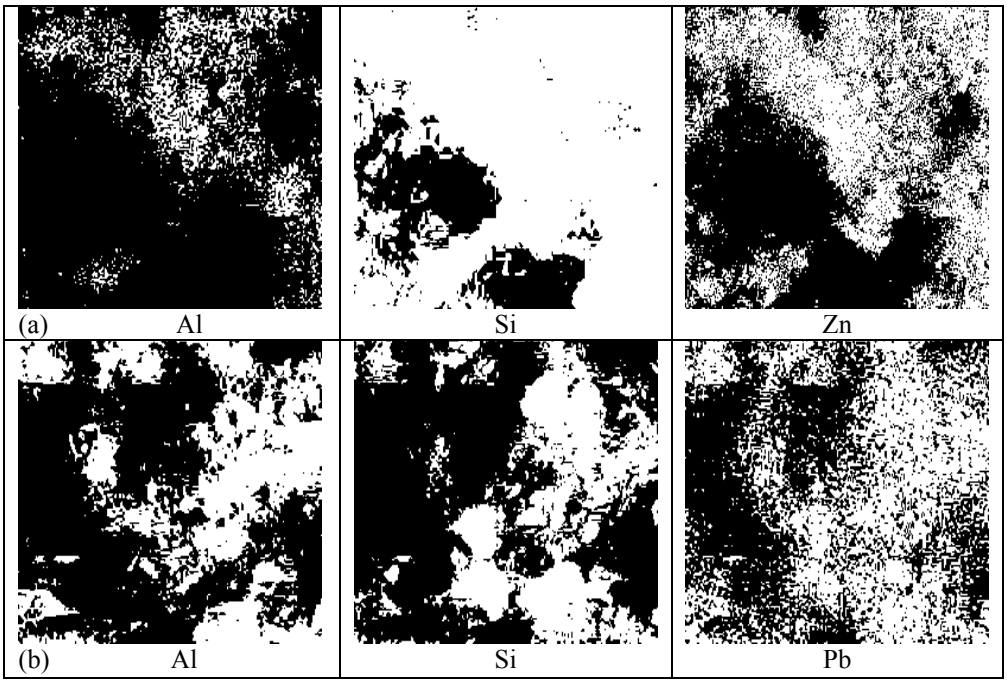

Figure 3.17. EDS maps showing the distribution of (a) Al, Si, and Zn (b) Al, Si, and Pb on kaolinite surface.

3.2.2. Sorption of Zn^{2+} and Pb^{2+} on Natural Clinoptilolite

3.2.2.1. Effect of Time

To study the effect of time, aliquots of 50 ml $Pb(NO_3)_2$ and $Zn(NO_3)_2$ .6(H_2O) solutions for 1, 100, 1000 mg/L were mixed with 0.5 g of clinoptilolite samples. The mixtures were then stirred for 10 minutes, 30 minutes, 2 hours, 8 hours, 24 hours and 48 hours, contact periods. The obtained results are drawn in Figure 3.18 and Figure 3.19. As was observed in kaolinite case, for the initial concentration of 1 and 100 mg/L, the results indicated faster attainment of equilibrium than at the higher concentration of 1000 mg/L. Compared with the results of sorption of both cations on kaolinite (section 3.2.1), the results for sorption on clinoptilolite indicated that in particular at higher

loading, the sorption kinetics are faster for kaolinite than for clinoptilolite. This could be referred to the presence of pore film diffusion which acts as an extra barrier against sorption on the internal channels in the matrix of clinoptilolite. In general, Pb and Zn ions sorption on clinoptilolite can reach equilibrium within the 48 hours of mixing. Based on this, further experiments were carried out at this mixing period.

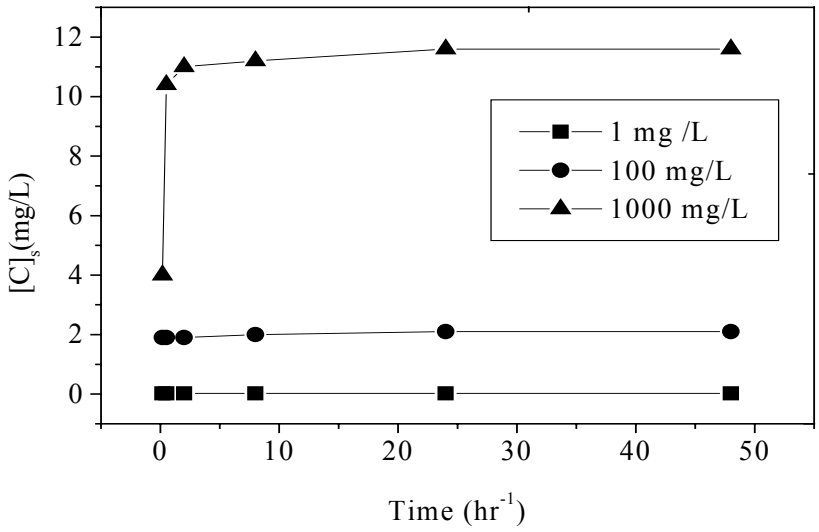

Figure 3.18. The effect of time of mixing on the sorption of Zn ions on clinoptilolite

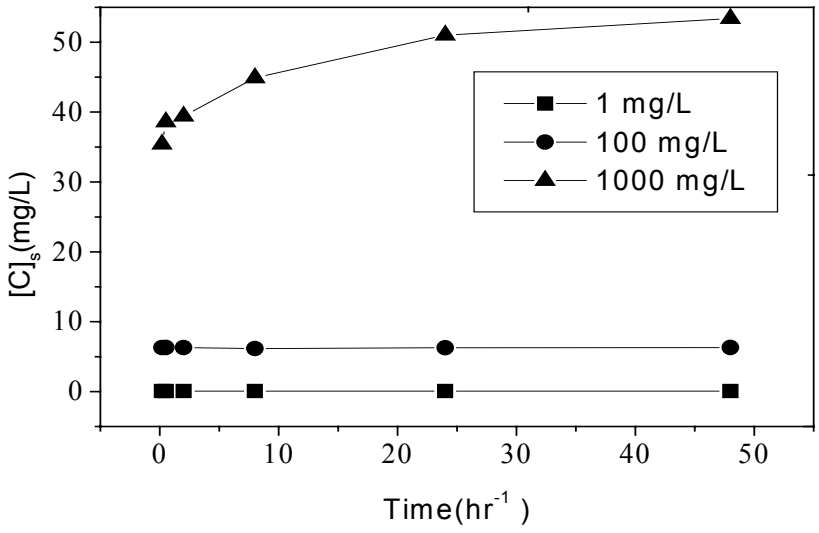

Figure 3.19. The effect of time of mixing on the sorption of Pb ions on Clinoptilolite.

3.2.2.2. Effect of Concentration

In these experiments, sorption was carried out at neutral pH for the initial concentration of $Pb(NO_3)_2$ and $Zn(NO_3)_2.6H_2O$ of 1, 100, 500, 3000, and 10000 mg/L. The obtained data for both cations, were used to calculate percentage sorption, as given in Table 3.6. The results showed that almost a 100% removal of both ions by clinoptilolite for the initial concentrations of 1 and 100 mg/L. The percentage sorption decreased with further increase in the initial concentrations. The overall results indicate that clinoptilolite is more effective in sorption of both ion compared to kaolinite. Comparing the amounts of fixed ions, it can be seen that Pb^{2+} uptake is more favoured, but, at higher values of loading, Zn^{2+} sorption becomes competitive with that of Pb^{2+}. A similar trend was observed for sorption on kaolinite (section 3.2.1.2). The sorption data of both ions on clinoptilolite was then examined using Freundlich isotherm model.

Table 3.6. The values of percentage sorption of Zn^{2+} and Pb^{2+}on individual clinoptilolite

	% Sorption on Clinoptilolite	
Initial Conc (mg/L)	Zn^{2+}	Pb^{2+}
1	>99.9	>99.9
100	95.5	>99.9
500	31.8	98.7
3000	22.9	52.3
10000	15.0	14.4

3.2.2.3. Freundlich Isotherms of Loaded Clinoptilolite

As was seen in kaolinite case, Freundlich isotherms described adequately the sorption data on clinoptilolite. Freundlich isotherms shown in Figure 3.20 and Figure 3.21 reveal the non-linearity of sorption, leading to a decrease in percentage sorptionh with further increase in the initial concentration. The values of Freundlich constants, n, k are provided in Table 3.17. As previously stated, the small n values means that the

energy barrier against sorption becomes increasingly effective. Based on the values of k, it is seen that the affinity of the mineral towards Pb^{2+} sorption is higher than its sorption affinity towards Zn^2.

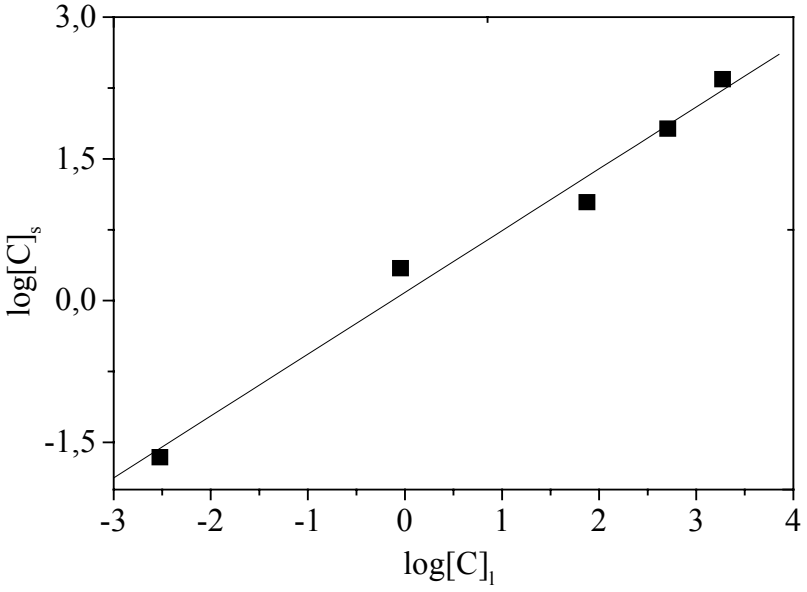

Figure 3.20. Freundlich plots corresponding to sorption of Zn^{2+} ions on clinoptilolite.

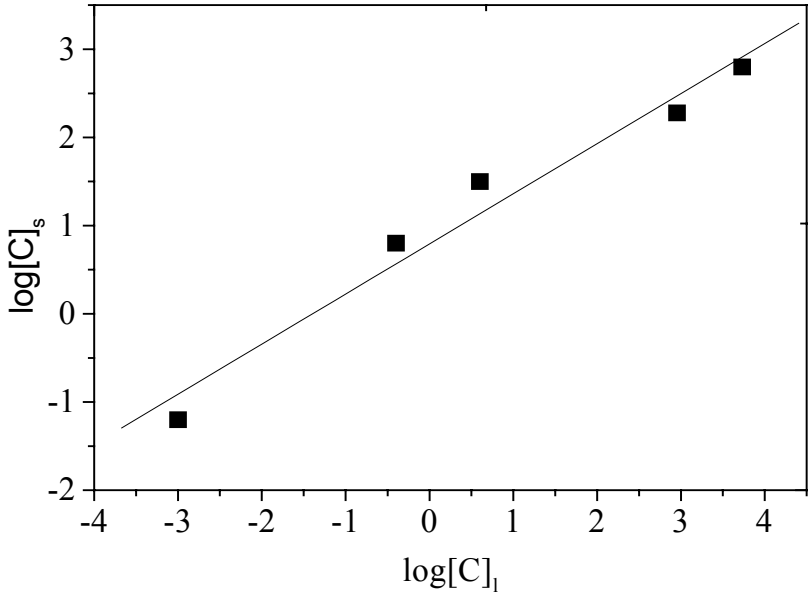

Figure 3.21. Freundlich plots corresponding to sorption of Pb^{2+} ions on clinoptilolite.

Table 3.7. Freundlich parameters, n and k, obtained from the fits of the sorption data of Zn^{2+} and Pb^{2+} ion on clinoptilolite. R corresponds to the linear correlation coefficient of the plots.

	n	k	R
Zn-clinoptilolite	0.6538	1.22	0.99075
Pb-clinoptilolite	0.56796	6.204	0.98337

3.2.2.4. XRPD and SEM \EDS Analysis of Sorbed Clinoptilolite

The XRPD characterization of Zn-, and Pb-reacted clinoptilolite samples showed that no significant changes in the position and/or intensity of the basic reflections of clinoptilolite were associated with sorption, indicating that the structure of clinoptilolite was not affected by sorption. This was also supported by the SEM analysis which showed no distinguishable change in the morphology or size of clinoptilolite crystals. In addition, Zn- and Pb- loaded clinoptilolite samples were characterized using EDS mapping analysis as given by Figure 3.22. The results indicate an even distribution of Zn and Pb signals on the surface of clinoptilolite. No selectivity of either cation towards aluminol or silanol sites is observed, as was observed in kaolinite case.

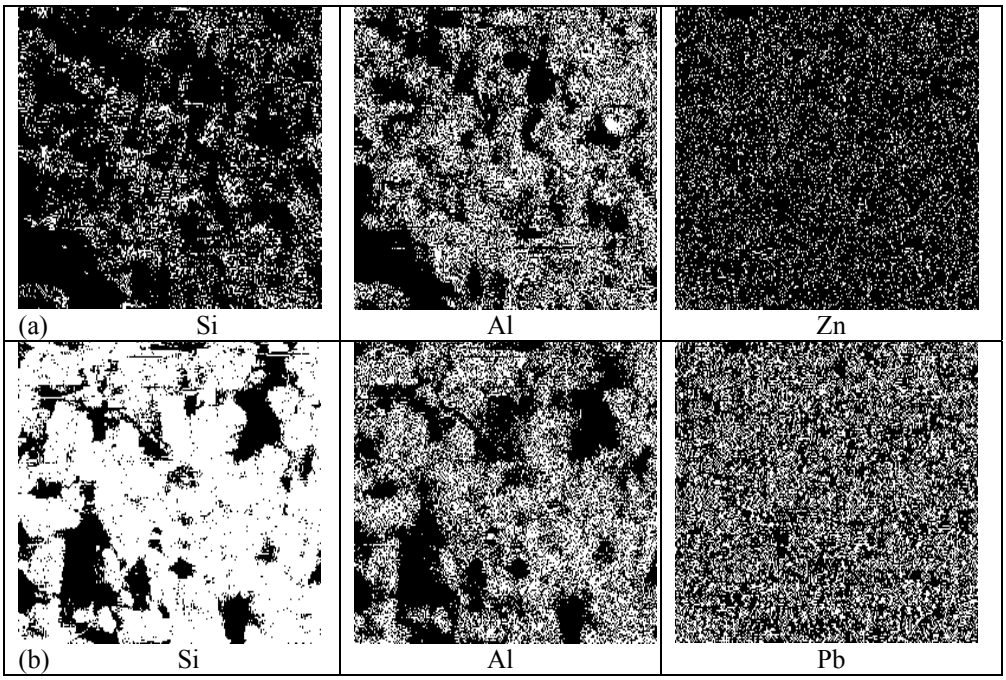

Figure 3.22. EDS maps showing the distribution of (a) Si, Al, and Zn, (b) Si, Al, and Pb on clinoptilolite surface.

3.3. Sorption Studies on Mineral Mixtures

These experiments were performed at initial concentrations of 1, 100, 500, 3000, and 10000 mg/L for solution of $Pb(NO_3)_2$ and $Zn(NO_3)_2.6H_2O$. The mineral mixtures were prepared by mixing appropriate amounts of calcite or magnesite with kaolinite and clinoptilolite to yield percentage (by mass) of 5, 10, 25, and 60 of carbonate. The findings of these experiments are discussed in the sub-sections, following.

3.3.1. Sorption of Zn^{2+} and Pb^{2+} on Calcite – Kaolinite Mixtures

The percentage sorption of Zn^{2+} and Pb^{2+} ions on the calcite-kaolinite mixtures are given in Table 3.8 and 3.9. The tables provide also the percentage sorption of both minerals on individual kaolinite and calcite. The results obtained from these sorption experiments is clearly showing an increase in the amount of scavenged Zn^{2+} and Pb^{2+} ions with the increase in the fraction of calcite in the mixtures.

Table 3.8. The values of percentage sorption of Zn^{2+} on individual kaolinite and calcite minerals, in addition to calcite-kaolinite mixtures.

Initial Conc. (mg/L)	kaolinite	%5 calcite	%10 calcite	%25 calcite	%60 calcite	calcite
1	>99.9	>99.9	>99.9	>99.9	>99.9	>99.9
100	86.4	>99.9	>99.9	>99.9	>99.9	>99.9
500	36.4	60.0	77.3	93.6	97.3	96.4
3000	31.8	48.0	45.5	51.1	79.7	88.6
10000	9.5	10.1	10.9	37.0	42.0	71.6

Table 3.9. The values of percentage sorption of Pb^{2+} on individual kaolinite, and calcite minerals, in addition to calcite-kaolinite mixtures.

Initial Conc. (mg/L)	kaolinite	%5 calcite	%10 calcite	%25 calcite	%60 calcite	calcite
1	>99.9	>99.9	>99.9	>99.9	>99.9	92.4
100	98.4	98.4	>99.9	>99.9	>99.9	99.97
500	45.4	>99.9	>99.9	>99.9	>99.9	99.92
3000	28.3	84.5	97.5	98.1	99.7	99.293
10000	5.2	18.4	29.7	79.6	99.8	99.98

As was discussed previously, kaolinite is able to scavenge Zn^{2+} and Pb^{2+} ions almost totally at concentrations lower than 100 mg/L. But as the initial concentration is increased beyond this value, the efficiency of removal of this mineral decreases largely. The results in Table 3.8 and Table 3.9 demonstrate that the sorption capacity of the solid mixture increases significantly with the increase in calcite fractions in calcite-kaolinite mixtures. The large difference between the sorption capacity of kaolinite and calcite is distinctly observed when pure calcite is used. It can be seen that the percentage sorption

on calcite at the highest studied concentration (10000 mg/L $Zn(NO_3)_2.6H_2O$, $Pb(NO_3)_2$) is almost eight-folds the percentage sorption of Zn^{2+} -pure kaolinite and about twenty fold that of Pb^{2+} on the same mineral. Therefore, within the studied experimental conditions, calcite stands as the prominent sink for zinc and lead among these two minerals. Based on this, it can be concluded that , at neutral and high pH media, calcareous soils is expected to possess outstanding sorption capacities towards both cations, thus regulating the dispersion of these cations in the geosphere. Tables 3.8, and 3.9 show that, the percentage sorption values of Pb^{2+} are higher than that of Zn^{2+} in all calcite containing mixtures.

The variation of the sorbed amounts of Zn^{2+} and Pb^{2+} ions with their equilibrium liquid concentrations on calcite-kaolinite mixtures are given in Fig. 3.23 and Fig. 3.24. The amount of retarded Zn^{2+} and Pb^{2+} appears to approximately approach the linear sorption as the mixtures become richer in calcite.

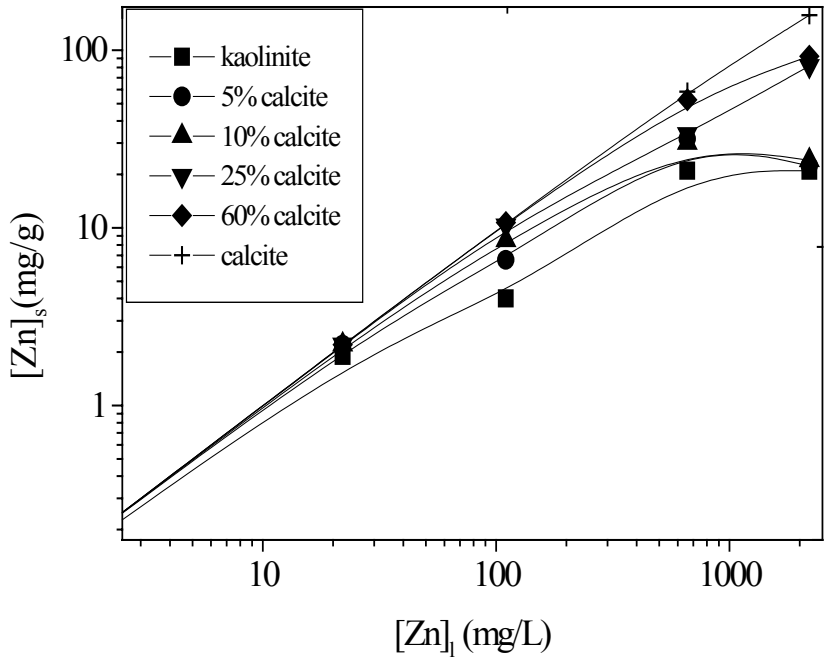

Figure 3.23. Variation of the equilibrium concentration on the solid phase with that in the liquid phase for different Zn^{2+} loading, at various mixture compositions for calcite-kaolinite

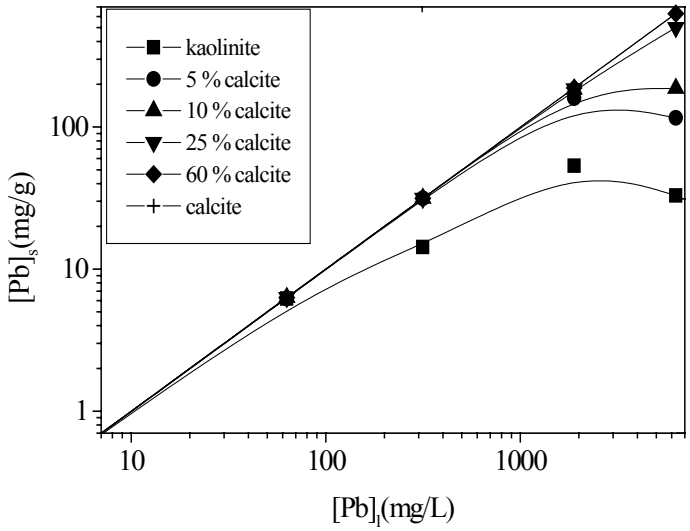

Figure 3.24. Variation of the equilibrium concentration on the solid phase with that in the liquid phase for different Pb^{2+} loadings, at various mixture compositions for calcite-kaolinite.

If the mixtures were behaving ideally, then the total percentage sorption would be predicted using the equation:

$$PS = \frac{m_A}{m_A + m_B}(PS)_A + \frac{m_B}{m_A + m_B}(PS)_B \qquad 3.3$$

where ;

PS: the percentage sorption

m_A and m_B : masses of components A and B in their solid mixture.

The variation of percentage sorption obtained for the initial concentrations of 500, 3000, and 10000 mg/L of is plotted as a function of calcite fraction in the mixtures as given by Fig. 3.25 and Figure 3.26. The same figure provides also the values predicted by equation 3.3 (dotted lines). The figure suggests an exponential increase in the percentage sorption of both ions as the fraction of calcite in the mixtures is increased. It can be noticed that as the initial concentration of $Zn(NO_3)_2$.$6H_2O$ and $Pb(NO_3)_2$ solution is increased to 10000 mg/L, the experimental values of percentage sorption become closer to those predicted by equation 3.3. This is merely stemming from the fact that at higher loading, kaolinite becomes inefficient in sorption which is in turn predominantly controlled by calcite, so that equation 3.3 can be approximated to:

$$PS \cong \frac{m_{Caclcite}}{m_{Calcite} + m_{Kaolinite}} (PS)_{Calcite} \qquad 3.4$$

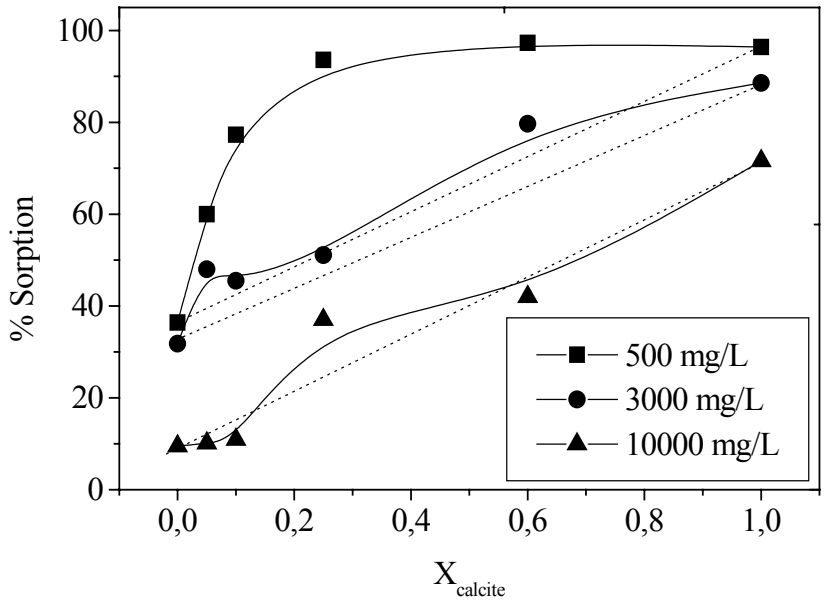

Figure 3.25. The change of percentage sorption with the fraction of calcite at initial loadings of 500, 3000, and 10000 mg/L of $Zn(NO_3)_2 .6H_2O$ on calcite-kaolinite.

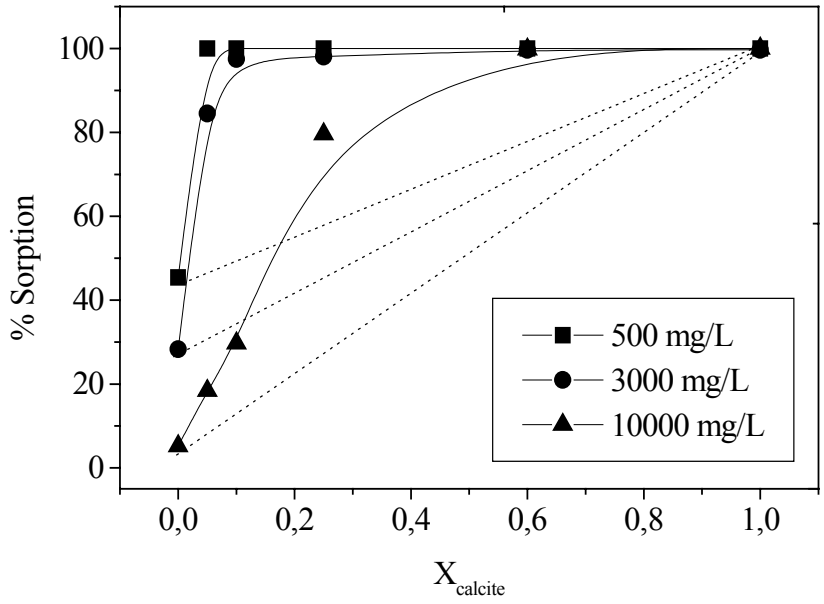

Figure 3.26. The change of percentage sorption with the fraction of calcite at initial loadings of 500, 3000, and 10000 mg/L of $Pb(NO_3)_2$ on calcite-kaolinite.

It is obvious from the above discussion that calcite fractions in the mixtures are responsible for the large retention of both cations. The data indicates also a larger affinity for Pb^{2+} uptake compared to that of Zn^{2+}. The differences between the sorbed amounts of Pb and Zn cations by calcite fractions might be referred to their different types of incorporation mechanisms. It is reported that, at low concentrations, the ionic radii of the divalent cations determines the extent of uptake of these cations by calcite so that ions with smaller radii are more preferably sorbed (Zachara et al, 1991, p.1549). Although the ionic radii criterion proved to be successful in explaining the preferential sorption of various ions on calcite (Zachara et al. 1991, p. 1549, Curti 1999, p.437), it can not be used to explain the higher selectivity of calcite towards Pb^{2+} ions over that of Zn^{2+} as the size of the latter is smaller than that of the former ($r(Pb^{2+})$ = 1.18 Å, $r(Zn^{2+})$ = 0.745 Å). Similar deviations of the ionic radii criteria were observed also for pairs of cations possessing similar ionic radii like and Mg^{2+}, Na^{+} and La^{3+} ions (Curti 1999, p.437). The explanation offered for such anomalies relied on the hypothesis suggesting that ions with lower partition coefficients are trapped within the limited number of interstitial positions in calcite rather than exchanging with Ca^{2+} in lattice positions (Busenberg et al. 1985, p.713).

The larger partition coefficient for Pb^{2+} can be verified from a thermodynamic approach that is based on the Gibbs free energies of formation of carbonate phases and ions in solution (Sverjinsky et al. 1992, p.232). These data can be used to estimate the partition coefficients at the solid/solution interface utilizing the equation (Böttcher 1997, p.661):

$$\log D_{Me,ideal} = (\Delta G^{o}_{f,\,CaCO3(s)} - \Delta G^{o}_{f,\,MeCO3(s)} - \Delta G^{o}_{f,\,Ca^{2+}(aq)} + \Delta G^{o}_{f,Me^{2+}(aq)}) / ((\ln (10))RT) \qquad 3.5$$

Where ΔG^{o}_{f} correspond to the standard Gibbs free energies of formation for the rhombohedral solid carbonates and the aqueous cations, T is the temperature in K, and R is the gas constant. Based on the equation above and the corresponding values of ΔG^{o}_{f} given in Table 3.10, it is possible to calculate log $D_{Me,ideal}$ of Zn^{2+} and Pb^{2+} as 0.053 and 1.8, respectively. This approach is useful in particular at lower metal concentrations where the possibility of incorporation of the sorbed metal ions by the rhombohedral calcite sites is higher. The larger uptake of Pb^{2+} ions compared with Zn^{2+} ions could be

indicative of a larger ability of Pb^{2+} ions in replacing Ca^{2+} ions in the regular matrix sites of calcite, while a large fraction of Zn^{2+} ions apparently trapped in the limited number of structural defects formed in the course of dissolution/recrystallization of calcite.

Table 3.10. The ionic radii of Ca^{2+}, Zn^{2+}, and Pb^{2+} and Gibbs free energies of formation of the aqueous cations in addition to their rhombohedral carbonates. The table provides also the calculated log $D_{Me,\ ideal}$ which shows the theoretical partitioning at the calcite/solution interface.

Cation	**Radius (Å)**	**$\Delta G^{o}_{f,cation}$ (kcal/mol)**	**$\Delta G^{o}_{f,MeCO3}$ (kcal/mol)**	**log $D_{Me,\ ideal}$**
Ca^{2+}	1	-132.12	-270.0	-
Zn^{2+}	0.745	-35.17	-175.1	0.053
Pb^{2+}	1.18	-5.79	-146.0	1.8

The preference of Pb^{2+} uptake by calcite is also supported by the predictions of another model (Wang et al. 2001, p.1530). This model makes use also of linear free energy and correlates metal partition coefficients with metal cation properties. It states that metal partitioning between minerals and aqueous solutions is controlled by three factors; the chemical bonding energies of substituent cation with the host mineral structure, the excessive energies created by the size difference between substituent and host cations, and the difference in chemical potential between substituent and host cations in solution. With all these factors taken into consideration, the partition coefficient of aqueous Zn^{2+} and Pb^{2+} with calcite were given as 0.59 and 2.5 logarithmic units, respectively.

At high loadings, the extent of precipitate overgrowth of a given cation can be related with the K_{sp} of the cation-anion pair forming the precipitate. Theoretically, in a mixture where the reactants are highly dispersed, the extent to which cation species reacts with calcite can be estimated using the individual K_{sp} values (Hay et al., 2003, p.3727):

$$CaCO_3 + Me^{2+} \rightarrow Ca^{2+} + Me^{2+} + CO_3^{2-} \rightarrow MeCO_3 + Ca^{2+}$$

Where Me^{2+} stands for a divalent metal ion. The net solubility product is then:

$$K_{CaCO_3 \rightarrow MeCO_3} = \frac{K_{sp,CaCO_3}}{K_{sp,MeCO_3}} = \frac{[Ca^{2+}]}{[Me^{2+}]} \qquad 3.6$$

Utilizing the K_{sp} values of 4.5×10^{-9}, 7.4×10^{-14}, and 1.4×10^{-11} for $CaCO_3$ (calcite polymorph), $PbCO_3$, and $ZnCO_3$, respectively (Petrucci et al. 1997, p.A26), the net solubility products are calculated to be ~ 61 000 and ~ 321 for cerussite and zincite formation respectively. These results are indicative that while the reaction between Zn^{2+} and CO_3^{2-} would be –to a certain extent- driven towards zincite formation, the reaction of Pb^{2+} with CO_3^{2-} would proceed until almost all calcite is dissolved leading to formation into cerussite. These predictions are supported also by Fajans' coprecipitation rule used for a qualitative prediction of the extent of precipitate formation of radioelements with counter ions (Curti 1999, p.438). According to this law: ' the lower the solubility of the compound formed by the radioelement with the anion of the precipitate, the greater is the amount of the radioelement carried down as cation'. It is obvious that these predictions qualitatively explain the larger removal of Pb^{2+} ions (in the form of cerussite) compared to the removal of Zn^{2+} (via zincite overgrowth) at higher loadings of these ions on calcite.

Although the model predictions outlined above are qualitatively inline with our experimental results which showed that Pb^{2+} retention by calcite is more favored, it must be noted that the above discussion is based solely on a thermodynamic approach, and thus careful comparison between experimental and these theoretical predictions should be done, as such models usually lack a kinetic perspective.

3.3.2. Sorption of Zn^{2+} and Pb^{2+} on Magnesite-Kaolinite Mixtures

In these experiments, calcite was replaced with magnesite. As discussed in section 1.3.3, the structural arrangement of both minerals is similar. However, the solubility products are different with that of calcite being 4.5×10^{-9}, and that of magnesite being 3.5×10^{-8}.

Tables 3.11 and 3.12 give the percentage sorption of Zn^{2+} and Pb^{2+} ions on individual kaolinite and magnesite in addition to the magnesite-kaolinite mixtures. As it was the case in calcite-kaolinite mixtures, the results reveals an increase in the amount of scavenged Zn^{2+} and Pb^{2+} ions with the increase in the fraction of magnesite in the mixtures, demonstrating the role of carbonate minerals in the fixation of this ions.

Table 3.11. The values of percentage sorption of Zn^{2+} on individual kaolinite and magnesite minerals, in addition to magnesite-kaolinite mixtures

Initial Conc. (mg/L)	kaolinite	%5 magnesite	%10 magnesite	%25 magnesite	%60 magnesite	magnesite
1	>99.9	>99.9	>99.9	>99.9	>99.9	>99.9
100	86.4	>99.9	>99.9	>99.9	>99.9	>99.9
500	36.4	63.6	97.3	>99.9	>99.9	>99.9
3000	31.8	53.5	42.1	94.5	99.98	>99.9
10000	9.5	17.5	17.3	25.2	57.23	98.7

Table 3.12. The values of percentage sorption of Pb^{2+} on individual kaolinite, and magnesite minerals, in addition to magnesite-kaolinite mixtures.

Initial Conc. (mg/L)	Kaolinite	%5 magnesite	%10 magnesite	%25 magnesite	%60 magnesite	magnesite
1	>99.9	>99.9	>99.9	>99.9	>99.9	>99.9
100	98.4	>99.9	>99.9	>99.9	>99.9	99.44
500	45.4	>99.9	>99.9	>99.9	>99.9	99.88
3000	28.3	84.4	99.4	99.7	99.9	99.96
10000	5.2	33.3	51.7	82.0	85.2	99.976

The variation of equilibrium concentration on the solid as a function of that in the liquid for both of Zn^{2+}, and Pb^{2+} ions are given in Fig. 3.27 and Fig. 3.28. In this Figure, the sorbed amounts of zinc and lead ions shows nearly a perfect linearity with the increase in magnesite fraction. The effect of increasing the fraction of magnesite becomes clearer, in particular at higher loadings. For the initial concentrations of 500, 3000, and 10000 mg/L of $Zn(NO_3)_2 .6H_2O$ and $Pb(NO_3)_2$, the percentage sorption is plotted versus the amount of magnesite (as shown in Figure 3.29 and Figure 3.30). The figure includes also the data corresponding the sorption of Zn^{2+} and Pb^{2+} ion on pure magnesite. If the mixtures were behaving ideally, the total percentage sorption would be predicted using the equation 3.3. Zn^{2+} and Pb^{2+} ions seems to be almost linearly sorbed at higher magnesite fractions. The shift towards linearity shows an enhancement in the sorption capacity of the solids. The data of the percentage sorption of Zn^{2+} and Pb^{2+} indicate a more preferential sorption of the latter ion. It is reported that magnesite is predicted to possess the largest partition coefficient among all carbonates with a calcite structure, and therefore is a good scavenger of heavy metals (Wang at. al. 2001, pp.1529-1530). According to the predictions presented by that study, the partition coefficient of aqueous Zn^{2+} and Pb^{2+} with magnesite were 1.97 and 4.26 logarithmic units, respectively.

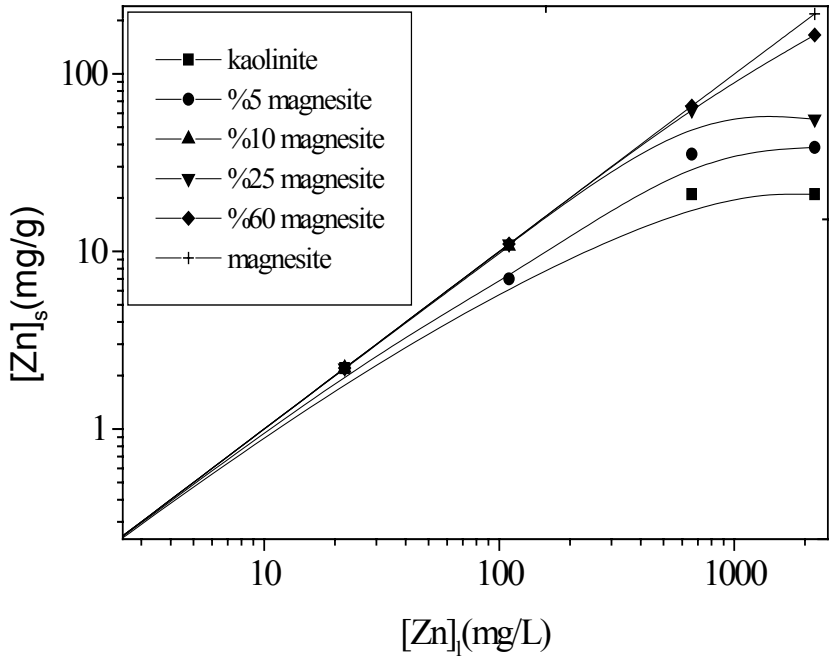

Figure 3.27. Variation of the concentration of sorbed Zn^{2+}(mg/g) ions with the equilibrium liquid concentration (mg/L) on magnesite-kaolinite.

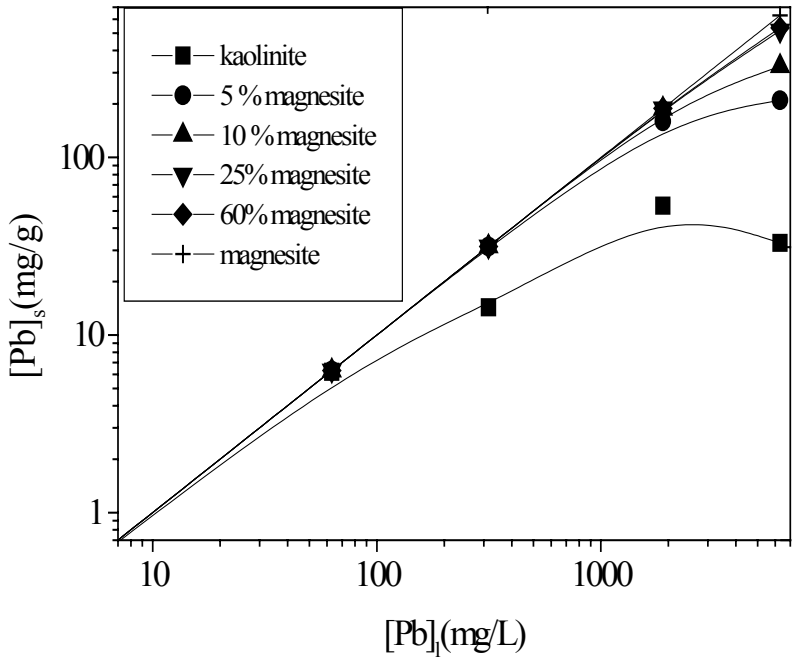

Figure 3.28. Variation of the concentration of sorbed Pb^{2+}(mg/g) ions with the equilibrium liquid concentration (mg/L) on magnesite-kaolinite.

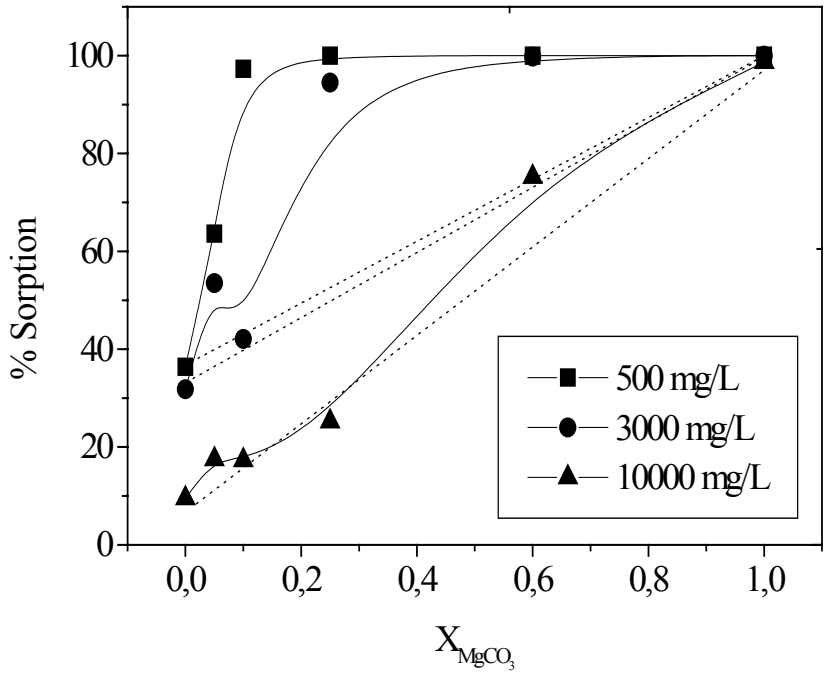

Figure 3.29. Change in the percentage sorption of Zn with the amount of magnesite in the mixtures of magnesite-kaolinite.

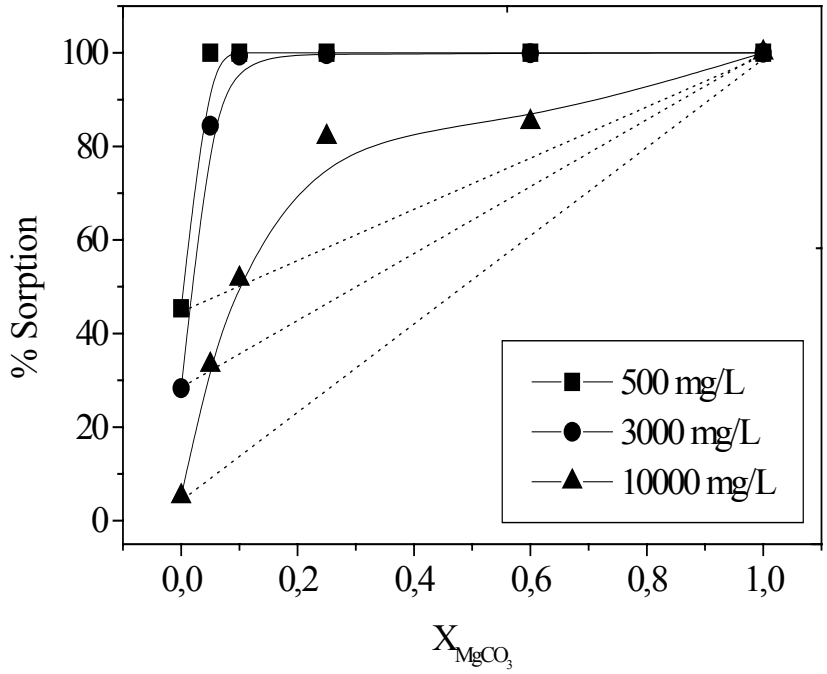

Figure 3.30. Change in the percentage sorption of Pb ions with the amount of magnesite in the mixtures of magnesite-kaolinite .

Comparing the sorption capacity of magnesite to that of calcite in their mixtures with kaolinite, it can be seen that magnesite fractions were slightly more efficient in the fixation of both cations. However, the detailed explanation of this result on a mechanistic basis requires a seperate detailed study.

3.3.3. Sorption of Zn^{2+} and Pb^{2+} on Calcite- Clinoptilolite

In these experiments, the effect of calcite association with clinoptilolite is investigated. The mixtures were prepared by mixing calcite with appropriate amount of clinoptilolite to yield percentage compositions (weight percentages of calcite) of 5, 10, 25, and 60.

As in the case of calcite -kaolinite mixtures, the results showed an increase in the amount of scavenged Zn^{2+} and Pb^{2+} ion with the increase of the fraction of calcite in the mixtures as given Table 3.13 and Table 3.14.

The variation of the sorbed amounts of Zn^{2+} and Pb^{2+} ion with its equilibrium liquid concentrations on calcite -clinoptilolite mixtures are given in Fig.3.31 and Fig. 3.32. The variation of percentage sorption of Zn^{2+} and Pb^{2+} at loadings of 500, 3000, and 10000 mg/L with the fraction of calcite are illustrated by Figure 3.33 and Figure 3.34. The figure suggests an exponential increase in the percentage sorption of both ions as the fraction of calcite in the mixtures is increased, the thing data observed in calcite - kaolinite mixture, demonstrating again the high uptake capacity of calcite fractions.

Table 3.13. The values of percentage sorption of Zn^{2+} on individual clinoptilolite and calcite minerals, in addition to calcite-clinoptilolite mixtures

Initial Conc (mg/L)	Clino	%5 calcite	%10 calcite	%25 calcite	%60 calcite	calcite
1	>99.9	>99.9	>99.9	>99.9	>99.9	>99.9
100	95.5	>99.9	>99.9	>99.9	>99.9	>99.9
500	31.8	72.7	92.7	95.5	98.2	96.4
3000	22.9	4.7	48.6	61.5	86.4	88.6
10000	15.0	16.1	33.6	66.8	67.7	71.6

Table 3.14. The values of percentage sorption of Pb^{2+} on individual clinoptilolite and calcite minerals, in addition to calcite-clinoptilolite mixtures

Initial Conc (mg/L)	Clino	%5 calcite	%10 calcite	%25 calcite	%60 calcite	calcite
1	>99.9	>99.9	>99.9	>99.9	>99.9	>99.9
100	>99.9	>99.9	>99.9	>99.9	>99.9	>99.9
500	98.7	99.7	99.7	>99.9	99.7	>99.9
3000	52.3	84,6	82.1	99.5	99.6	99.7
10000	14.4	27.8	43.7	73.7	>99.9	>99.9

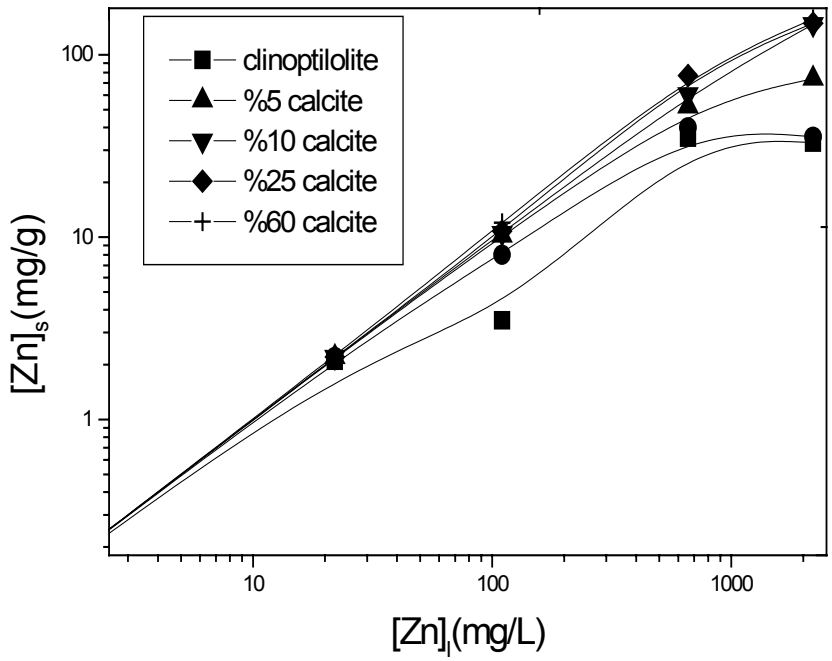

Figure 3.31. Variation of the equilibrium concentration on the solid phase with that in the liquid phase for different Zn^{2+} loadings, and mixture compositions for calcite-clinoptilolite.

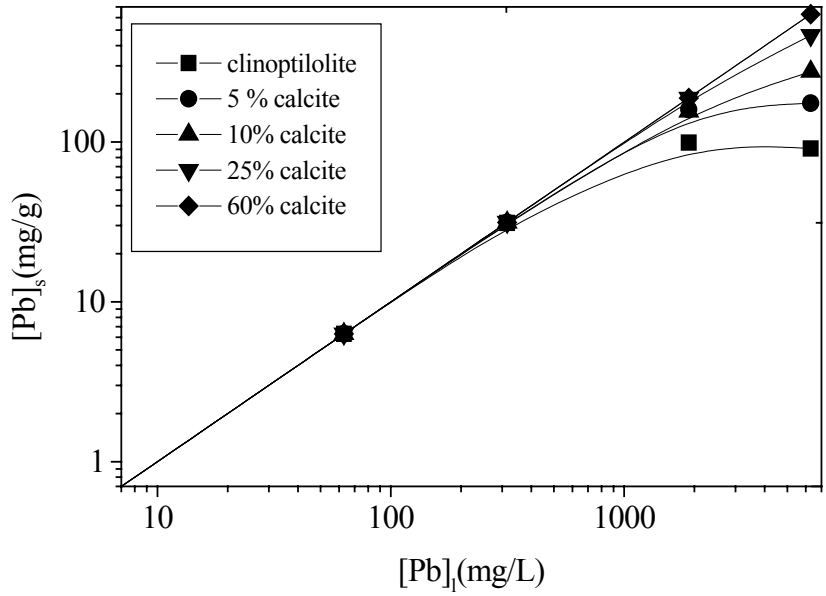

Figure 3.32. Variation of the equilibrium concentration on the solid phase with that in the liquid phase for different Pb^{2+} loadings, and mixture compositions for calcite-clinoptilolite.

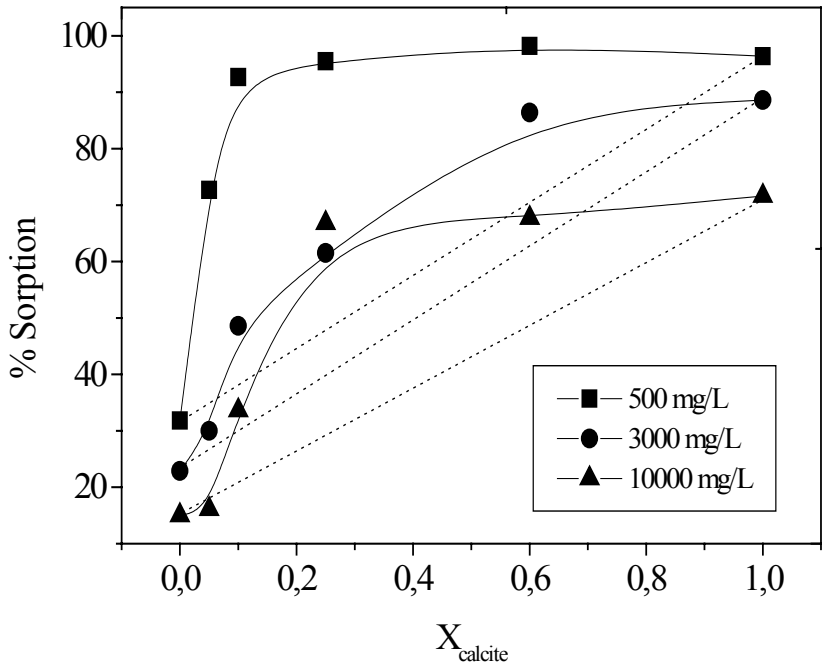

Figure 3.33. The change of percentage sorption with the fraction of calcite at initial loadings of 500, 3000, and 10000 mg/L of $Zn(NO_3)_2.6H_2O$ on calcite-clinoptilolite.

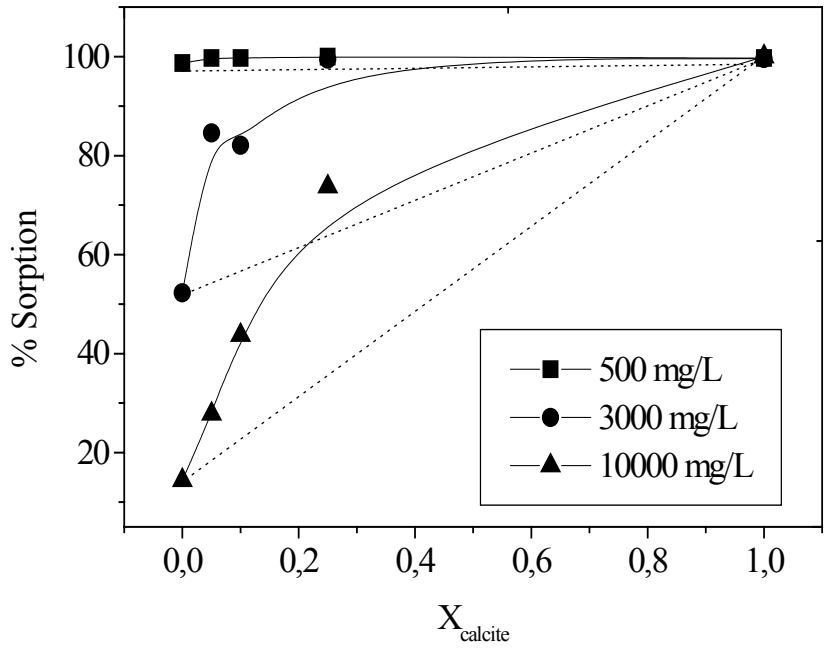

Figure 3.34. The change of percentage sorption with the fraction of calcite at initial loadings of 500, 3000, and 10000 mg/L of $Pb(NO_3)_2$ on calcite-clinoptilolite.

3.3.4. Sorption of Zn^{2+} and Pb^{2+} on Magnesite –Clinoptilolite

In these experiments, calcite was replaced by magnesite to study the effect of the latter on the sorption capacity of clinoptilolite. The results showed that Pb^{2+} and Zn^{2+} ions are increasing with the increase in the fraction of magnesite in the mixtures of clinoptilolite as given Table 3.15 and Table 3.16. Figure 3.35 and Figure 3.36 show the variation of the sorbed amounts of lead and zinc ions with their equilibrium liquid concentration on magnesite - clinoptilolite mixtures. Lead and zinc ions seem to be almost linearly sorbed at higher carbonate fractions. Here, it should be noted that, even at lower magnesite fractions, the extent of curvature of the fits of experimental data is less pronounced compared to the case of magnesite -kaolinite mixtures. This observation is stimming from the higher sorption capacity of clinoptilolite, as compared to that of kaolinite.

In addition, the variations of the percentage sorption with the amount of magnesite in the mixtures at the initial concentrations of 500, 3000, and 10000 mg/L of

$Pb(NO_3)_2$ and $Zn(NO_3)_2.6H_2O$ solutions are given in Figure 3.37 and Figure 3.38. The figure shows that initial concentration of lead and zinc ion is increased, then the experimentel values of percentage sorption becomes closer to its predicted by equation 3.3, suggesting again that sorption becomes controlled by the carbonate phase in the mixtures.

Table 3.15. The values of percentage sorption of Zn^{2+} on individual clinoptilolite and magnesite minerals, in addition to magnesite-clinoptilolite mixtures

Initial Conc (mg/L)	Clino	%5 magnesite	%10 magnesite	%25 magnesite	%60 magnesite	magnesite
1	>99.9	>99.9	>99.9	>99.9	>99.9	>99.9
100	>99.9	>99.9	>99.9	>99.9	>99.9	>99.9
500	31.8	79.1	99.1	>99.9	>99.9	>99.9
3000	22.9	14.7	61.5	77.3	97.9	>99.9
10000	15.0	34.1	46.4	63.2	92.0	98.7

Table 3.16. The values of percentage sorption of Pb^{2+} on individual clinoptilolite and magnesite minerals, in addition to magnesite-clinoptilolite mixtures

Initial Conc (mg/L)	Clino.	%5 magnesite	%10 magnesite	%25 magnesite	%60 magnesite	magnesite
1	>99.9	>99.9	>99.9	>99.9	>99.9	>99.9
100	>99.9	>99.9	>99.9	>99.9	>99.9	>99.9
500	98.7	99.7	99.7	99.7	99.7	>99.9
3000	52.3	86.0	99.5	99.8	99.9	>99.9
10000	14.4	33.5	63.8	92.9	99.9	>99.9

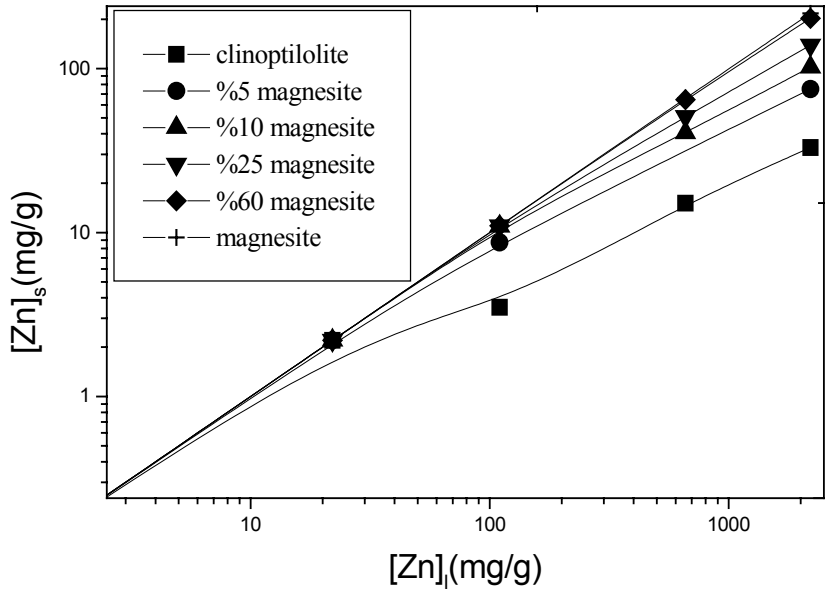

Figure 3.35. Variation of the concentration of sorbed Zn ion (mg/g) with the equilibrium liquid concentration (mg/L) on magnesite-clinoptilolite mixture

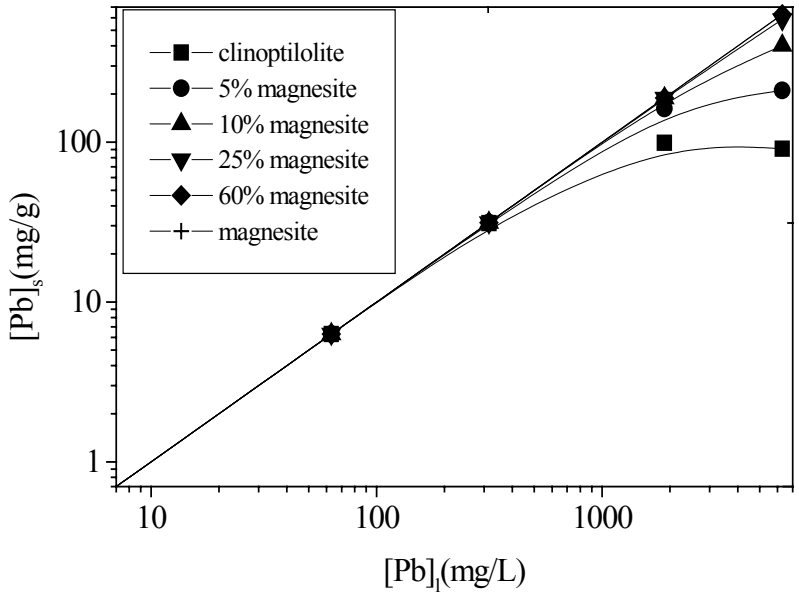

Figure 3.36. Variation of the concentration of sorbed Pb ion (mg/g) with the equilibrium liquid concentration (mg/L) on magnesite-clinoptilolite mixture

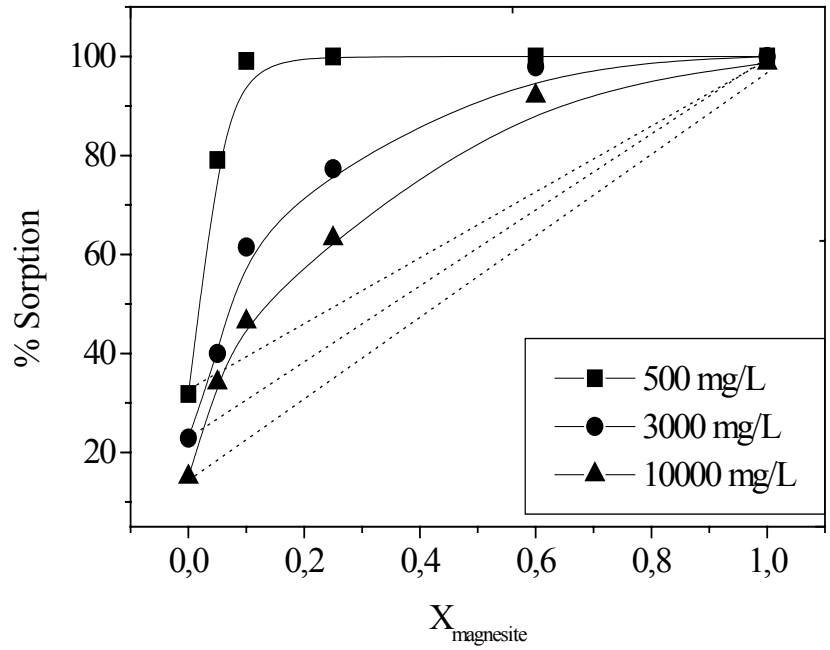

Figure 3.37. Change in the percentage sorption of Zn ions with the amount of magnesite in the mixtures of clinoptilolite-magnesite

.

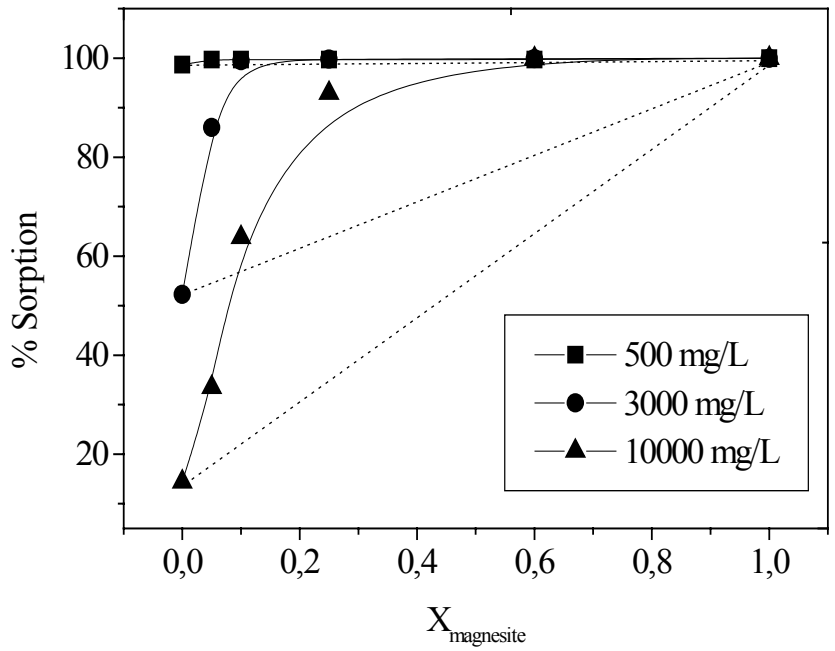

Figure 3.38. Change in the percentage sorption of Pb ion with the amount of magnesite in the mixtures of clinoptilolite-magnesite

3.4. Formation of Carbonate Phases of Zn^{2+} and Pb^{2+} Ions

3.4.1. Carbonate Phases of Lead

With the increase of calcite and magnesite fractions in the solid mixtures, the formation of Pb- carbonate phases was observed. The formation of such phases was documented using X-ray diffraction measurements, which showed that these phases were associated with the mixtures containing 60% calcite or magnesite in addition to pure calcite and magnesite. For the Pb-loaded mixtures of calcite, Figure 3.39 indicates the formation of cerussite ($PbCO_3$) in the samples that were prepared without any initial pH control. When the initial pH was raised to 10.0, formation of hydrocerussite, ($Pb_3(CO_3)_2(OH)_2$), was observed, indicating that this form is more stable at high pH values. However, in the case of Pb^{2+} sorption on magnesite, the formation of a mixture of cerussite and hydrocerussite was detected in the samples prepared with out any pH control, as seen in Figure 3.40(a). As the initial pH was increased to 10.0, an entire precipitation of hydrocerussite alone was seen in Figure 3.40(b).

The topic of relative stability of cerussite and hydrocerussite phases, formed upon exposure of Pb ions to carbonate minerals , is a matter of dispute among different researchers of this field. It is reported that cerussite and hydrocerussite equilibrium, which is given by the reaction: $3\ PbCO_{3(s)} + H_2O \Leftrightarrow Pb(OH)_2.(PbCO_3)_{2(s)} + CO_{2(g)}$, lies very close to the partial pressure in the atmosphere (Godelitsas et al. 2003, p.3358). In the same study, it was also argued that hydrocerussite formation might result from a rapid pH increment but that a subsequent equilibrium with the atmospheric $CO_{2(g)}$ can lead to a higher stability of cerussite. Our studies confirmed the fact that the formation of hydrocerussite was caused by the increment in the pH, but it revealed also that exchanging CO_2 with the atmosphere during a period of four hours did not lead to any conversion of hydrocerussite into cerussite. It must be stressed here that a time period of four hours is very short to be able to draw a sharp conclusion about the relative stability of cerussite/hydrocerussite within the solution medium as phase transitions might sometimes be kinetically controlled.

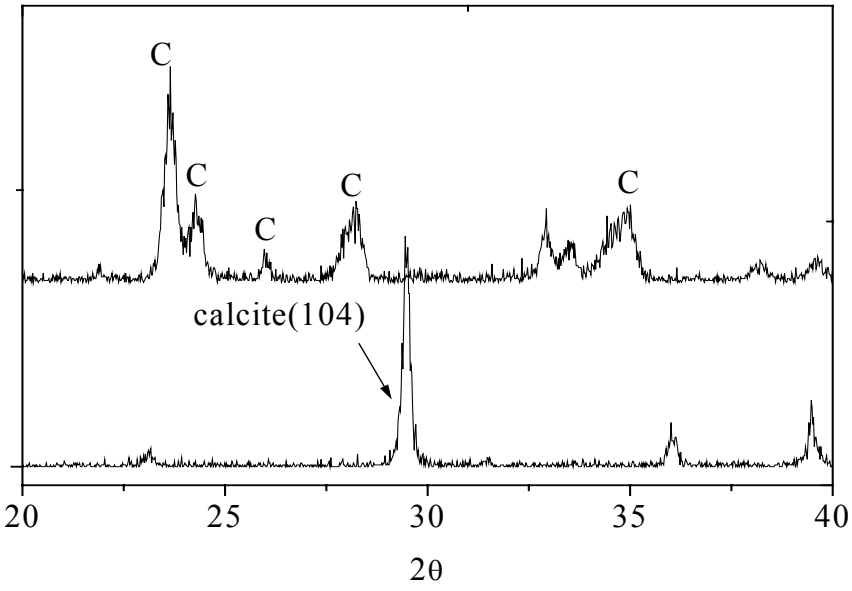

Figure 3.39. XRPD patterns showing the features of cerussite and hydrocerussite obtained upon interaction of Pb ions with calcite with no pH modification, C: Cerussite, HydC: Hydrocerussite

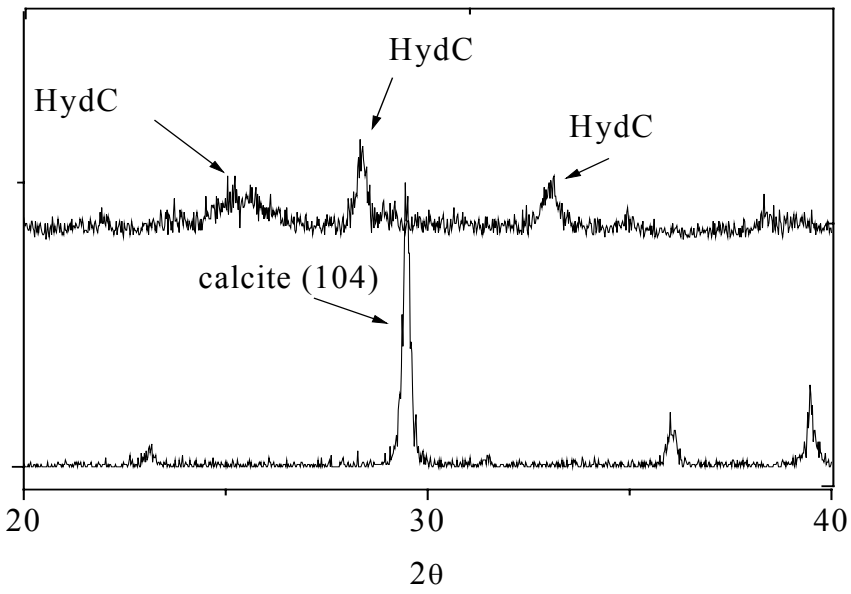

Figure 3.40. XRPD patterns showing the features of hydrocerussite obtained upon interaction of Pb ions with calcite with initial pH of 10.0. C: Cerussite, HydC: Hydrocerussite.

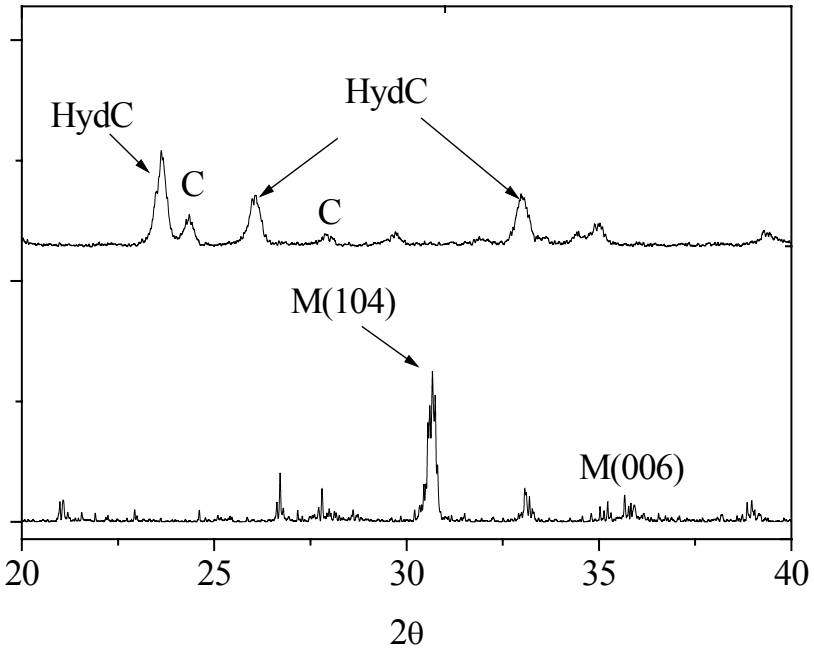

Figure 3.41. XRPD patterns showing: features of cerussite and hydrocerussite obtained upon interaction of Pb ions with magnesite with no pH modification M: Magnesite, C: cerussite, HydC: Hydrocerussite.

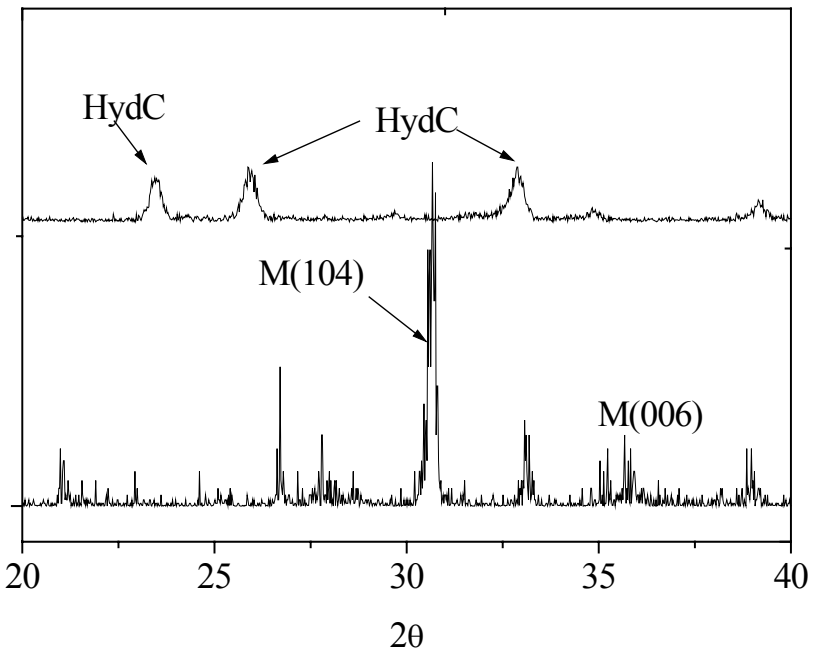

Figure 3.42. XRPD patterns showing the features of hydrocerussite with pH=10 . M: Magnesite, C: cerussite, HydC: Hydrocerussite.

The morphologies of cerussite and hydrocerussite were investigated using SEM. Figure 3.43 gives the SEM micrographs of cerussite and hydrocerussite obtained from the contact of Pb^{2+} with calcite. Figure 3.43 (a) shows that the cerussite crystals possess a columnar prismatic morphology with crystal length ranging 1-2 μm and cross section diameter of about 0.5 μm. On the other hand, hydrocerussite crystals appeared to have tabular hexagonal shape (as shown in Figure 3.43 (b)). The figure demonstrates also an edge size of about 1μm of the crystals.

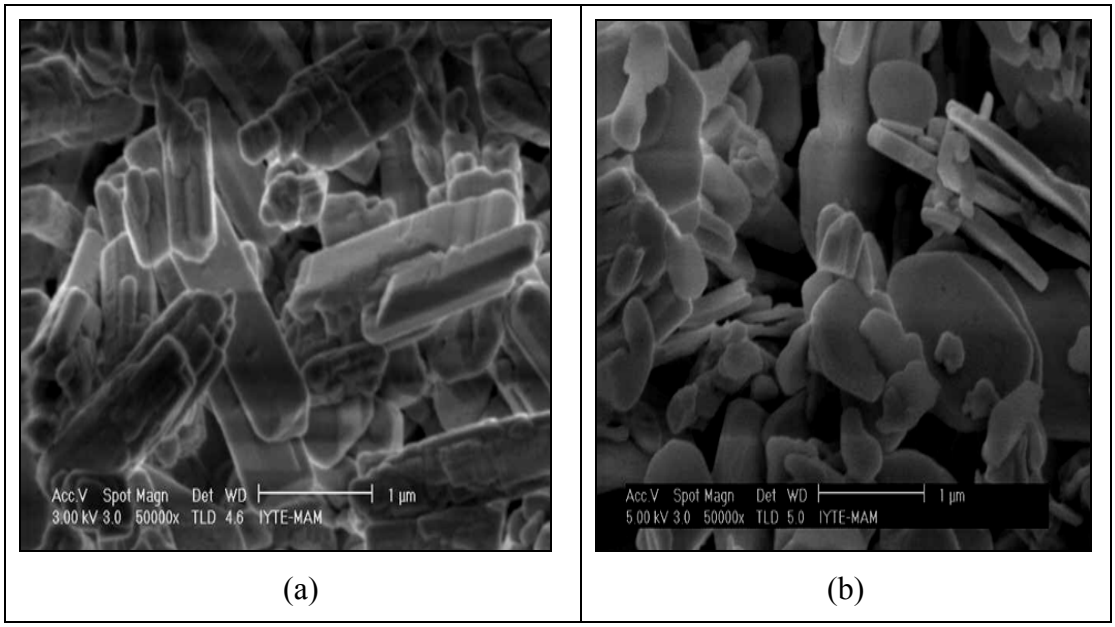

(a) (b)

Figure 3.43. Typical SEM microimages showing the features of cerussite and hydrocerussite obtained upon interaction of Pb ions with calcite with (a) no pH modification, and (b) the features of hydrocerussite obtained upon interaction of Pb ions with calcite with initial pH of 10.0.

In addition, Figure 3.44 gives the SEM micrographs of cerussite and hydrocerussite obtained from the contact of Pb^{2+} with magnesite. In the samples prepared with no pH control, the cerussite crystals appear to be embedded into hydrocerussite crystals. As, the initial pH is increased to 10.0, the samples were entirely composed of hydrocerussite, in line with the XRPD predictions. The cerussite crystals possess a columnar prismatic morphology as in the case of Pb^{2+} sorption on calcite fraction. Hydrocerussite crystals, however, seems to have plate like morphology that

posses a shape close to hexagonal but with rounded edges, and variable edge lengths ranging 0.5-2 μm.

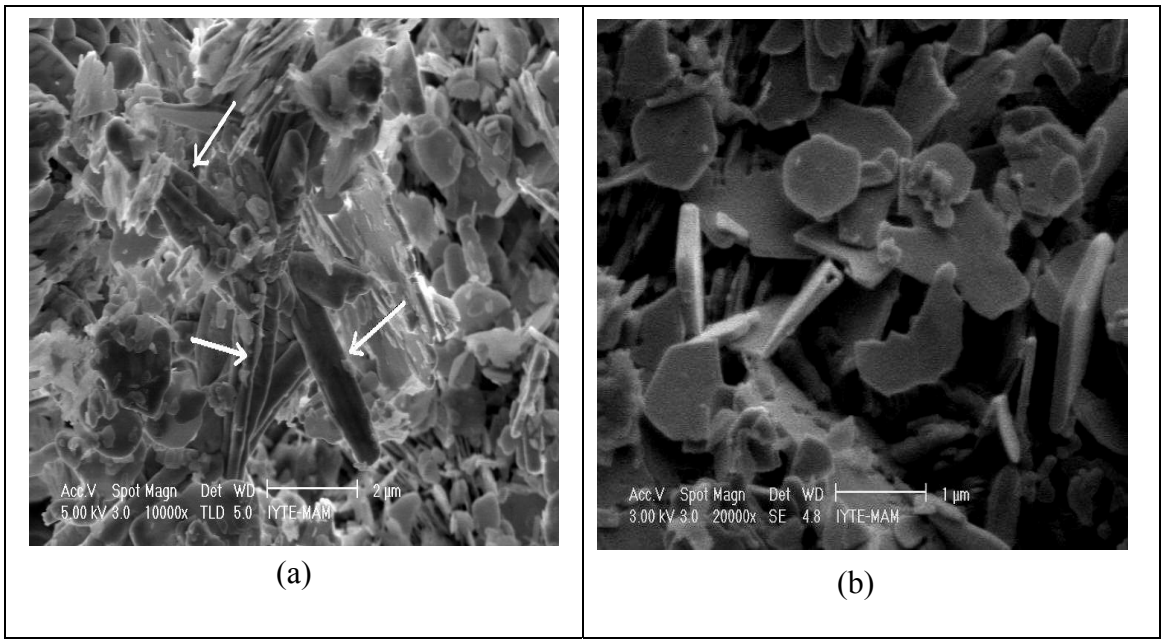

(a) (b)

Figure 3.44. Typical SEM microimages showing; (a) cerussite crystals embedded in between crystals of hydrocerussite and magnesite (b)hydrocerussite crystals.

The morphological stability of cerussite and hydrocerussite was also examined over long periods of time. SEM and EDS analysis of the dried samples that were kept under ambient conditions for a period of nine months revealed that while hydrocerussite retained its morphologic configuration and chemical composition over this time period, a slow morphological transition was observed in the case of cerussite from columnar prismatic shape to what seems to be a rectangular plate-like shape, as shown in Fig. 3.45.

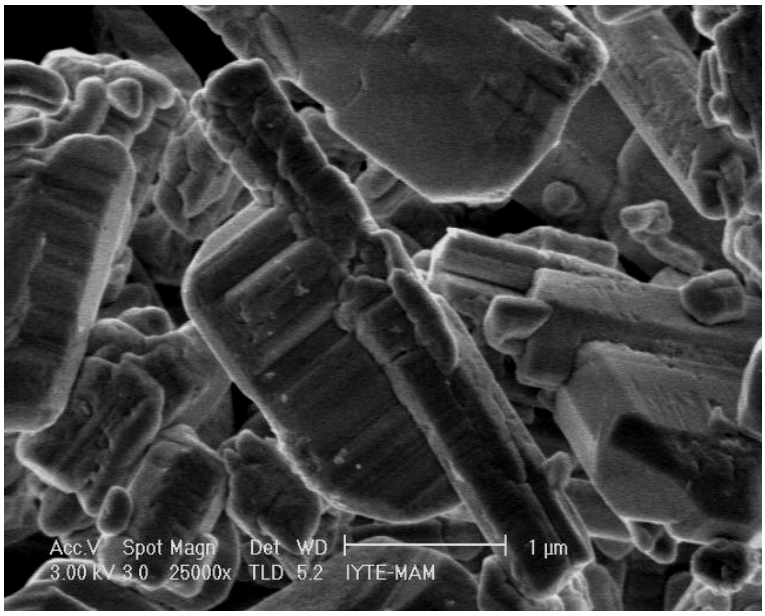

Fig. 3.45. SEM micrographs of: cerussite powder stored under ambient conditions for nine months (magnification of ×25 000)

The carbonate specie formed upon contact of Pb^{2+} with calcite and magnesite were also examined using FTIR spectroscopy. Figure 3.46 shows IR modes of Pb-loaded calcite compared to that of pure calcite. The band at 1074 cm^{-1} in the spectra of Pb-loaded calcite belongs to the ν1 vibrational mode (symmetric stretching) that is IR inactive in the spectrum of pure calcite. Moreover, a broadening is observed in the asymmetric stretching peak (ν3)- which occured at 1437 cm^{-1} in calcite accompanied by a slight splitting, particularly in the samples of Pb-loaded calcite. The split could be caused by difference in chemical environment of lattice carbonate and surface carbonate. Furhermore, the originally weak feature, appearing near 847 cm^{-1} in calcite, is becoming more intense upon sorption of Pb^{2+} ions. The observed variations in various vibrational bands of calcite indicate a decrease in the carbonate symmetry upon the uptake of lead ions by calcite. As illustrated in Figure 3.47, the band occuring at 3538 cm^{-1} comes plausibly from the stretching vibrations of the structural –OH groups in hydrocerussite. As in cerussite, hydrocerussite formation caused a slight split in the band arising from the ν3 (asymetric stretching of carbonate) mode originally at 1437 cm^{-1}, accompanied by a red shift of the band center to 1376 cm^{-1}. The band corresponding to the ν1 mode (symmetric stretching that is IR inactive in calcite) became more distinct upon hydrocerussite overgrowth compared to the case of

cerussite. Moreover, it is evident from the spectra that hydrocerussite formation weakened the ν2 band (out-of-plane bending) and caused a shift in the ν4 band (in plane bending) from 712 cm^{-1} (in calcite) to 676 cm^{-1}. As was previously stated, the splits in the ν3 and ν4 modes and the activation of the ν1 mode all point to geometrical modifications resulting in a decrease in the symmetry of the carbonate group upon the uptake of Pb^{2+} ions by calcite.

As can be deduced from Fig. 3.48 and Fig. 3.49, the FTIR spectra of magnesite and Pb-loaded magnesite (where cerussite and hydrocerussite formation was observed), less significant modification in the original bands of magnesite is observed compared to the case of loading Pb-calcite. Apart from some changes in the intensity of the vibrational bands, no significant change in the band positions is seen. This is suggesting that cerussite and hydrocerussite formed by reacting Pb^{2+} ions with magnesite possess a microscopic (atomic) structural environment that is not much different from that of magnesite. This result is different from the one observed in the case of calcite, were cerussite and hydrocerussite growth appeared to lead to more significant structural changes, as discussed peviously. Never the less, the validation of these findings necessitates application of advanced structural techniques.

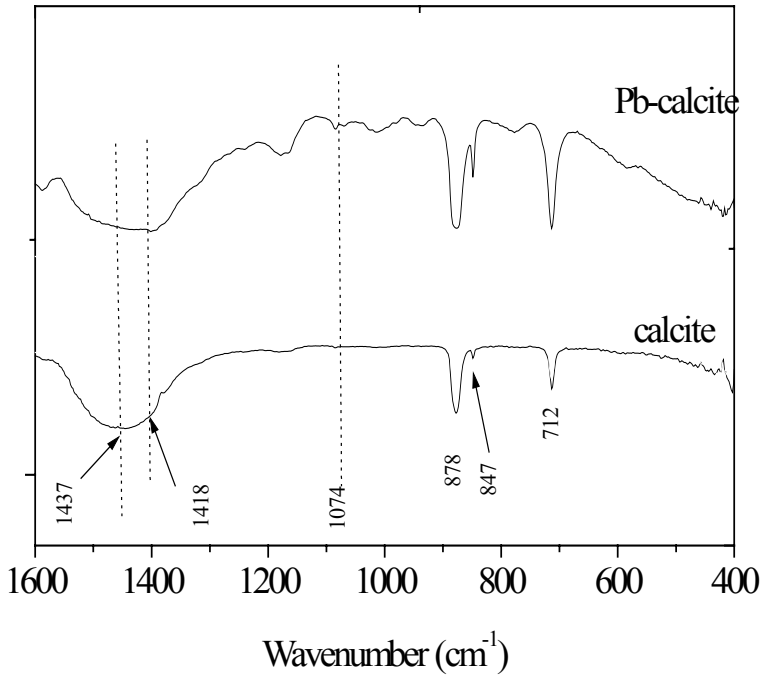

Figure 3.46. FTIR spectra of calcite and Pb-loaded calcite under no pH control.

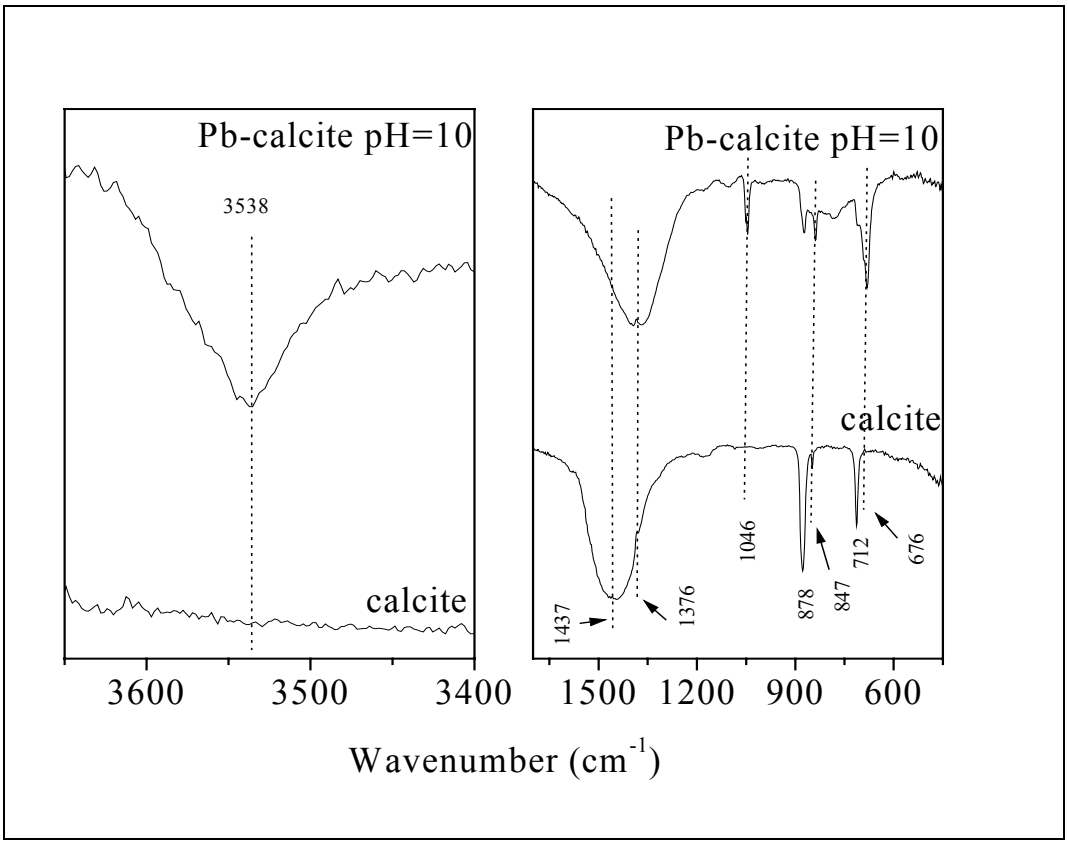

Figure 3.47. FTIR spectra of calcite and Pb-loaded calcite under pH=10.

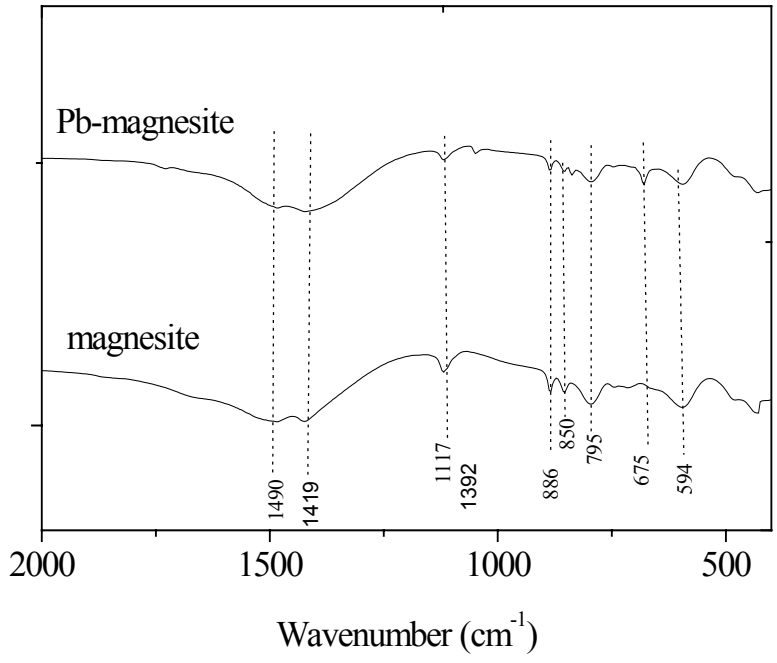

Figure 3.48. FTIR spectra of Pb-loaded magnesite

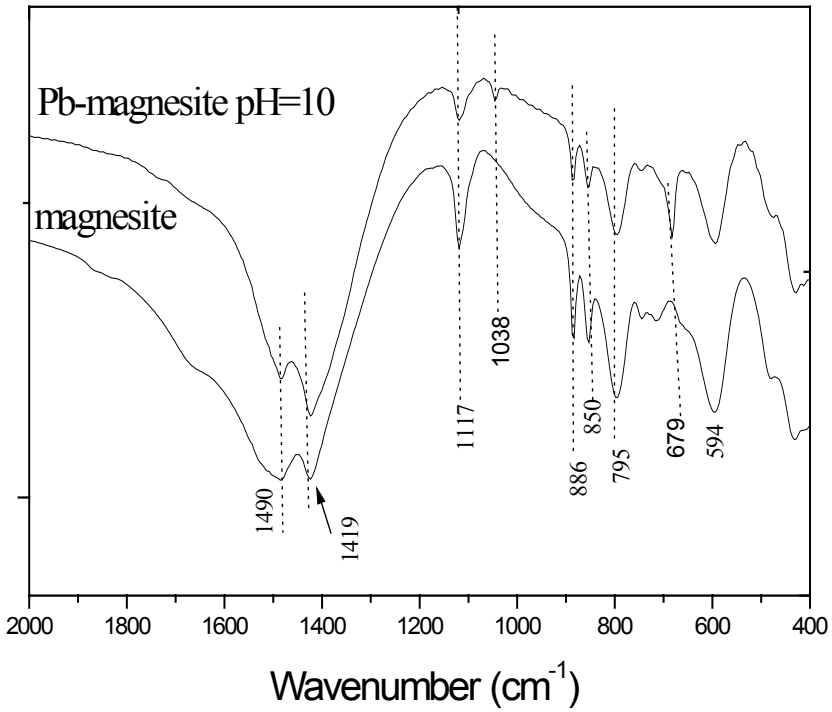

Figure 3.49. FTIR spectra of Pb-loaded magnesite for pH=10

3.4.2. Carbonate Phases of Zinc

XRPD examination of the Zn- loaded mixtures of both of calcite and magnesite in addition to kaolinite and clinoptilolite mixtures containing 60% of magnesite and calcite, revealed the formation of hydrozincite species as shown in Figure 3.50 and 3.51. It is reported that in the presence of carbonate and hydroxide ions, zinc can form precipitates that exhibit the general formula $Zn(CO_3)_x(OH)_{2-2x}$ with $0<x<1$, where the value of x can be controlled by the synthesis procedure (Zhang et al. 2004, p.1944). Increasing the initial pH to 10.0 did not change the type of precipitated specie indicating the stability of hydrozincite. The particles of this crystal did not show a distinct morphology as it was the case in cerussite and hydrocerussite. A typical SEM image is provided in Figures 3.52 (a) and (b) for hydrozincite.

The effect of Zn^{2+} retention on the structure of calcite and magnesite was also followed using FTIR spectroscopy. Fig. 3.53 provides the FTIR spectra of calcite prior to and after Zn^{2+} loading at the highest studied concentration of 10000 mg/L $Zn(NO_3)_2$

.6H_2O. Again, incorporation of Zn^{2+} in the form of hydrozincite is seen to cause changes in the vibrational bands. These changes include a split in the asymmetric vibrational band of the mineral occurring initially at 1443 cm^{-1}, activation of the initially inactive symmetric stretching feature located at 1056 cm^{-1}, development of a hydroxide stretching feature at 3344 cm^{-1}, possibly arising from the hydroxide groups in the hydrozincite structure, and splitting of the in-plane and out-of-plane bending modes occurring at 716 , 876 cm^{-1}, respectively.

The FTIR spectra of magnesite is compared to that of Zn-loaded magnesite in which hydrozincite formation was documented. The overgrowth of hydrozincite leads to no significant modifications in the original vibrational bands. Interestingly, this result resembles the one observed upon overgrowth of cerussite and hydrocerussite resulting from sorption of Pb^{2+} on magnesite as shown in Fig. 3.54.

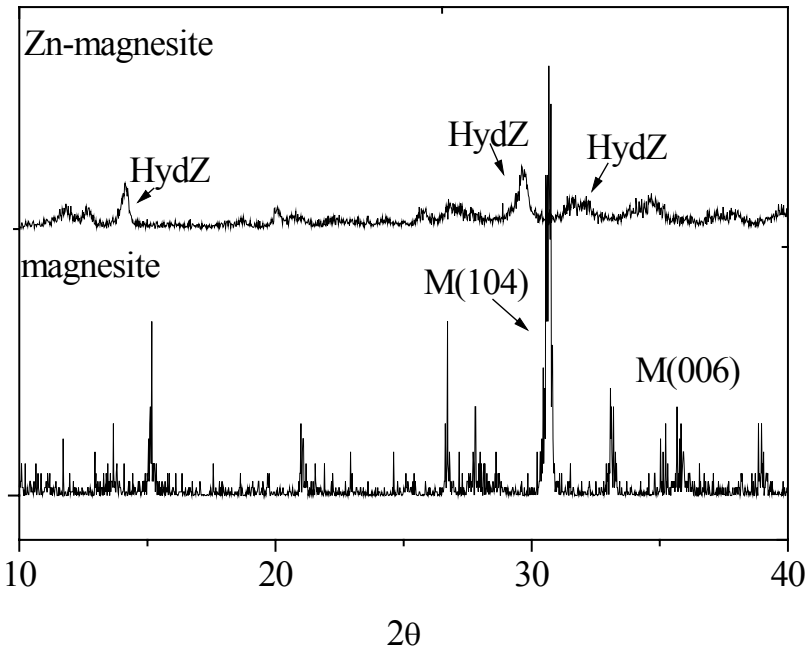

Figure 3.50. XRPD patterns showing the features of hydronzincite obtained upon interaction of Zn ions with magnesite. M: magnesite, HydZ: hydrozincite

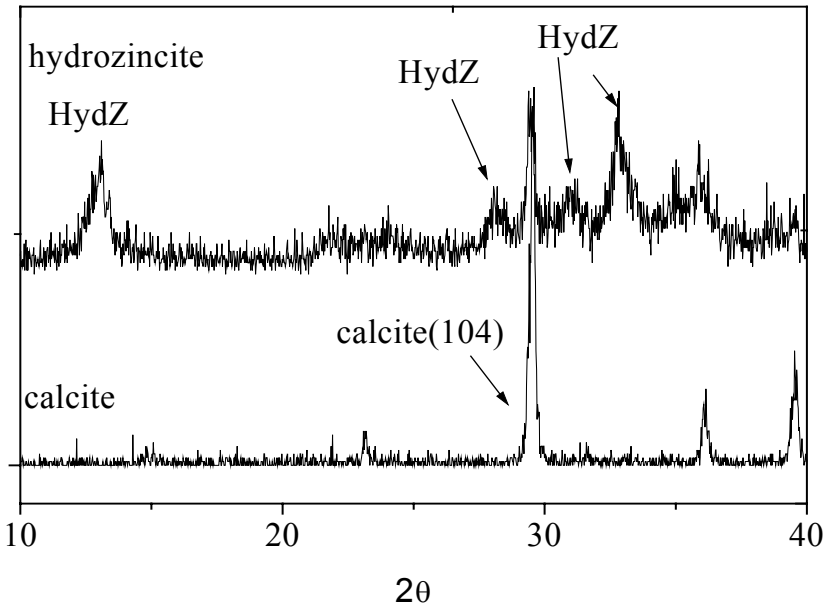

Figure 3.51. XRPD patterns showing the features of hydronzincite obtained upon interaction of Zn ions with calcite. HydZ: hydrozincite

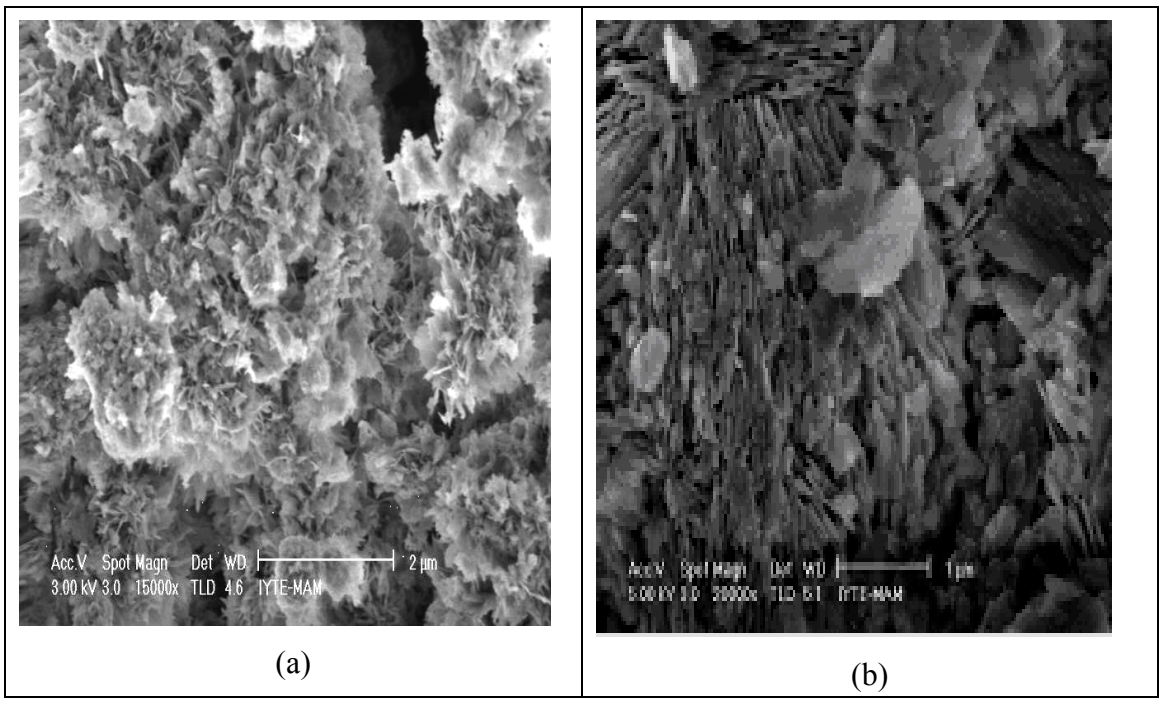

Figure 3.52. Typical SEM microimages of hydrozincite for (a) calcite (b) magnesite

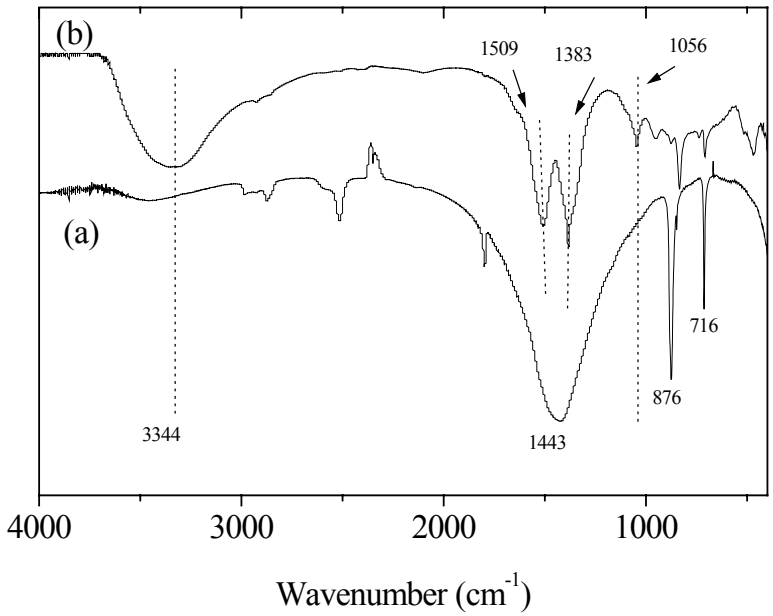

Figure 3.53. FTIR spectra of (a)calcite, (b) Zn-loaded calcite.

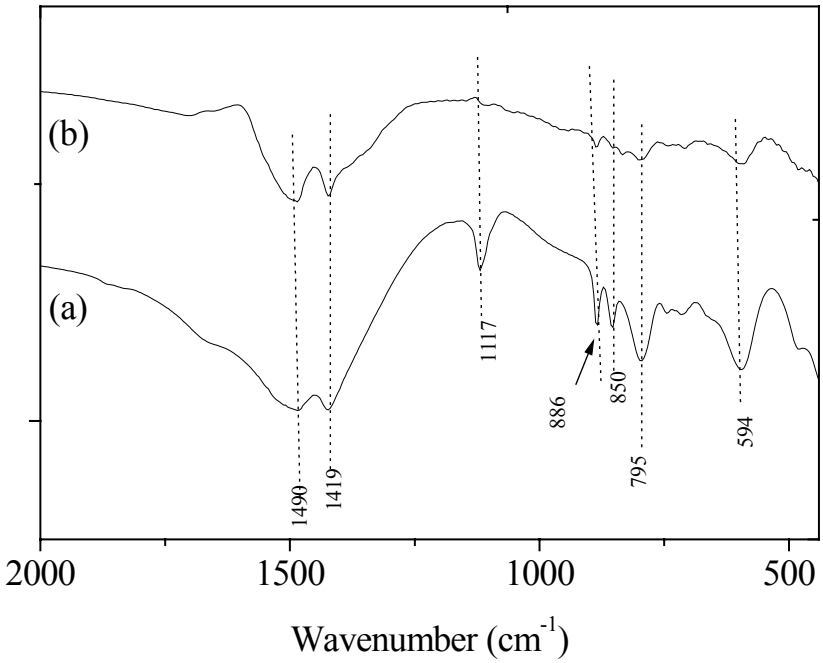

Figure 3.54. FTIR spectra of (a) magnesite, and (b) Zn-loaded magnesite.

CHAPTER 4

CONCLUSIONS AND RECOMMENDATIONS

The effect of magnesite and calcite on the uptake of lead and zinc by mixtures of these carbonates with kaolinite and clinoptilolite was investigated. The study included determination of kinetics and sorption isotherms of lead and zinc on pure kaolinite and clinoptilolite. In addition, the mechanisms of uptake of lead and zinc at different concentration levels for different mixtures and pH conditions, the morphologies of the formed precipitates, the plausible structural changes in the lattice of calcite, magnesite, kaolinite, and clinoptilolite, originating from sorption of lead and zinc ions were discussed. The specific conclusions are listed below:

1. The sorption affinity of both of kaolinite and clinoptilolite towards Pb is larger than their affinity towards Zn. The process of sorption appears to achieve equilibrium rapidly. The sorption data are described by Freudlich isotherm model.
2. The large increase in the scavenged amounts of Zn and Pb ions with the increase in the fraction of magnesite and calcite in the mixtures suggests that carbonates are a more favorable sink for these ions. Hence, carbonate presence as a soil component is expected to correlate positively with the sorption properties of soil, in particular in the alkaline media. The efficiency of calcite and magnesite becomes clearer at higher loadings, where the sorption process becomes predominantly controlled by the amount of calcite and magnesite in the mixtures.
3. Precipitation mechanism of carbonate specie of Zn and Pb took place at higher fractions of magnesite and calcite and higher loadings leading to enhancement in the removal of both ions from the aqueous medium.
4. When the initial concentration of Zn and Pb ions is raised, a rapid overgrowth of hydrozincite, and cerussite was observed. Increasing the initial pH to 10.0 caused enhancement in the dissolution of calcite and magnesite, increasing in

the amount of precipitated hydrozincite and the formation of hydrocerussite instead of cerussite.

5. The SEM images showed that the morphologies of cerussite, and hydrocerussite have columnar prismatic- like, and tabular hexagonal-like shapes, respectively. The size of the crystals are roughly in the range 1-2 μm. Alternatively, hydrozincite did not have a distinct morphology. Examination of the morphological stability of the samples stored in dry conditions over a period of nine months, indicated that hydrocerussite is more stable than cerussite.
6. The uptake of Pb^{2+} and Zn^{2+} results in decreasing the symmetry of the carbonate group leading to activating the initially inactive symmetric stretching mode and splitting the degenerate modes . By virtue of being able to trace the changes in symmetry in the structure of a given sorbent, FTIR analysis could be helpful in confirming the uptake of foreign ions by that sorbent, in particular, when the concentration of these ions is so small that their sorption might not be clearly followed by techniques like XRPD and SEM.
7. On the overall, magnesite fractions appears to show a slightly better sorption capacity compared to calcite fractions. This observation needs to be validated on a mechanistic basis in a separate detailed study in which kinetic and thermodynamic factors should be examined in depth.

REFERENCES

Allen, H.E., Huang, C.P., Bailey, G.W., Bowers, A.R., 1995. *Metal Speciation and Contamination of Soil,* (Lewis Publishers, Florida,), p.255

Appel, C., Ma, L. 2002. "Concentration, pH, and surface charge effects on cadmium and lead sorption in three tropical soils", *JEQ*, Vol. 31, pp.581-589.

Auboiroux, M., Baillif, P., Touray, J.C., Bergaya F. 1996. "Fixation of Zn^{2+} and Pb^{2+} by a Ca –montmorillonite in brines and dilute solutions: Preliminary results", *Applied Clay Science*, Vol. 11, pp.117-126.

Badawy, S.H., Helal, M.I.D., Chaudri, A., Lawlor, K. and McGrath, S.P. 2002. "Solid solid-phase controls lead activity in soil solution", *JEQ*, Vol. 31, pp.162-167.

Busenberg, E. and Plummer, L.N. 1985. "Kinetics and thermodynamics factore controlling the distribution of SO_4^{2-} and Na^+ in calcites and selected arogonites", *Geochimica et Cosmochimica Acta,* Vol. 49, pp.713-725.

Badillo-Almaraz, V., Trocellier P., Davilla- Rangel I. 2003. "Adsorption of aqueous Zn(II) species on synthetic zeolites", *Nuclear Instruments and Methods in Physics Research*, Vol. 210, pp.424 –428.

Böttcher, M. E., Gehlken, P., and Steele, D.F. 1997. "Characterization of inorganic and biogenic magnesian calcites by Fourier Transform Infrared Spectroscopy.", *Solid State Ionics*, Vol. 101-103, pp.1379-1385.

Bradl, H.B. 2004. "Adsorption of heavy metal ions on soils and soils constituents", *Journal of Colloid and Interface Science*, Vol. 277, pp. 1-18.

Chiron, N., Guilet, R., Deydier, E. 2003. "Adsorption of Cu(II) and Pb(II) onto a grafted silica: isotherms and kinetic models", *Water Research*, Vol. 37, pp.3079-3086.

Coles, C.A., Yong, R.N. 2002. "Aspects of kaolinite characterization and retention of Pb and Cd", *Applied Clay Science*, Vol. 22, pp.39-45.

Connor, D.J., Sexton, B.A., Smart, R. 2003. *Surface Analysis Methods in Materials Science*, (Springer-Verlag, Germany), pp.91, 98, 203-205.

Curti, E. 1999. " Coprecipitation of radionuclides with calcite: estimation of partition coefficients based on a rewiew of laboratory investigations and geochemical data", *Applied Geochemistry,* Vol.14, pp. 433-445.

Çulfaz, M., Yağız, M. 2003. "Ion exchange properties of natural clinoptilolite:lead –sodium and cadmium –sodium equilibria", *Seperation and Purification Technology*, Elsevier, Vol.37, pp. 95-105.

Echeverria, J.C, Morera, M.T., Mazkiaran, C., Garrido, J.J. 1998. "Competitive sorption of heavy metal by soils.Isotherms and fractional factorial experiments", *Environmental Pollution*, Vol. 101, pp.275-284.

El-Korashy, S.A. 2003. "Studies on diavalent ion uptake of transition metal cations by calcite through crystallization and cation exchange process", *Journal of Materials Science*, Vol. 38, pp. 1709-1719.

Elzinga, E.J., Reeder, R. J. 2002. " X-ray absorption spectroscopy study of Cu^{2+} and Zn^{2+} adsorption complexes at the calcite surface: Implications for site-specific metal incorporation preferences during calcite crystal growth", *Geochimica et Cosmochimica Acta*, Vol. 66, pp.3943-3954.

Erten, H.N., Gökmenoğlu, Z. 1994. "Sorption behaviour of Co^{2+}, Zn^{2+} and Ba^{2+} ions on alumina, kaolinite and magnesite", *Journal of Radioanalytical and Nuclear Chemistry, Articles*, Vol. 182, pp.375-384.

Esalah, J.O., Weber, M.E., Vera, J.H. 2000. "Removal of lead from aqueous solutions by precipitation with sodium di-(n-octyl) phosphinate", *Seperation and Purification Technology*, Vol. 18, pp. 25-36.

Feng, D., Aldrich, C., Tan, H. 2000. "Removal of heavy metal ions by carrier magnetic separation of adsorptive particulates", *Hydrometallurgy*, Vol. 56, pp.359-368.

Garcia-Sanchez, A., Alvarez-Ayasu, E. 2002. "Sorption of Zn, Cd and Cr on calcite. Application to purification of industrial waste waters", *Minerals Engineering*, Vol. 15, pp.539-547.

Godelitsas, A., Astilleros J.M., Hallam, K., Harissopoulos, S. and Putnis, A. 2003. " Interaction of calcium carbonates with lead in aqueous solutions", *Environ. Sci. Technol*., Vol. 37, pp.3351-3360.

Gupta, V., K., Gupta, M., and Sharma S. 2001. "Process development for the removal of lead and chromium from aqueous solutions using red mud –an aluminium industry waste", *Water Research*, Vol. 35, pp.1125-113 .

Haswell, S.J. 1991. *Atomic Absorption Spectrometry: Theory, Design and Applications* , (Elsevier, Amsterdam,), p.22

Hay, M.B., Workman, R.K., and Manne, S. 2003. "Mechanisms of metal ion sorption on calcite: composition mapping by Lateral Force Microscopy, *Langmuir*, Vol. 19, pp. 3727-3740

Hooda, P.S., Alloway, B.J. 1998. "Cadmium and lead sorption behaviour of selected English and Indian soils", *Geoderma*, Vol. 84, pp. 121-134.

Hu, Y., Liu, X. 2003. "Chemical composition and surface property of kaolins" , *Minerals Engineering*, Vol.16, pp.1279-1284.

Inglezakis, V. J., Loizidou, M.D., and Grigoropoulou, H. P. 2003. "Ion exchange of Pb^{+2}, Cu^{+2}, Fe^{+3}, and Cr^{+3} on natural clinoptilolite; Selectivity determination and influence of acidity on metal uptake.", *Journal of colloid and Interface Science*, Vol. 261, pp.49-54.

Ikhsan, J., Johnson, B.B., and Wells, D. 1999. "A comparative study of the adsorption of transition metals on kaolinite", *Journal of Colloid and Interface Science*, Vol. 217, pp.403-410.

Jain, C. K., and Ram, D. 1997. "Adsorption of lead and zinc on bed sediments of the River Kali", *Wat. Res*., Vol. 31, pp.154-162.

Kissel, D.E., Dixon, J.B., and Weed S.B. 1989. *SSA Book series:1 Minerals in Soil Environments*, (Soil Science Society of America, Madison, Wisconsin USA), p.488.

Kuriyavar, S.I., Vetrivel, R., Hegde, S.G., Ramaswamy, A.V., Chakrabarty, D. and Mahapatra, S. 2000. "Insights into the formation of hydroxyl ions in calcium carbonate: temperature dependent FTIR and molecular modelling studies". *J. Mater. Chem.*, Vol. 10, pp. 1835-1840.

Langella, A., Pansini, M., Capeletti, P., Gennaro, B., Gennaro,M., Colella, C., 2000. "NH_4^+, Cu^{2+}, Zn^{2+}, Cd^{2+} and Pb^{2+} exchange for Na^+ in a sedimentary clinoptilolite, North Sardinia, Italy", *Microporous and Mesoporous Materials*, Vol. 37, pp.337-343.

Lee, S., Z., Chang, L., Yang, H., Chen, C., M., and Liu, M.C. 1998. "Adsorption characterictics of lead onto soils", *Journal of Hazardous Materials*, Vol. 63, pp.37-49.

Li, Z., Alessi, D., and Allen, L. 2002. "Influence of quaternary ammonium on sorption of selected metal cations onto clinoptilolite zeolite", *JEO*, Vol. 31, pp.1106-1114.

Lim, T.T., Tay, J.H., and Teh, C.I., 2002. "Contamination time effect on lead and cadmium fractionation in a tropical coastal clay", *JEO*, Vol. 31, pp.806-812.

Lin, Z., Cormet, B., Qvarfort, U. and Herbert, R., 1995. "The chemical and mineralogical behaviour of Pb in shooting range soils from central Sweden", *Environmental Pollution*, 89, pp.303-309.

Liu, D., Hsu, C., Chuang, C. 1995. "Ion Exchange and sorption kinetics of cesium and strontium in soils", *Appl. Radiat. Isot*., Vol. 46, pp.839-846.

Mercy, M.A., Rock, P.A., Casey, W.H., Mokarrom, M.H. 1998. *Am. Mineral*, Vol. 83, pp.739-745

Mesquita, M.E., Silva, J.M., 1996. "Zinc adsorption by a calcareous soil. Copper interaction.", *Geoderma*, Vol. 69, pp.137-146.

Miranda-Trevino, J.C., Coles, C.A., 2003. "Kaolinite properties, structure and influence of metal retention on pH", *Applied Clay Science*, Vol. 23, pp.133-139.

Nachtegaal, M., Sparks, D. 2004. "Effect of iron oxide coatings on zinc sorption mechanisms at the clay-mineral/water interface", *Journal of Colloid and Interface Science*, Vol. 276, pp.13-23.

Nakamoto, K. 1986. *Infrared and Raman Spectra of Inorganic and Coordination Compounds,* (John Wiley & Sons), pp.86-87.

Narin, G.,A. 2001. Chromotographic Study of Carbonmonoxide Adsorption in Clinoptolite, MSc Thesis, İzmir Institue of Technology, İzmir, p.15

Ohnesorge, C.K., and Withem, M.,. 1991. *Metals and Their Compounds in the Environment*. (VCH publishers, Germany,), pp.971-974, 1309

Özkan, S. F. 1996. Adsorbent Yataklarının Dinamik Davranışının incelenmesi ve Doğal Kaynakların Adsorbent olarak Değerlendirimesi, Ph.D., Ege University, İzmir, p.2.

Pardo-Botello, R., Fernandez-Gonzalez, C., Pinilla-Gil, E., Cuerda Correa, E.M., Gomez-Serrano, V. 2004. "Adsorption kinetics of zinc in multicomponent ionic systems", *Elsevier, Journal of Colloid and Interface Science*, Vol. 277, pp.292-298.

Peric, J., Trgo, M., Medvidovic, N.V. 2004. "Removal of zinc, copper and lead by natural zeolite – acomparison of adsorption isotherms", *Water Research*, Vol. 38, pp.1893-1899.

Petrucci, R.H., Harwood, W.S. 1997. *General Chemistry*, (Prentice-Hall International, New Jersey), p.A26.

Pierzynski, G.M., Thomas, J. S., Vance, G. F., 1994. *Soils and Environmental Quality,* (Lewis Publishers, Florida), p.167.

Pokrovsky, O.S., 1998. "Precipitation of calcium and magnesium carbonates from homogeneous supersaturated solutions", *Journal of Crystal Growth*, Vol. 186, pp. 233-239.

Prasad M., Saxena S., Amritphale S.S., and Chandra N. 2000. "Kinetics and isoterms for aqueous lead adsorption by natural minerals", *Ind. Eng. Chem. Res.,* Vol. 39, pp.3034-3037.

Reig, F.B., Gimeno Adelantado, J.V. and Moya Moreno, M.C.M. 2002. "FTIR quantitative analysis of calcium carbonate (calcite) and silica (quartz) mixtures using the constant ratio method. Application to geological samples", *Talanta*, Vol. 58, pp.811-821.

Rouquerol, F., Rouquerol, J., and Sing, K., 1999. *Adsorption by Powder and Porous Solids Principles, Methology and Applications,* (Academic Pres Inc. USA), pp. 355, 358.

Settle, F.A. 1997. *Handbook of Instrumental Techniques for Analytical Chemistry*, (Prentice Hall PTR), pp.341-342

Shahwan, T. 2000. "Radiochemical and spectroscopic studies of cesium, barium, and cobalt sorption on some natural clays", Ph. D. Thesis, Bilkent University, Ankara , pp.8, 18

Shahwan, T., Atesin, A.C., Erten, H.N., Zarasız, A., 2002. "Uptake of Ba^{2+} ions by natural bentonite and $CaCO_3$: A radiotracer, EDXRF and PXRD study", *Journal of Radioanalytical and Nüclear Chemistry*, Vol. 254, pp.563-568.

Shahwan, T., Sayan, S., Erten, H. N., Black, L., Hallam, K.R. and Allen, G.C. 2000. "Surface spectroscopic studies of Cs^{+}, and Ba^{2+} sorption on chloride –illite mixed clay", *Radiochim. Acta*, Vol. 88, pp.681-686 .

Sheta A.S., Falatah, A.M., Al-Sewailem, M.s., Khaled, E.M., Salam, A.S.H. 2003. "Sorption characteristics of zinc and iron by natural zeolinite and bentonite", *Microporous and Mesoporous Materials,* Vol. 61, pp.127-136.

Singh, S.P., Ma, L.Q. and Harris, W.G. 2001. "Heavy metal interactions with phosphatic clay", *JEO*, Vol. 30, pp.1961-1968.

Sipos, P., Nemeth, T., Mohai, I., Dodony, I. 2004. "Effect of soil composition on adsorption of lead as reflected by a study on a natural forest soil profile", Geoderma, Vol. 124, pp.363-374.

Skoog, D.A., and West, D.M., 1971. *Principles of instrumental analysis* , (Hardcover, NewYork), p.549.

Smyth, J.R., Ahrens, T.J., 1997. "The crystal structure of calcite III", *Geophysical Research Letters*, Vol. 24, pp.1595-1598.

Stumm, W., and Morgan, J.J. 1996. *Aquatic Chemistry*, (John Wiley& Sons, New York, USA), p.296.

Sverjensky, D.A. and Molling, P.A. 1992. "A linear free energy relationship for crystalline solids and aqueous ions.", *Nature,* Vol. 356, pp. 231–234.

Tanaka, H., Yamasaki, N., Muratani, M., Hino, R., 2003 "Structure and formation process of (K,Na)- clinoptilolite", *Material Research Bulletin*", Vol.38, pp. 713-722 .

Top, A. 2001. Cation Exchange (Ag^{+}, Zn^{+2}, Cu^{+2}) behaviour of natural zeolites, MSc Thesis, IYTE, İzmir, pp.23-24

Trgo, M., and Peric, J., 2003. "Interaction of the zeolitic tuff with zinc containing simulated pollutant solutions", *Journal of Colloid and Interface Science*, Vol. 260, pp.1656-175.

Van Olphen, H., 1977. *An Introduction to Clay Colloid Chemistry, 2nd ed.*; (Wiley, New York,), p.59.

Wang, Y., Xu, H., 2001. "Prediction of trace metal partitioning between minerals and aqueous solutions: a linear free energy correlation approach", *Geochim. Cosmochim. Acta* , Vol. 65, pp.1529-1543.

Wenming, D., Zhijun, G., Jinzhou, D., Liying, Z., Zuyi, T., 2001. "Sorption characteristic of zinc(II) by calcareous soil radiotracer study", *Applied Radiation and Isotopes*, Vol. 54, pp. 371-375.

Wilson, M.J. 1994. *Clay Mineralogy: Spectroscopic and Chemical Determinative Methods.* (Chapman& Hall, New York,), pp.52-55.

Xu N., Hochella, M.F., Brown, G.E., Parks G.A., Parks, J. 1996. "Co(II) sorption at the calcite-water interface: X-ray photoelectron spectroscopic study", *Geochimica et Cosmochimica Acta ,* Vol. 60, pp.2801-2815

Yariv, S., Cross H. 2002. *Organo Clay Complexes and Interactions*, (Marcel Dekker, Inc, Newyork-Basel), pp.2-9

Yu, B., Zhang, Y., Shukla, A.S., Dorris, S., and K., 2001. "The removal of heavy metals from aqueous solutions by sawdust adsorption removal of lead and comparison of its adsorption with copper", *Journal of Hazardous Materials*, Vol. 84, pp.83-94.

Zachara, J.M., Cowan, C.e. and Resch, C.T. 1991 " Sorption of divalent metals on calcite", *Geochimica et Cosmochimica Acta*, Vol. 55 , pp.1549-1562.

Zhang, S., Fortier, H., and Dahn, J., 2004. "Characterization of zinc carbonate hydroxides synthesized by precipitation from zinc acetate and potassium carbonate solutions", *Mater. Res. Bullet*., Vol. 39, pp. 1939-1948

WEB_1, 2002. TMMOB, 05.04.2004. http://www.maden.org.tr/yeni3/ english/mining sector in Turkey.pdf

WEB_2, 1996. Mouter River Co, 10.02.2004. http://www.moutere.com

WEB_3, 2004. Chemsoc, 01.01.2005. http://www.rsc.org.pdf

WEB_4, 1996. University of Melbourne. http://www.ph.unimelb.edu.au. htm

WEB_5, 2002. Nunnauuni, 10.01.2005. http://www.nunnauuni.com/english /soapstone /rakenneosat.html

WEB_6, 1996. Science Hypermedia Home Page, 08.03.2003. http://elchem. kaist .ac.kr/vt/ chem-ed/spec/ atomic/aa.htm

APPENDIX A

APPENDIX A1: Experimental Data Corresponding to Sorption of Pb^{2+} on Kaolinite

Table A1-1. Concentration in liquid phase (mg/L), obtained from studies on the effect of time on sorption of Pb^{2+} ions on kaolinite.

Initial Conc of $Pb(NO_3)_2$ (mg/L)	10 min	30 min	120 min	480 min	1440 min	2880 min
1	0	0	0	0	0	0
100	17	15	14	3	1	1
1000	460	468	476	456	464	468

Table A1-2. Concentration in solid phase (mg/g) obtained from studies on the effect of time on sorption of Pb^{2+} ions on kaolinite.

Initial Conc of $Pb(NO_3)_2$ (mg/L)	10 min	30 min	120 min	480 min	1440 min	2880 min
1	0.063	0.063	0.063	0.063	0.063	0.063
100	4.600	4.800	4.900	6.000	6.200	6.200
1000	17.000	16.200	15.400	17.400	16.600	16.200

Table A1-3. % Sorption Pb^{2+} ions on kaolinite at various contact times.

Initial Conc of $Pb(NO_3)_2$ (mg/L)	10 min	30 min	120 min	480 min	1440 min	2880 min
1	>99.9	>99.9	>99.9	>99.9	>99.9	>99.9
100	73.0	76.2	77.8	95.2	98.4	98.4
1000	27.0	25.7	24.4	27.6	26.3	25.7

APPENDIX A2: Experimental Data Corresponding to Sorption of Zn^{2+} on Kaolinite

Table A2-1. Concentration in liquid phase (mg/L) obtained from studies on the effect of time on sorption of Zn^{2+} ions on kaolinite

Initial Conc. of $Zn(NO_3)_2.6H_2O$ (mg/L)	10 min	30 min	120 min	480 min	1440 min	2880 min
1	0	0	0	0	0	0
100	14	13	11	9	5	3
1000	118	116	122	118	108	104

Table A2-2. Concentration in solid phase (mg/g) obtained from studies on the effect of time on sorption of Zn^{2+} ions on kaolinite

Initial Conc. of $Zn(NO_3)_2.6H_2O$ (mg/L)	10 min	30 min	120 min	480 min	1440 min	2880 min
1	0.022	0.022	0.022	0.022	0.022	0.022
100	0.800	0.900	1.100	1.300	1.700	1.900
1000	10.200	10.400	9.800	10.200	11.200	11.600

Table A2-3. % Sorption Zn^{2+} ions on kaolinite at various contact times.

Initial Conc. of $Zn(NO_3)_2.6H_2O$ (mg/L)	10 min	30 min	120 min	480 min	1440 min	2880 min
1	>99.9	>99.9	>99.9	>99.9	>99.9	>99.9
100	36.4	40.9	50.0	59.1	77.3	86.4
1000	46.4	47.3	44.5	46.4	50.9	52.7

APPENDIX B

APPENDIX B1: Experimental Data Corresponding to Sorption of Pb^{2+} on Clinoptilolite

Table B1-1. Concentration in liquid phase (mg/L), obtained from studies on the effect of time on sorption of Pb^{2+} ions on clinoptilolite

Initial Conc of $Pb(NO_3)_2$ (mg/L)	10 min	30 min	120 min	480 min	1440 min	2880 min
1	0	0	0	0	0	0
100	0.2	0	0.1	1.4	0.3	0
1000	276	244	236	181	120	96

Table B1-2. Concentration in solid phase (mg/g) obtained from studies on the effect of time on sorption of Pb^{2+} ions on clinoptilolite

Initial Conc of $Pb(NO_3)_2$ (mg/L)	10 min	30 min	120 min	480 min	1440 min	2880 min
1	0.063	0.063	0.063	0.063	0.063	0.063
100	6.280	6.300	6.290	6.160	6.270	6.300
1000	35.400	38.600	39.400	44.900	51.000	53.400

Table B1-3. % Sorption Pb^{2+} ions on clinoptilolite at various contact times

Initial Conc of $Pb(NO_3)_2$ (mg/L)	10 min	30 min	120 min	480 min	1440 min	2880 min
1	>99.9	>99.9	>99.9	>99.9	>99.9	>99.9
100	99.7	100.0	99.8	97.8	99.5	100.0
1000	56.2	61.3	62.5	71.3	81.0	84.8

APPENDIX B2: Experimental Data Corresponding to Sorption of Zn^{2+} on Clinoptilolite

Table B2-1. Concentration in liquid phase (mg/L), obtained from studies on the effect of time on sorption of Zn^{2+} ions on clinoptilolite

Initial Conc. of $Zn(NO_3)_2.6H_2O$ (mg/L)	10 min	30 min	120 min	480 min	1440 min	2880 min
1	0	0	0	0	0	0
100	3	3	3	2	1	1
1000	180	116	110	108	104	104

Table B2-2. Concentration in solid phase (mg/g)), obtained from studies on the effect of time on sorption of Zn^{2+} ions on clinoptilolite

Initial Conc. of $Zn(NO_3)_2.6H_2O$ (mg/L)	10 min	30 min	120 min	480 min	1440 min	2880 min
1	0.022	0.022	0.022	0.022	0.022	0.022
100	1.900	1.900	1.900	2.000	2.100	2.100
1000	4.000	10.400	11.000	11.200	11.600	11.600

Table B2-3. % Sorption of effect of time on sorption of zinc ions on clinoptilolite

Initial Conc. of $Zn(NO_3)_2.6H_2O$ (mg/L)	10 min	30 min	120 min	480 min	1440 min	2880 min
1	>99.9	>99.9	>99.9	>99.9	>99.9	>99.9
100	86.4	86.4	86.4	90.9	95.5	95.5
1000	18.2	47.3	50.0	50.9	52.7	52.7

APPENDIX C

APPENDIX C1: Experimental Data Corresponding to Sorption of Zn^{2+} and Pb^{2+} on Calcite-Kaolinite Mixtures

Table C1-1. Concentrations in liquid phase (mg/L) of Pb^{2+} obtained from the sorption experiments on calcite-kaolinite mixtures

Initial Conc of $Pb(NO_3)_2$ (mg/L)	Kaolinite	%5 calcite	%10 calcite	%25 calcite	%60 calcite	calcite
1	0	0	0	0	0	0
100	1	1	0	0	0	0
500	172	0	0	0	0	0
3000	1356	293	47	35	5	5
10000	5970	5140	4430	1285	10	1

pH=10						
Initial Conc of $Pb(NO_3)_2$ (mg/L)	Kaolinite	%5 calcite	%10 calcite	%25 calcite	%60 calcite	calcite
100	3	2	1	1	1	1
10000	3	2	2	3	1	4

Table C1-2. Concentrations in solid phase (mg/L) of Pb^{2+} obtained from the sorption experiments on calcite-kaolinite mixtures

Initial Conc of $Pb(NO_3)_2$ (mg/L)	Kaolinite	%5 calcite	%10 calcite	%25 calcite	%60 calcite	calcite
1	0.063	0.063	0.063	0.063	0.063	0.063
100	6.2	6.2	6.3	6.3	6.3	6.3
500	14.3	31.5	31.5	31.5	31.5	31.5
3000	53.4	159.7	184.3	185.5	188.5	188.5
10000	33	116	187	501.5	629	629.9

pH=10						
Initial Conc of $Pb(NO_3)_2$ (mg/L)	Kaolinite	%5 calcite	%10 calcite	%25 calcite	%60 calcite	calcite
100	6	6.1	6.2	6.2	6.2	6.2
10000	629.7	629.8	629.8	629.7	629.9	629.6

Table C1-3. % Sorption of Pb^{2+} on calcite-kaolinite mixtures

Initial Conc of $Pb(NO_3)_2$ (mg/L)	Kaolinite	%5 calcite	%10 calcite	%25 calcite	%60 calcite	calcite
1	>99.9	>99.9	>99.9	>99.9	>99.9	>99.9
100	98.4	98.4	>99.9	>99.9	>99.9	>99.9
500	45.4	>99.9	>99.9	>99.9	>99.9	>99.9
3000	28.3	84.5	97.5	98.1	99.7	99.7
10000	5.2	18.4	29.7	79.6	99.8	100.0

pH=10						
Initial Conc of $Pb(NO_3)_2$ (mg/L)	Kaolinite	%5 calcite	%10 calcite	%25 calcite	%60 calcite	calcite
100	95.2	96.8	98.4	98.4	98.4	98.4
10000	>99.9	>99.9	>99.9	>99.9	>99.9	99.9

Table C1-4. Concentrations in liquid phase (mg/L) of Zn^{2+} obtained from the sorption experiments on calcite-kaolinite mixtures

Initial Conc of $Zn(NO_3)_2.6H_2O$ (mg/L)	Kaolinite	%5 calcite	%10 calcite	%25 calcite	%60 calcite	calcite
1	0	0	0	0	0	0
100	3	0	0	0	0	0
500	70	44	25	7	3	4
3000	450	343	360	323	134	75
10000	1990	1977	1960	1385	1275	625

pH=10						
Initial Conc $Zn(NO_3)_2.6H_2O$ (mg/L)	Kaolinite	%5 calcite	%10 calcite	%25 calcite	%60 calcite	calcite
100	1	4	1	2	1	0
10000	17	3	4	14	6	4

Table C1-5. Concentrations in solid phase (mg/L) of Zn^{2+} obtained from the sorption experiments on calcite-kaolinite mixtures

Initial Conc of $Zn(NO_3)_2.6H_2O$ (mg/L)	Kaolinite	%5 calcite	%10 calcite	%25 calcite	%60 calcite	calcite
1	0.022	0.022	0.022	0.022	0.022	0.022
100	1.9	2.2	2.2	2.2	2.2	2.2
500	4	6.6	8.5	10.3	10.7	10.6
3000	21	31.7	30	33.7	52.6	58.5
10000	21	22.3	24	81.5	92.5	157.5

pH=10						
Initial Conc $Zn(NO_3)_2.6H_2O$ (mg/L)	Kaolinite	%5 calcite	%10 calcite	%25 calcite	%60 calcite	calcite
100	2.1	1.8	2.1	2	2.1	2.2
10000	218.3	219.7	219.6	218.6	219.4	219.6

Table C1-6. %Sorption of Zn^{2+} on calcite-kaolinite mixtures

Initial Conc of $Zn(NO_3)_2.6H_2O$ (mg/L)	Kaolinite	%5 calcite	%10 calcite	%25 calcite	%60 calcite	calcite
1	>99.9	>99.9	>99.9	>99.9	>99.9	>99.9
100	86.4	>99.9	>99.9	>99.9	>99.9	>99.9
500	36.4	60.0	77.3	93.6	97.3	96.4
3000	31.8	48.0	45.5	51.1	79.7	88.6
10000	9.5	10.1	10.9	37.0	42.0	71.6

pH=10						
Initial Conc $Zn(NO_3)_2.6H_2O$ (mg/L)	Kaolinite	%5 calcite	%10 calcite	%25 calcite	%60 calcite	calcite
100	95.5	81.8	95.5	90.9	95.5	>99.9
10000	99.2	99.9	99.8	99.4	99.7	99.8

APPENDIX C2: Experimental Data Corresponding to Sorption of Zn^{2+} and Pb^{2+} on Calcite-Clinoptilolite Mixtures

Table C2-1. Concentrations in liquid phase (mg/L) of Pb^{2+} obtained from the sorption experiments on calcite-clinoptilolite mixtures

Initial Conc of $Pb(NO_3)_2$ (mg/L)	Clino.	%5 calcite	%10 calcite	%25 calcite	%60 calcite	calcite
1	0	0	0	0	0	0
100	0	0	0	0	0	0
500	4	1	1	0	1	0
3000	901	291	339	9	8	5
10000	5390	4550	3545	1660	2	0

pH=10						
Initial Conc of $Pb(NO_3)_2$ (mg/L)	Clino	%5 calcite	%10 calcite	%25 calcite	%60 calcite	calcite
100	1	0	1	0	1	1
10000	210	2	8	0	1	4

Table C2-2. Concentrations in solid phase (mg/g) of Pb^{2+} obtained from the sorption experiments on calcite-clinoptilolite mixtures

Initial Conc of $Pb(NO_3)_2$ (mg/L)	Clino	%5 calcite	%10 calcite	%25 calcite	%60 calcite	calcite
1	0.063	0.063	0.063	0.063	0.063	0.063
100	6.3	6.3	6.3	6.3	6.3	6.3
500	31.1	31.4	31.4	31.5	31.4	31.5
3000	98.9	159.9	155.1	188.1	188.2	188.5
10000	91	175	275.5	464	629.8	630

pH=10						
Initial Conc of $Pb(NO_3)_2$ (mg/L)	Clino	%5 calcite	%10 calcite	%25 calcite	%60 calcite	calcite
100	6.2	6.3	6.2	6.3	6.2	6.2
10000	609	629.8	629.2	630	629.9	629.6

Table C2-3. % Sorption of Pb^{2+} on calcite-clinoptilolite mixtures

Initial Conc of $Pb(NO_3)_2$ (mg/L)	Clino	%5 calcite	%10 calcite	%25 calcite	%60 calcite	calcite
1	>99.9	>99.9	>99.9	>99.9	>99.9	>99.9
100	>99.9	>99.9	>99.9	>99.9	>99.9	>99.9
500	98.7	99.7	99.7	>99.9	99.7	>99.9
3000	52.3	84,6	82.1	99.5	99.6	99.7
10000	14.4	27.8	43.7	73.7	>99.9	>99.9

pH=10						
Initial Conc of $Pb(NO_3)_2$ (mg/L)	Clino	%5 calcite	%10 calcite	%25 calcite	%60 calcite	calcite
100	98.4	>99.9	98.4	>99.9	98.4	98.4
10000	96.7	>99.9	99.9	>99.9	>99.9	99.9

Table C2-4. Concentrations in liquid phase (mg/L) of Zn^{2+} obtained from the sorption experiments on calcite-clinoptilolite mixtures

Initial Conc of $Zn(NO_3)_2.6H_2O$ (mg/L)	Clino	%5 calcite	%10 calcite	%25 calcite	%60 calcite	calcite
1	0	0	0	0	0	0
100	1	0	0	0	0	0
500	75	30	8	5	2	4
3000	509	629	339	254	90	75
10000	1870	1845	1460	730	710	625

pH=10						
Initial Conc of $Zn(NO_3)_2.6H_2O$ (mg/L)	Clino	%5 calcite	%10 calcite	%25 calcite	%60 calcite	calcite
100	0	0	1	0	0	0
10000	5	3	4	4	3	4

Table C2-5. Concentrations in solid phase (mg/g) of Zn^{2+} obtained from the sorption experiments on calcite-clinoptilolite mixtures

Initial Conc of $Zn(NO_3)_2.6H_2O$ (mg/L)	Clino	%5 calcite	%10 calcite	%25 calcite	%60 calcite	calcite
1	0.022	0.022	0.022	0.022	0.022	0.022
100	2.1	2.2	2.2	2.2	2.2	2.2
500	3.5	8	10.2	10.5	10.8	10.6
3000	35.1	23.1	52.1	60.6	77	78.5
10000	33	35.5	74	147	149	157.5

pH=10						
Initial Conc of $Zn(NO_3)_2.6H_2O$ (mg/L)	Clino	%5 calcite	%10 calcite	%25 calcite	%60 calcite	calcite
100	2.2	2.2	2.1	2.2	2.2	2.2
10000	219.5	219.7	219.6	219.6	219.7	219.,6

Table C2-6. % Sorption of Zn^{2+}on calcite-clinoptilolite mixtures

Initial Conc of $Zn(NO_3)_2.6H_2O$ (mg/L)	Clino	%5 calcite	%10 calcite	%25 calcite	%60 calcite	calcite
1	>99.9	>99.9	>99.9	>99.9	>99.9	>99.9
100	95.5	>99.9	>99.9	>99.9	>99.9	>99.9
500	31.8	72.7	92.7	95.5	98.2	96.4
3000	22.9	4.7	48.6	61.5	86.4	88.6
10000	15.0	16.1	33.6	66.8	67.7	71.6

pH=10						
Initial Conc of $Zn(NO_3)_2.6H_2O$ (mg/L)	Clino	%5 calcite	%10 calcite	%25 calcite	%60 calcite	calcite
100	>99.9	>99.9	95,5	>99.9	>99.9	>99.9
10000	99.8	99.9	99.8	99.8	99.9	99.8

APPENDIX C3: Experimental Data Corresponding to Sorption of Pb^{2+} and Zn^{2+} on Magnesite-Kaolinite Mixtures

Table C3-1. Concentrations in liquid phase (mg/L) of Pb^{2+} obtained from the sorption experiments on magnesite-kaolinite.

Initial Conc of $Pb(NO_3)_2$ (mg/L)	Kaolinite	%5 magnesite	%10 magnesite	%25 magnesite	%60 magnesite	magnesite
1	0	0	0	0	0	0
100	1	0	0	0	0	0
500	172	0	0	0	0	0
3000	1356	294	11	6	2	0
10000	5970	4200	3040	1135	935	1

pH=10						
Initial Conc of $Pb(NO_3)_2$ (mg/L)	Kaolinite	%5 magnesite	%10 magnesite	%25 magnesite	%60 magnesite	magnesite
100	3	1	3	2	2	2
10000	3	1	2	1	3	1

Table C3-2**.** Concentrations in solid phase (mg/g) of Pb^{2+} obtained from the sorption experiments on magnesite-kaolinite.

Initial Conc of $Pb(NO_3)_2$ (mg/L)	Kaolinite	%5 magnesite	%10 magnesite	%25 magnesite	%60 magnesite	magnesite
1	0.063	0.063	0.063	0.063	0.063	0.063
100	6.2	6.3	6.3	6.3	6.3	6.3
500	14.3	31.5	31.5	31.5	31.5	31.5
3000	53.4	159.6	187.9	188.4	188.8	189
10000	33	210	326	516.5	536.5	629.9

pH=10						
Initial Conc of $Pb(NO_3)_2$ (mg/L)	Kaolinite	%5 magnesite	%10 magnesite	%25 magnesite	%60 magnesite	magnesite
100	6	6.2	6	6.1	6.1	6.1
10000	629.7	629.9	629.8	629.9	629.7	629.9

Table C3-3. % Sorption of Pb^{2+} on magnesite-kaolinite mixtures

Initial Conc of $Pb(NO_3)_2$ (mg/L)	Kaolinite	%5 magnesite	%10 magnesite	%25 magnesite	%60 magnesite	magnesite
1	>99.9	>99.9	>99.9	>99.9	>99.9	>99.9
100	98.4	>99.9	>99.9	>99.9	>99.9	>99.9
500	45.4	>99.9	>99.9	>99.9	>99.9	>99.9
3000	28.3	84.4	99.4	99.7	99.9	>99.9
10000	5.2	33.3	51.7	82.0	85.2	>99.9

pH=10						
Initial Conc of $Pb(NO_3)_2$ (mg/L)	Kaolinite	%5 magnesite	%10 magnesite	%25 magnesite	%60 magnesite	magnesite
100	95.2	98.4	95.2	96.8	96.8	96.8
10000	>99.9	>99.9	>99.9	>99.9	>99.9	>99.9

Table C3-4. Concentrations in liquid phase (mg/L) of Zn^{2+} obtained from the sorption experiments on magnesite-kaolinite.

Initial Conc of $Zn(NO_3)_2.6H_2O$ (mg/L)	Kaolinite	%5 magnesite	%10 magnesite	%25 magnesite	%60 magnesite	magnesite
1	0	0	0	0	0	0
100	0	0	0	0	0	0
500	70	40	3	0	0	0
3000	450	307	382	36	1	0
10000	1990	1815	1820	1645	546	29

pH=10						
Initial Conc of $Zn(NO_3)_2.6H_2O$ (mg/L)	Kaolinite	%5 magnesite	%10 magnesite	%25 magnesite	%60 magnesite	magnesite
100	1	1	2	3	2	1
10000	17	11	2	2	1	2

Table C3-5. Concentrations in solid phase (mg/g) of Zn^{2+} obtained from the sorption experiments on magnesite-kaolinite.

Initial Conc of $Zn(NO_3)_2.6H_2O$ (mg/L)	Kaolinite	%5 magnesite	%10 magnesite	%25 magnesite	%60 magnesite	magnesite
1	0.022	0.022	0.022	0.022	0.022	0.022
100	2.2	2.2	2.2	2.2	2.2	2.2
500	4	7	10.7	11	11	11
3000	21	35.3	27.8	62.4	65.9	66
10000	21	38.5	38	55.5	165.4	217.1

pH=10						
Initial Conc of $Zn(NO_3)_2.6H_2O$ (mg/L)	Kaolinite	%5 magnesite	%10 magnesite	%25 magnesite	%60 magnesite	magnesite
100	2.1	2.1	2	1.9	2	2.1
10000	218.3	218.9	219.8	219.8	219.9	219.8

Table C3-6. % Sorption of Zn^{2+} on magnesite-kaolinite mixtures

Initial Conc of $Zn(NO_3)_2.6H_2O$ (mg/L)	Kaolinite	%5 magnesite	%10 magnesite	%25 magnesite	%60 magnesite	magnesite
1	>99.9	>99.9	>99.9	>99.9	>99.9	>99.9
100	>99.9	>99.9	>99.9	>99.9	>99.9	>99.9
500	36.4	63.6	97.3	>99.9	>99.9	>99.9
3000	31.8	53.5	42.1	94.5	99.8	>99.9
10000	9.5	17.5	17.3	25.2	75.2	98.7

pH=10						
Initial Conc of $Zn(NO_3)_2.6H_2O$ (mg/L)	Kaolinite	%5 magnesite	%10 magnesite	%25 magnesite	%60 magnesite	magnesite
100	95.5	95.5	90.9	86.4	90.9	95.5
10000	99.2	99.5	99.9	99.9	>99.9	99.9

APPENDIX C4: Experimental Data Corresponding to Sorption of Pb^{2+} and Zn^{2+} on Magnesite-Clinoptilolite Mixtures

Table C4-1. Concentrations in liquid phase (mg/L) of Pb^{2+} obtained from the sorption experiments on magnesite-clinoptilolite.

Initial Conc of $Pb(NO_3)_2$ (mg/L)	Clino	%5 magnesite	%10 magnesite	%25 magnesite	%60 magnesite	magnesite
1	0	0	0	0	0	0
100	0	0	0	0	0	0
500	4	1	1	1	1	0
3000	901	264	10	3	1	0
10000	5390	4190	2280	445	4	1

pH=10						
Initial Conc of $Pb(NO_3)_2$ (mg/L)	Clino	%5 magnesite	%10 magnesite	%25 magnesite	%60 magnesite	magnesite
100	3	1	1	3	2	3
10000	3	1	3	1	1	1

Table C4-2. Concentrations in solid phase (mg/g) of Pb^{2+}obtained from the sorption experiments on magnesite-clinoptilolite

Initial Conc of $Pb(NO_3)_2$ (mg/L)	Clino	%5 magnesite	%10 magnesite	%25 magnesite	%60 magnesite	magnesite
1	0.063	0.063	0.063	0.063	0.063	0.063
100	6.3	6.3	6.3	6.3	6.3	6.3
500	31.1	31.4	31.4	31.4	31.4	31.5
3000	98.9	162.6	188	188.7	188.9	189
10000	91	211	402	585.5	629.6	629.9

pH=10						
Initial Conc of $Pb(NO_3)_2$ (mg/L)	Clino	%5 magnesite	%10 magnesite	%25 magnesite	%60 magnesite	magnesite
100	6	6.2	6.2	6	6.1	6
10000	629.7	629.9	629.7	629.9	629.9	629.9

Table C4-3**.** % Sorption of Pb^{2+}on magnesite-clinoptilolite mixtures

Initial Conc of $Pb(NO_3)_2$ (mg/L)	Clino.	%5 magnesite	%10 magnesite	%25 magnesite	%60 magnesite	magnesite
1	>99.9	>99.9	>99.9	>99.9	>99.9	>99.9
100	>99.9	>99.9	>99.9	>99.9	>99.9	>99.9
500	98.7	99.7	99.7	99.7	99.7	>99.9
3000	52.3	86.0	99.5	99.8	99.9	>99.9
10000	14.4	33.5	63.8	92.9	99.9	>99.9

pH=10						
Initial Conc of $Pb(NO_3)_2$ (mg/L)	Clino.	%5 magnesite	%10 magnesite	%25 magnesite	%60 magnesite	magnesite
100	95.2	98.4	98.4	95.2	96.8	95.2
10000	>99.9	>99.9	>99.9	>99.9	>99.9	>99.9

Table C4-4**.** Concentrations in liquid phase (mg/L) of Zn^{2+}obtained from the sorption experiments on magnesite-clinoptilolite

Initial Conc of $Zn(NO_3)_2.6H_2O$ (mg/L)	Clino.	%5 magnesite	%10 magnesite	%25 magnesite	%60 magnesite	magnesite
1	0	0	0	0	0	0
100	0	0	0	0	0	0
500	75	23	1	0	0	0
3000	509	563	254	150	14	0
10000	1870	1450	1180	810	177	29

pH=10						
Initial Conc of $Zn(NO_3)_2.6H_2O$ (mg/L)	Clino.	%5 magnesite	%10 magnesite	%25 magnesite	%60 magnesite	magnesite
100	0	0	0	1	2	1
10000	5	1	0	1	1	2

Table C4-5. Concentrations in solid phase (mg/g) of Zn^{2+}obtained from the sorption experiments on magnesite-clinoptilolite.

Initial Conc of $Zn(NO_3)_2.6H_2O$ (mg/L)	Clino	%5 magnesite	%10 magnesite	%25 magnesite	%60 magnesite	magnesite
1	0.022	0.022	0.022	0.022	0.022	0.022
100	2.2	2.2	2.2	2.2	2.2	2.2
500	3.5	8.7	10.9	11	11	11
3000	15.1	9.7	40.6	51	64.6	66
10000	33	75	102	139	202.3	217.1

pH=10						
Initial Conc of $Zn(NO_3)_2.6H_2O$ (mg/L)	Clino	%5 magnesite	%10 magnesite	%25 magnesite	%60 magnesite	magnesite
100	2.2	2.2	2.2	2.1	2	2.1
10000	219.5	219.9	220	219.9	219.9	219.8

Table C4-6. % Sorption of Zn^{2+} on magnesite-clinoptilolite mixtures

Initial Conc of $Zn(NO_3)_2.6H_2O$ (mg/L)	Clino	%5 magnesite	%10 magnesite	%25 magnesite	%60 magnesite	magnesite
1	>99.9	>99.9	>99.9	>99.9	>99.9	>99.9
100	>99.9	>99.9	>99.9	>99.9	>99.9	>99.9
500	31.8	79.1	99.1	>99.9	>99.9	>99.9
3000	22.9	14.7	61.5	77.3	97.9	>99.9
10000	15.0	34.1	46.4	63.2	92.0	98.7

pH=10						
Initial Conc of $Zn(NO_3)_2.6H_2O$ (mg/L)	Clino	%5 magnesite	%10 magnesite	%25 magnesite	%60 magnesite	magnesite
100	>99.9	>99.9	>99.9	95.5	90.9	95.5
10000	99.8	>99.9	>99.9	>99.9	>99.9	99.9

APPENDIX D

APPENDIX D1: The pH Values Obtained From Sorption Data of Lead Ion

Pb-Kaolinite						
Initial Conc of $Pb(NO_3)_2$ (mg/l)	10 min	30 min	120 min	480 min	1440 min	2880 min
1	6.86-7.01	6.76-7.01	6.49-7.73	6.80-7.10	6.49-7.73	7.73-7.96
100	5.28-5.77	5.35-5.78	5.41-6.00	5.06-6.77	5.28-7.02	5.41-6.66
1000	4.13-4.25	3.63-4.04	5.4-6.64	5.73-4.96	6.50-6.82	5.82-4.82
Pb-Clinoptilolite						
Initial Conc of $Pb(NO_3)_2$ (mg/L)	10 min	30 min	120 min	480 min	1440 min	2880 min
1	8.8-8.0	9.02-7.8	8.68-8.06	8.50-8.33	9.15-8.52	8.68-7.96
100	6.42-6.83	6.81-7.07	6.47-7.31	6.66-7.67	5.66-7.83	6.48-7.91
1000	4.17-4.15	3.85-4.46	4.88-4.15	5.16-5.11	5.50-7.14	5.30-4.80

Pb-Mixtures						
Calcite-Kaolinite						
Initial Conc of $Pb(NO_3)_2$ (mg/L)	Kaolinite	%5 calcite	%10 calcite	%25 calcite	%60 calcite	calcite
1	7.73-7.96	9.36-8.91	9.36-8.92	9.38-8.96	9.40-9.20	9.32-9.39
100	6.5-7.06	6.00-7.03	5.81-6.92	8.05-6.89	8.09-6.89	6.5-7.06
500	5.27-5.88	5.67-7.92	5.50-7.91	5.42-7.96	5.42-7.96	5.35-8.06
3000	4.77-5.35	5.7-6.20	5.53-6.25	5.08-7.62	4.91-7.79	4.84-7.75
10000	4.13-4.71	5.57-4.35	5.32-4.65	4.96-4.12	4.48-4.35	4.29-6.69
pH=10						
Initial Conc of $Pb(NO_3)_2$ (mg/L)	Kaolinite	%5 calcite	%10 calcite	%25 calcite	%60 calcite	calcite
100	10.53	9.52	10.5	10.09	9.76	10.45
10000	9.88	10.08	10,86	11.00	11.08	11.02

Magnesite-Kaolinite						
Initial Conc of $Pb(NO_3)_2$ (mg/L)	Kaolinite	%5 magnesite	%10 magnesite	%25 magnesite	%60 magnesite	magnesite
1	7.73-7.960	9.56-9.18	9.33-9.45	9.78-9.38	9.73-9.67	9.93-9.84
100	6.5-7.06	6.53-8.53	6.61-8.19	8.21-8.79	9.14-9.4	9.61-9.33
500	5.27-5.88	5.34-9.34	5.24-9.47	5.28-9.42	5.23-9.58	5.28-9.55
3000	4.77-5.35	5.0-5.58	5.00-6.62	4.92-8.65	4.90-8.88	4.90-9.00
10000	4.13-4.71	4.23-4.55	3.96-4.59	3.96-4.96	3.97-5.05	4.05-7.65
pH=10						
Initial Conc of $Pb(NO_3)_2$ (mg/L)	Kaolinite	%5 magnesite	%10 magnesite	%25 magnesite	%60 magnesite	magnesite
100	10.53	9.75	9.73	9.99	10.04	10.07
10000	9.88	10.64	10.62	10.45	10.39	9.37
Calcite-Clinoptilolite						
Initial Conc of $Pb(NO_3)_2$ (mg/L)	Clino	%5 calcite	%10 calcite	%25 calcite	%60 calcite	calcite
1	8.68-7.96	9.23-8.91	9.34-8.94	9.30-8.81	9.48-9.14	9.32-9.39
100	6.48-7.91	8.8-6.86	9.11-7.25	8.62-7.30	8.69-7.14	8.09-6.89
500	6.32-7.55	6.56-8.30	6.56-8.37	6.32-8.39	6.34-8.49	5.35-8.06
3000	4.04-4.96	4.00-5.55	4.38-5.12	4.49-5.92	4.79-7.09	4.84-7.75
10000	3.91-4.36	4.05-4.65	4.10-4.81	4.14-5.03	4.02-7.07	4.48-4.35
pH=10						
Initial Conc of $Pb(NO_3)_2$ (mg/L)	Clino	%5 calcite	%10 calcite	%25 calcite	%60 calcite	calcite
100	9.39	9.46	9.16	9.49	9.78	8.75
10000	7.86	10.72	10.91	10.96	10.90	11.02

Magnesite-Clinoptilolite						
Initial Conc of $Pb(NO_3)_2$ (mg/L)	Clino	%5 magnesite	%10 magnesite	%25 magnesite	%60 magnesite	magnesite
1	5.30-4.80	9.38-8.83	9.31-9.03	9.10-8.91	9.21-9.19	9.93-9.84
100	6.48-7.91	7.82-9.06	7.63-9.12	9.14-8.65	9.59-9.07	9.61-9.33
500	6.32-7.55	6.34-9.09	6.41-9.06	6.21-9.59	6.00-9.19	5.28-9.55
3000	4.04-4.96	4.35-5.07	4.46-8.36	4.06-8.83	5.62-9.20	4.90-9.00
10000	3.91-4.36	3.85-4.59	3.81-4.81	3.76-5.35	3.72-8.45	4.05-7.65
pH=10						
Initial Conc of $Pb(NO_3)_2$ (mg/L)	Clino	%5 magnesite	%10 magnesite	%25 magnesite	%60 magnesite	magnesite
100	9.39	9.7	9.7	9.8	9.53	10.07
10000	7.86	10.14	10.18	10.18	10.09	9.37

APPENDIX D2: The pH Values Obtained From Sorption Data of Zinc Ion

Zn-Kaolinite						
Initial Conc of $Zn(NO_3)_2.6H_2O$ (mg/L)	10 min	30 min	120 min	480 min	1440 min	2880 min
1	7.26-8.21	7.24-8.19	7.22-8.32	6.99-9.09	6.5-7.64	7.25-8.92
100	5.97-6.44	6.09-6.56	5.99-6.84	5.47-7.13	6.15-7.34	6.44-7.04
1000	4.64-5.19	5.28-5.63	5.28-5.52	5.76-5.88	5.84-6.84	5.30-4.80
Zn-Clinoptilolite						
Initial Conc of $Zn(NO_3)_2.6H_2O$ (mg/L)	10 min	30 min	120 min	480 min	1440 min	2880 min
1	8.20-7.5	8.48-8.16	8.63-8.50	7.85-7.80	8.43-8.14	8.35-8.01
100	6.01-6.39	6.43-7.08	7.00-6.79	6.25-7.07	6.05-7.5	6.68-7.44
1000	4.84-5.43	5.10-5.92	6.29-5.73	6.44-6.04	6.02-6.90	5.94-6.75

Zn-Mixtures						
Calcite -Kaolinite						
Initial Conc of $Zn(NO_3)_2.6H_2O$ (mg/L)	Kaolinite	%5 calcite	%10 calcite	%25 calcite	%60 calcite	calcite
1	7.25-8.92	9.16-8.37	9.05-8.84	9.24-9.13	9.62-9.15	9.71-9.37
100	6.44-7.04	7.05-7.85	7.03-7.62	7.26-7.86	7.54-8.32	7.69-8.93
500	6.93-6.78	6.95-6.85	6.91-6.56	6.84-6.85	6.90-7.26	6.98-7.33
3000	6.48-6.79	5.92-5.94	6.00-6.01	6.13-6.32	6.26-6.46	6.3-6.46
10000	6.02-6.15	5.38-6.00	5.83-5.88	5.91-5.78	5.94-5.83	5.97-5.93
pH=10						
Initial Conc of $Zn(NO_3)_2.6H_2O$ (mg/L)	Kaolinite	%5 calcite	%10 calcite	%25 calcite	%60 calcite	calcite
100	10.29	10.1	9.45	9.84	9.92	8.08
10000	9.12	9.1	8.84	8.76	8.72	8.75

Magnesite-Kaolinite						
Initial Conc of $Zn(NO_3)_2.6H_2O$ (mg/L)	Kaolinite	%5 magnesite	%10 magnesite	%25 magnesite	%60 magnesite	magnesite
1	7.25-8.92	9.48-9.65	9.60-9.64	10.10-9.3	10.05-9.78	10.08-10.0
100	6.44-7.04	7.52-9.09	7.42-9.37	7.23-9.38	7.71-9.35	7.99-9.61
500	5.27-5.88	5.34-9.34	5.24-9.47	5.28-9.42	5.23-9.58	5.28-9.55
3000	6.48-6.79	6.49-6.82	6.54-5.66	6.55-6.79	6.58-8.65	6.60-7.55
10000	6.02-6.15	6.03-6.06	6.05-5.93	6.06-6.05	6.07-7.06	6.09-6.24
pH=10						
Initial Conc of $Zn(NO_3)_2.6H_2O$ (mg/L)	Kaolinite	%5 magnesite	%10 magnesite	%25 magnesite	%60 magnesite	magnesite
100	10.29	10.06	9.99	10.03	10.11	9.99
10000	9.12	10.11	10.01	9.99	10.1	9.9

Calcite-Clinoptilolite						
Initial Conc of $Zn(NO_3)_2.6H_2O$ (mg/L)	Clino	%5 calcite	%10 calcite	%25 calcite	%60 calcite	calcite
1	8.35-8.01	9.78-8.99	9.60-8.51	9.62-9.00	9.60-9.34	9.71-9.37
100	6.68-7.44	7.49-8.14	7.33-7.85	8.9-8.30	8.49-8.67	7.69-8.93
500	6.32-7.55	6.56-8.30	6.56-8.37	6.32-8.39	6.34-8.49	5.35-8.06
3000	6.05-6.24	6.70-6.55	5.48-6.48	5.80-6.44	6.15-6.64	6.3-6.46
10000	6.08-5.98	5.70-5.83	5.83-5.90	5.89-5.87	5.97-6.13	5.97-5.93
pH=10						
Initial Conc of $Zn(NO_3)_2.6H_2O$ (mg/L)	Clino	%5 calcite	%10 calcite	%25 calcite	%60 calcite	calcite
100	9.39	9.46	9.16	9.49	9.78	10.45
10000	8.83	9.27	8.92	8.78	8.78	8.75

Magnesite-Clinoptilolite						
Initial Conc of $Zn(NO_3)_2.6H_2O$ (mg/L)	Clino	%5 magnesite	%10 magnesite	%25 magnesite	%60 magnesite	magnesite
1	8.35-8.01	9.49-9.47	9.42-9.47	9.61-9.3	10.03-9.41	10.08-10.0
100	6.68-7.44	7.21-9.05	7.83-9.3	8.69-9.27	8.05-9.17	7.99-9.61
500	6.32-7.55	6.34-9.09	6.41-9.06	6.21-9.59	6.00-9.19	5.28-9.55
3000	6.05-6.24	6.36-6.34	6.36-6.63	6.34-8.25	6.32-8.29	6.60-7.55
10000	6.08-5.98	6.13-5.92	6.14-5.85	6.18-6.09	6.08-7.23	6.09-6.24
pH=10						
Initial Conc of $Zn(NO_3)_2.6H_2O$ (mg/L)	Clino	%5 magnesite	%10 magnesite	%25 magnesite	%60 magnesite	magnesite
100	9.69	9.87	9.7	9.72	9.57	9.99
10000	8.83	9.73	9.86	9.85	9.78	9.9

APPENDIX D3: Speciation Figures of Pb^{2+} and Zn^{2+} in Aqueous Solution

Table D3-1. Speciation table of 10000 mg/L Pb^{2+} in aqueous solution as a function of pH

pH	Pb(OH)2 (aq)	Pb(OH)3-	Pb+2	Pb2OH+3	Pb3(OH)4+2	Pb4(OH)4+4	PbOH+
2	3,8794E-15	3,9E-24	0,048265	9,33E-08	1,45E-20	7E-19	1,22E-07
4	3,8783E-11	3,9E-18	0,048234	9,32E-06	1,45E-12	6,98E-11	1,22E-05
6	2,9512E-07	2,97E-12	0,036703	0,00054	6,38E-05	0,002341	0,000928
8	0,00003421	3,44E-08	0,000425	7,25E-06	0,009936	0,004227	0,001075
10	0,00085777	8,63E-05	1,07E-06	4,56E-09	0,015661	1,67E-05	0,00027
12	0,0043085	0,043348	5,36E-10	1,15E-13	0,000198	1,06E-10	1,35E-05

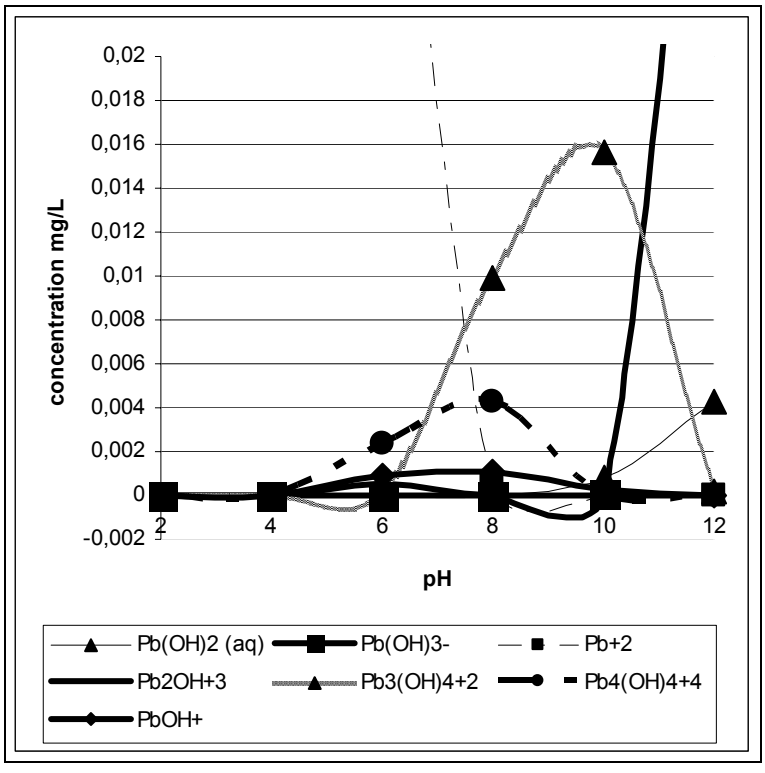

Figure D3-1. Speciation Figures of 10000 mg/L Pb^{2+} in aqueous solution as a function of pH

Table D3-2. Speciation table of 100 mg/L Pb^{2+} in aqueous solution as a function of pH

pH	Pb(OH)2 (aq)	Pb(OH)3-	Pb+2	Pb2OH+3	Pb3(OH)4+2	Pb4(OH)4+4	PbOH+
2	3,89E-17	3,91E-26	0,000483	9,34E-12	1,45E-26	7,02E-27	1,22E-09
4	3,89E-13	3,91E-20	0,000483	9,33E-10	1,45E-18	7,01E-19	1,22E-07
6	3,79E-09	3,82E-14	0,000471	8,88E-08	1,35E-10	6,34E-11	1,19E-05
8	6,26E-06	6,31E-09	7,78E-05	2,42E-07	6,09E-05	4,73E-06	0,000197
10	0,000153	1,54E-05	1,9E-07	1,45E-10	8,87E-05	1,68E-08	4,8E-05
12	4,36E-05	0,000439	5,41E-12	1,17E-17	2,05E-10	1,11E-18	1,37E-07

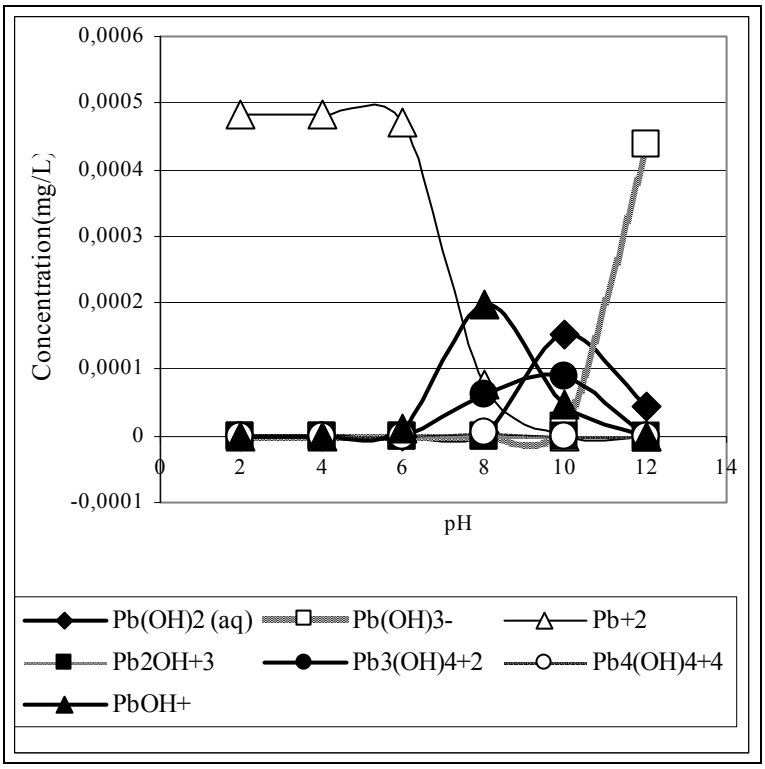

Figure D3-2. Speciation figure of 100 mg/L Pb^{2+} in aqueous solution as a function of pH

Table D3-3. Speciation table of 10000 mg/L Zn^{2+} in aqueous solution as a function of pH

pH	Zn(OH)2 (aq)	Zn(OH)3-	Zn(OH)4-2	Zn+2	Zn2OH+3	ZnOH+
2	1,94E-14	6,15E-24	9,78E-35	0,15298	2,35E-09	1,53E-08
4	1,94E-10	6,15E-18	9,79E-27	0,15297	2,35E-07	1,54E-06
6	1,94E-06	6,15E-12	9,77E-19	0,15277	2,34E-05	0,000153
8	0,015494	4,92E-06	7,82E-11	0,12222	0,001499	0,012264
10	0,14702	0,004666	7,42E-06	0,000116	1,35E-07	0,001164
12	0,032701	0,10377	0,016504	2,58E-09	6,68E-15	2,59E-06

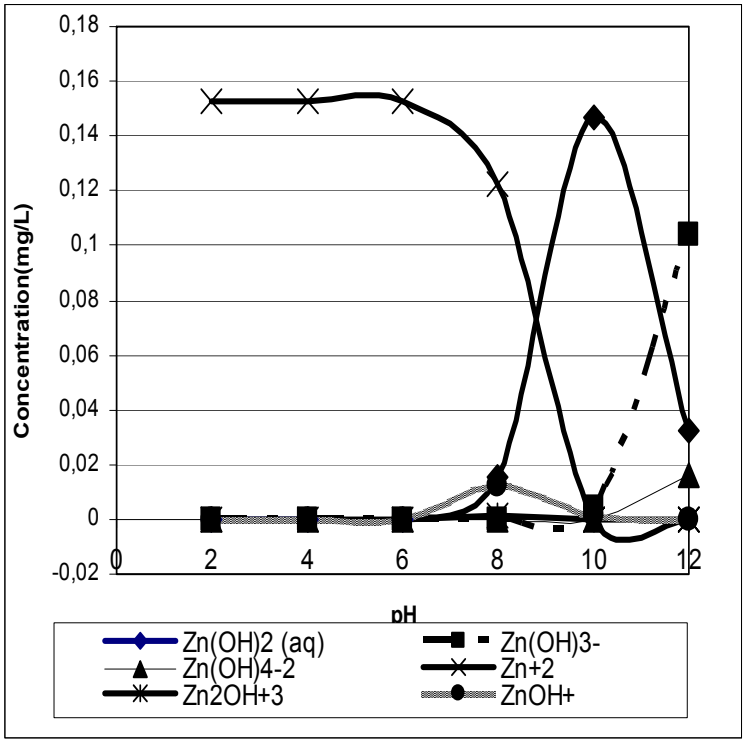

Figure D3-3. Speciation figure of 10000 mg/L Zn^{2+} in aqueous solution as a function of pH

Table D3-4. Speciation table of 100 mg/L Zn^{2+} in aqueous solution as a function of pH

pH	Zn(OH)2 (aq)	Zn(OH)3-	Zn(OH)4-2	Zn+2	Zn2OH+3	ZnOH+
2	1,95E-16	6,2E-26	9,88E-37	0,00153	2,354E-13	1,54E-10
4	1,95E-12	6,2E-20	9,89E-29	0,00153	2,3543E-11	1,54E-08
6	1,95E-08	6,2E-14	9,88E-21	0,001528	2,3496E-09	1,54E-06
8	0,000159	5,05E-08	8,05E-13	0,001245	1,5604E-07	0,000125
10	0,00147	4,68E-05	7,46E-08	1,15E-06	1,3391E-11	1,16E-05
12	0,000326	0,001038	0,000166	2,56E-11	6,5949E-19	2,58E-08

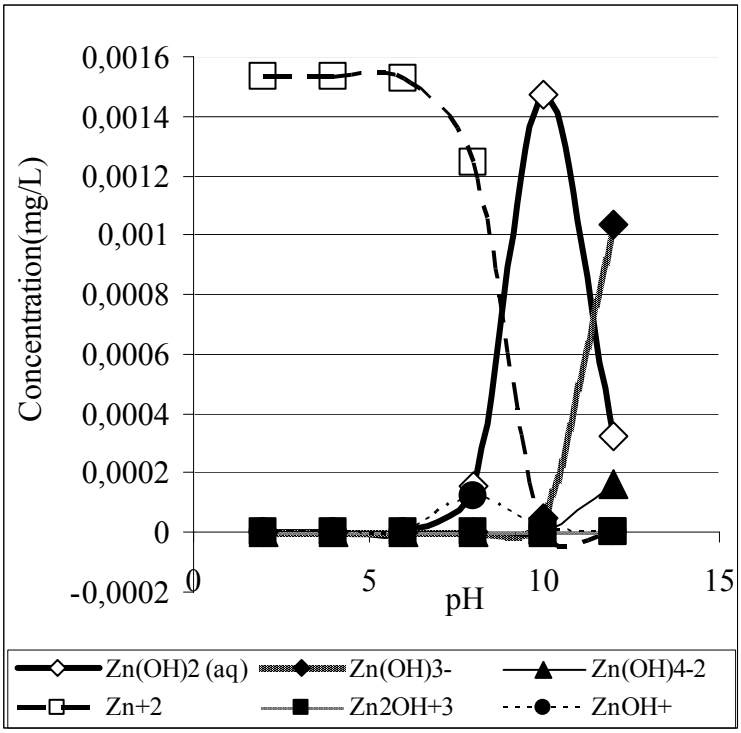

Figure D3-4. Speciation figure of 100 mg/L Zn^{2+} in aqueous solution as a function of pH